Chapter 1

THE GEOLOGY OF COLOMBIA

SERVICIO GEOLÓGICO COLOMBIANO

The Permian – Triassic History of Magmatic Rocks of the Northern Andes (Colombia and Ecuador): Supercontinent Assembly and Disassembly

Richard SPIKINGS[1]* and Andre PAUL[2]

1 richard.spikings@unige.ch
University of Geneva
Department of Earth Sciences and the Environment
Rue des Maraichers 13, Geneva 1205
Switzerland

2 andre.paul@unige.ch
University of Geneva
Department of Earth Sciences and the Environment
Rue des Maraichers 13, Geneva 1205
Switzerland

* Corresponding author

Abstract Northwestern South America and its conjugate margins record the Permian assembly of Pangaea, its Triassic fragmentation and opening of the proto–Caribbean ocean, and the onset of the Andean cycle at ca. 209 Ma. We review Permian and Triassic magmatic rocks exposed in the cordilleras and dispersed inliers in Colombia and Ecuador, and present a large geochronological, geochemical, isotopic, and thermochronological database. These data are used to develop a model for the evolution of rocks within Colombia and Ecuador during the formation and destruction of Pangaea. Similar data has been assembled from studies of the southern North American and western Caribbean plates, as well as Venezuela and further south within South America, and a large–scale reconstruction for western Pangaea is provided. Permian magmatic rocks in Colombia and Ecuador (288–253 Ma) formed within a continental arc system which extended from at least southern North America to southern Perú. The Permian arc within northwestern South America was dismembered during Cenozoic interactions with the Caribbean Plate, causing some blocks to be transferred eastwards. Compression and regional metamorphism at ca. 250 Ma is best recorded in the Sierra Nevada de Santa Marta, and represents the final stages of amalgamation and thickening of western Pangaea. Continental rifting prevailed within southern North America and the entire western margin of South America during 245–216 Ma. Significant back–arc extension in northwestern South America leads to a rift–to–drift transition in Colombia and Ecuador, forming oceanic lithosphere of the proto–Caribbean. Rifting failed south of the Huancabamba Deflection, and is preserved as Triassic basins in Perú, western Argentina, and Chile. Triassic rifting represents the early fragmentation of western Pangaea, and the attenuation of its margin may be a prelude to complete separation by enhancing mantle upwelling, inducing a Large Igneous Province and weakening the crust within a tensile regime.

Keywords: *Permian – Triassic, Pangaea, supercontinent, continental rift, anatexis.*

Resumen El noroccidente de Suramérica y sus márgenes conjugados registran la formación de Pangea durante el Pérmico, su fragmentación durante el Triásico y la apertura del océano proto–Caribe, así como el comienzo del ciclo andino hace ca. 209 Ma. En este capítulo presentamos una revisión de las rocas magmáticas del Pérmico y Triá-

Quaternary
Neogene
Paleogene
Cretaceous
Jurassic
Triassic
Permian
Carboniferous
Devonian
Silurian
Ordovician
Cambrian
Proterozoic

sico que afloran como fragmentos dispersos en las cordilleras de Colombia y Ecuador; además, presentamos una amplia base de datos geocronológica, geoquímica, isotópica y termocronológica. Estos datos se utilizan para desarrollar un modelo de la evolución de las rocas en Colombia y Ecuador durante la formación y la separación de Pangea. Otros estudios en el sur de la Placa de Norteamérica y en el occidente de la Placa del Caribe, así como en Venezuela y más al sur dentro de Suramérica, han sido también tenidos en cuenta para este análisis. Adicionalmente, se preparó una reconstrucción a gran escala del occidente de Pangea. Las rocas magmáticas del Pérmico de Colombia y Ecuador (288–253 Ma) se formaron en un ambiente de arco continental que se extendió al menos desde el sur de Norteamérica hasta el sur de Perú. En el noroccidente de Suramérica, este arco pérmico se separó durante las interacciones con la Placa del Caribe en el Cenozoico, de forma que algunos bloques fueron transferidos hacia el oriente. La compresión y el metamorfismo regional que ocurrieron hace ca. 250 Ma se observan claramente en la Sierra Nevada de Santa Marta y representan los estados finales de la amalgamación y engrosamiento del occidente de Pangea. El *rift* continental continuó en el sur de Norteamérica y todo el margen occidental de Suramérica durante 245–216 Ma. La extensión en el retroarco en Suramérica fue muy importante y llevó a una transición *rift–drift* en Colombia y Ecuador, lo que causó la formación de la litósfera oceánica del proto–Caribe. El *rift* fue abortado al sur de la deflexión de Huancabamba, pero se preservó como cuencas triásicas en Perú, el occidente de Argentina y Chile. Este *rift* triásico representa una separación temprana del occidente de Pangea y la atenuación de su margen podría ser el preludio de la separación completa de los continentes, ya que potencia el ascenso del manto y esto induce a la formación de una Gran Provincia Ígnea, debilitando la corteza en un régimen de extensión.

Palabras clave: *Pérmico–Triásico, Pangea, supercontinente, rift continental, anatexis.*

1. Introduction

The northwestern South American Plate hosts a Rodinia–aged (ca. 1 Ga) and Ordovician basement, which was modified during the amalgamation and disassembly of Pangaea. Subsequent active margin magmatism (209–115 Ma) within the proto–Caribbean and Pacific Wilson cycle occurred during a prolonged period of extension (Cochrane et al., 2014a; Spikings et al., 2015), which was interrupted by compression at ca. 115 Ma (Spikings et al., 2015) and the collision of the voluminous Caribbean Large Igneous Province at ca. 75 Ma (Vallejo et al., 2006), which added new crust to South America. This chapter is a review of crystalline and some sedimentary rocks exposed in Colombia and Ecuador that formed during the Permian and Triassic. These rocks record the period between the final assembly of Pangaea in the early Permian, and its early disassembly during the Triassic. Colombia and Ecuador are considered together because their Permian and Triassic rock records are extremely similar and complementary, and thus studying both countries increases our chances of observing poorly exposed sequences and obtaining an accurate geological model, and provides a means to identify plate margin trends. The studied units are mainly exposed in the Central Cordillera, Sierra Nevada de Santa Marta, and Santander Massif of Colombia, and the Cordillera Real and Amotape Complex of Ecuador. We will also consider Permian and Triassic crystalline rocks exposed in Perú and other regions of South America, as well as the southernmost North American and western Caribbean plates, which were coeval with and probably formed in the same general tectonic setting as crystalline rocks in northwestern South America, facilitating reconstructions of western Pangaea.

The amalgamation of Pangaea in the Permian coincided with a drastic reduction in plate velocities and an almost complete pause in continental drift during the late Permian – Early Jurassic (Vilas & Valencio, 1978). This relatively stationary period was characterised by heat accumulation, the production of large volumes of magmas (e.g., Kay et al., 1989), and geographically extensive extension along western South America (e.g., Charrier et al., 2007; Spikings et al., 2015, 2016). Increased plate velocities in the earliest Jurassic (e.g., Ramos, 1988) were coeval with the disassembly of Pangaea, although the relationship between Triassic extension and the rapid disassembly of Pangaea in the Early Jurassic is unclear.

This review presents geochronological (U–Pb zircon), geochemical, isotopic (Hf, Pb, Sr, Nd, O), and thermochronological (U–Pb and $^{40}Ar/^{39}Ar$) data from the Permian and Triassic magmatic rocks of the Central Cordillera of Colombia, and coeval magmatic and metasedimentary units of the Sierra Nevada de Santa Marta. The same techniques have been applied to the Tres Lagunas Granite, Sabanilla Migmatite (Cordillera Real, Ecua-

dor), and the Moromoro Granite (Amotape Complex, Ecuador), along with Triassic mafic units in both countries. These data are used to develop a temporally constrained tectonic framework for the Permian – Triassic, culminating with rifting along western Pangaea (proto–Caribbean; Jaillard et al., 1990, 1995; Pindell, 1985), and to investigate the relationship between initial Triassic rifting and the final disassembly of Pangaea.

2. Geological Framework and Previous Work

Phanerozoic rocks in the northern Andes (north of the Huancabamba Deflection; at 5° S; Figure 1) can be separated into a relatively undifferentiated oceanic Upper Cretaceous sequence, which is faulted against older, differentiated continental crust. The Upper Cretaceous oceanic rocks form the basement to the Western Cordillera and the forearcs of Colombia (Calima and Chocó–Panamá Terranes; Figure 1; e.g., Kerr et al., 1997, 2002) and Ecuador (Pallatanga–Piñon Terrane; e.g., Vallejo et al., 2009). Geochemical, isotopic, and geochronological data suggests these laterally accreted ultramafic and mafic rocks formed in an oceanic hot–spot setting during 99–87 Ma (e.g., Kerr et al., 1997; Vallejo et al., 2006; Villagómez et al., 2011), and that they are equivalent to the oceanic plateau rocks that form the Caribbean Plate (e.g., Sinton et al., 1998; van der Lelij et al., 2010). Field relationships and U–Pb zircon dates show that the oceanic plateau was intruded by an east–facing intra–oceanic arc prior to their collision with South America in the Campanian (e.g., Spikings et al., 2010; Vallejo et al., 2006, 2009), although this is not consistent with the plate reconstructions of Pindell & Kennan (2009), who suggest that arcs at this time were west–facing and were intruding the continental margin of South America. The accretion of allochthons of the Caribbean Large Igneous Province added at least $5 \times 10^6 – 1 \times 10^7 \, km^3$ of new crust to the South American Plate (Cochrane et al., 2014a). These terranes are bound to the east by the Cauca–Almaguer Fault (Colombia; Figure 1), and the buried Ingapirca Fault (Ecuador).

The Early Cretaceous continental margin hosts linear belts that are exposed within the Central Cordillera and Sierra Nevada de Santa Marta of Colombia, and the Cordillera Real and Amotape Complex of Ecuador (Figure 1). These belts mainly strike to the north, although they have been partially segmented and rotated, resulting in a NE (Sierra Nevada de Santa Marta, Colombia; Bayona et al., 2010) and E–W (Amotape Complex, Ecuador; Mitouard et al., 1990) strike. Traversing eastwards from the Campanian suture, these are M–HP/LT complexes of amphibolites, blueschists, and eclogites (e.g., Arquía and Barragán Complexes, Colombia; Raspas Complex, Ecuador; e.g., Bustamante et al., 2012; John et al., 2010; Spikings et al., 2015), Cretaceous arc rocks of the Quebradagrande (Colombia; Nivia et al., 2006) and Alao sequences (Ecuador; Cochrane et al., 2014a; Spikings et al., 2015), poorly differentiated Paleozo-

ic rocks that contain isolated exposures of Ordovician gneisses (e.g., Martens et al., 2014; Villagómez et al., 2011; Vinasco et al., 2006), minor Permian intrusions and extensive Triassic anatectites (Cochrane et al., 2014a; Paul et al., 2018; Spikings et al., 2015), foliated Jurassic arc rocks that are best exposed in Ecuador, and large unfoliated Jurassic batholiths along the eastern flank of the Central Cordillera in Colombia, and Cordillera Real in Ecuador (Figure 1). McCourt et al. (1984), Aspden & McCourt (1986), Aspden & Litherland (1992), and Litherland et al. (1994) suggest that these belts are in tectonic contact, and the Triassic and younger belts were juxtaposed during compression at 140–120 Ma. Alternatively, Pratt et al. (2005) suggest that the contacts are intrusive, and the rock units within Ecuador are autochthonous, which is similar to the model proposed by Villagómez & Spikings (2013), Cochrane et al. (2014a), and Spikings et al. (2015) for Colombia and Ecuador. The Permian and Triassic rocks form the focus of this review.

Traversing further eastwards, the Eastern Cordillera of Colombia has no equivalent topographic feature in Ecuador, and it includes the high plains of the Santander Massif in the north (Figure 1). The Santander Massif has an extensive metamorphic basement that is dominated by amphibolite grade Ordovician gneisses of the Bucaramanga Gneiss and Berlin Orthogneiss (van der Lelij et al., 2016). In contrast to the rocks exposed in the Central Cordillera, a significant magmatic hiatus exists between the Ordovician basement (500–415 Ma; van der Lelij et al., 2016), and intruding late Triassic (209 Ma; van der Lelij et al., 2016) and younger continental arc rocks of the Santander Plutonic Group. Triassic anatexis, which is extensively preserved in the cordilleras, did not affect the Ordovician basement exposed in the Santander Massif, and the Permian is only recorded by a single rhyolite (251 ± 4 Ma; van der Lelij et al., 2016) along the western margin of the massif. The Permian Diamante, Tiburón, and the fossiliferous Bocas sedimentary Formations are sporadically exposed across the Santander Massif, although the tectonic environment in which they were deposited is undetermined. Coeval Permian sedimentary successions in the juxtaposed Mérida Andes of Venezuela (Palmarito Formation; Figure 1) are interpreted to have deposited in a foreland basin (Laya & Tucker, 2012), which may have formed during the final stages of the Alleghanian Orogeny, culminating with the amalgamation of Pangaea by the early Permian (Hatcher, 2002).

The Sierra Nevada de Santa Marta resides within a triangular faulted block in northern Colombia (Figure 1). The northern margin of the Sierra Nevada de Santa Marta Block is truncated by the right–lateral Oca Fault, which is displacing Cretaceous and older continental crust of the Guajira Peninsula to the east (Figure 1). The western margin of the triangular block is defined by the Santa Marta–Bucaramanga Fault (Figure 1), which separates crystalline rocks in the east from the Oligocene – Miocene Plato–San Jorge Basin to the west, which is floored by Triassic rocks similar to those exposed in the Sierra Nevada
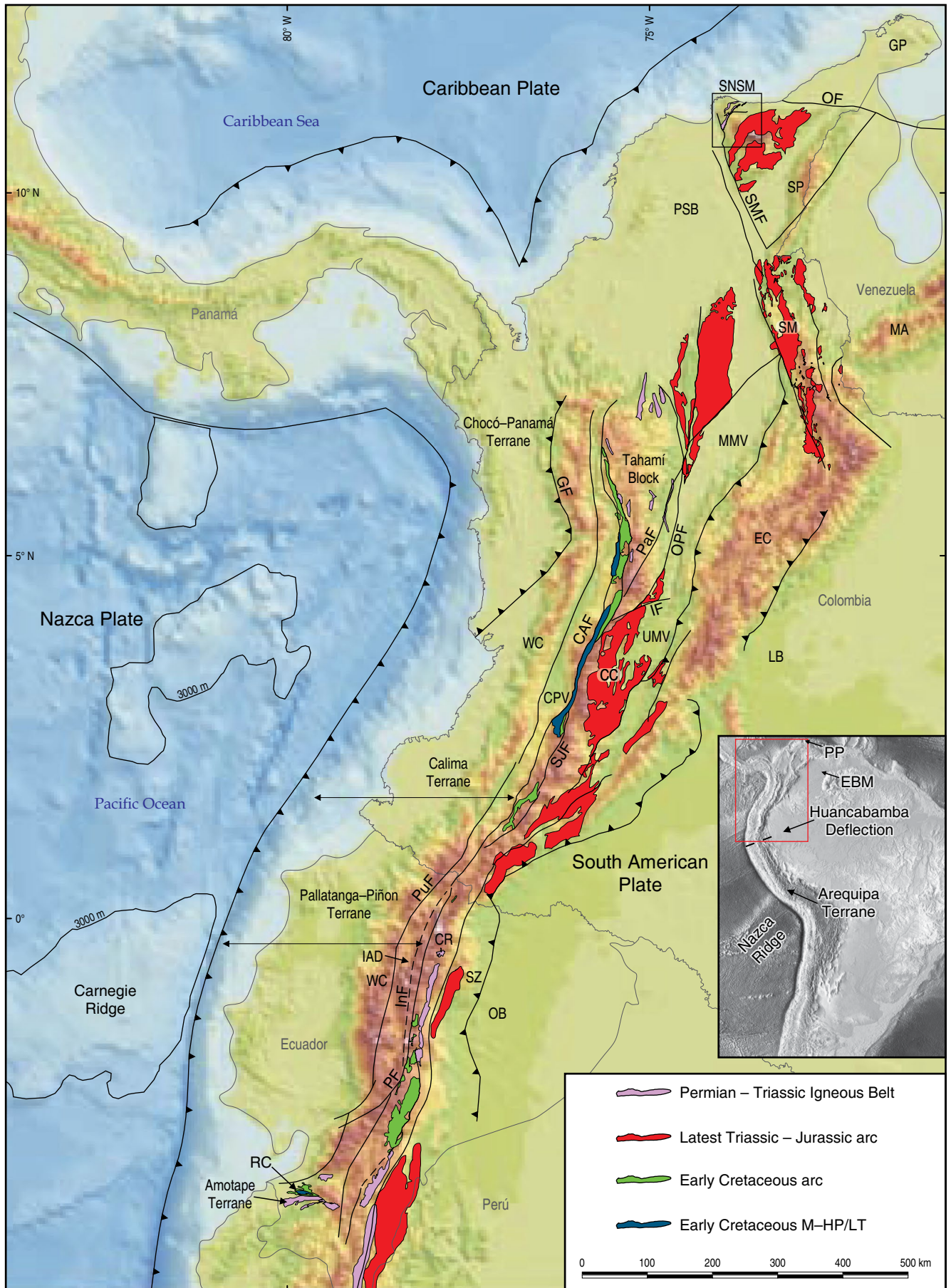
de Santa Marta (Montes et al., 2010). The Santa Marta–Bucaramanga Fault extends towards the SSE where it defines the western margin of the Santander Massif within the Colombian Eastern Cordillera (Figure 1). The present study follows the geological subdivisions of the Sierra Nevada de Santa Marta proposed by Tschanz et al. (1974), which were structurally revised by Colmenares et al. (2007a, 2007b) and better temporally constrained by Cardona et al. (2010a, 2010b) and Piraquive (2017). The Inner Santa Marta Metamorphic Belt of the Sierra Nevada de Santa Marta consists of Paleozoic orthogneisses and schists, which were intruded by Permian – Triassic syntectonic granitoids (Piraquive, 2017) that are studied in this review. Palaeomagnetic studies (Bayona et al., 2006, 2010) suggest that Jurassic rocks exposed along the southern border of the Sierra Nevada de Santa Marta rotated clockwise (17 ± 13°) between the Middle – Late Jurassic and Early Cretaceous, and thus it is likely that there is a genetic link between Permian – Triassic magmatic rocks exposed in the Central Cordillera and the Sierra Nevada de Santa Marta. Similarly, Pindell et al. (1998) used palinspastic reconstructions to reach the same conclusion.
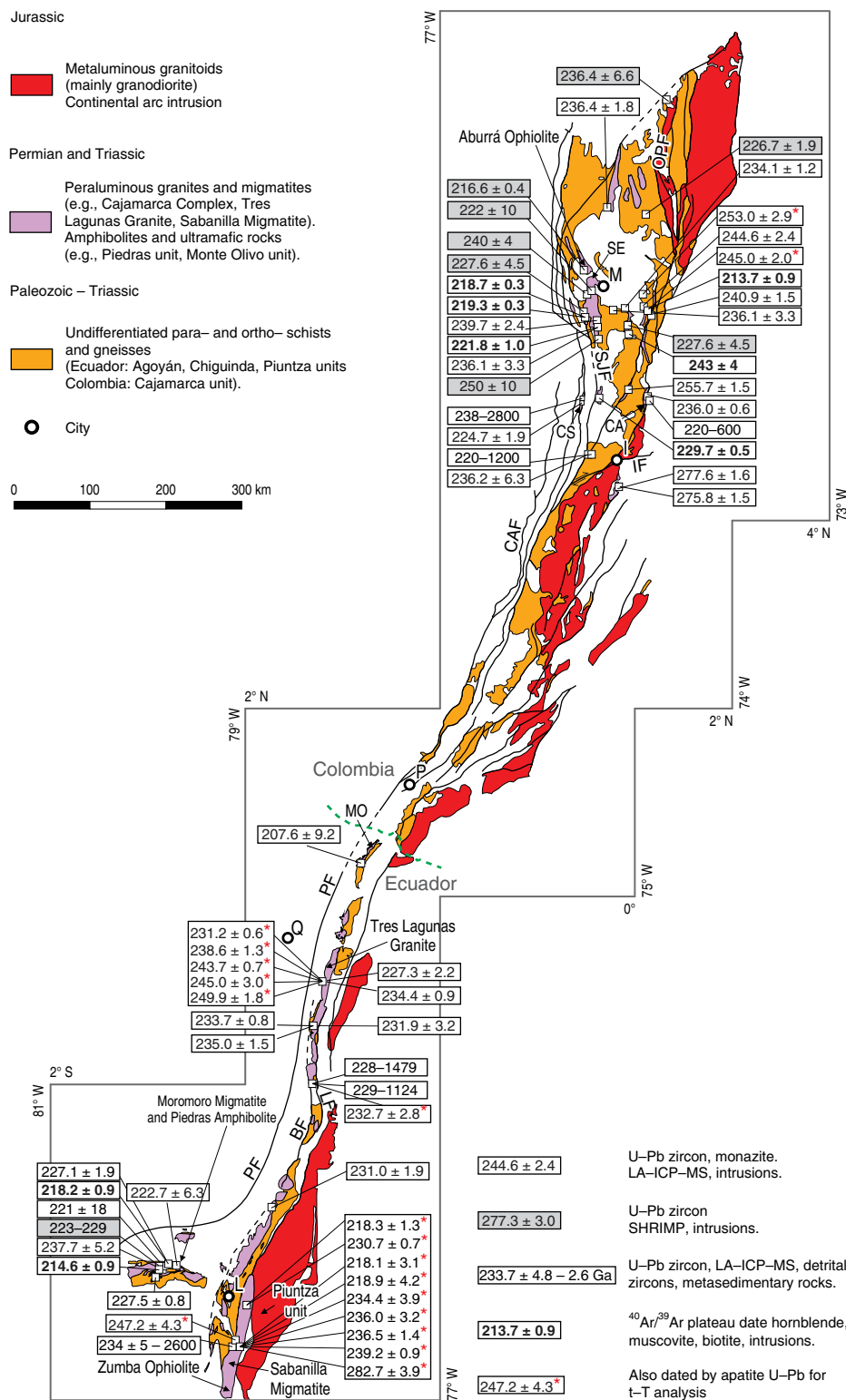
3. Historical Perspective and Occurrence of Permian – Triassic Igneous Rocks

Widely dispersed and variably deformed Permian and Triassic meta–granitoids, ultra–mafic – mafic rocks, and metasedimentary rocks occur within the northern Central Cordillera of Colombia (Figure 2). These rocks were initially described by Hall et al. (1972), Feininger et al. (1972), and González (1980), who considered them to be Permian – Triassic on the basis of K/Ar dates. Restrepo & Toussaint (1988) suggested the Permian – Triassic rocks defined the basement of the fault–bounded Tahamí Terrane, and placed them within the Central Cordillera Polymetamorphic Complex (Restrepo & Toussaint, 1982). The Tahamí Terrane of Restrepo & Toussaint (1988) is bound by the Otú–Pericos Fault to the east, which separates it from Grenvillian aged metamorphic basement of the postulated Chibcha Terrane (e.g., Ordóñez–Carmona et al., 2006), and the San Jerónimo Fault to the west, which separates it from the Cretaceous Quebradagrande Arc (Figure 1). Maya & González (1995) and Villagómez et al. (2011) group the Tri-

assic metamorphosed igneous and sedimentary rocks into the Cajamarca Complex, which will be adopted in this manuscript. The geological map of Colombia (Gómez et al., 2007) reveals a paucity of Triassic lithologies within the Central Cordillera south of the Ibagué Fault (Figure 2). Vinasco et al. (2006), Correa–Martínez (2007), Cardona et al. (2010a), Montes et al. (2010), Weber et al. (2010), Restrepo et al. (2011), Villagómez et al. (2011), Cochrane et al. (2014b), Martens et al. (2014), Spikings et al. (2015), Bustamante et al. (2017), and Paul et al. (2018) present a large quantity of geochemical data and concordant zircon U–Pb dates (Figure 2; Table 1) from the Cajamarca unit, confirming the Permian – Triassic crystallisation gneisses of the Central Cordillera, which are faulted against Paleozoic (mainly Ordovician) metamorphic rocks such as La Miel unit (e.g., Martens et al., 2014; Restrepo et al., 1991; Villagómez et al., 2011). In contrast, anatexis of undifferentiated Upper Devonian – Carboniferous metasedimentary rocks forming the Triassic Sabanilla Migmatite can be observed in the Cordillera Real. Correa–Martínez (2007) reports a series of metagabbros and amphibolites in the northern Central Cordillera, which she attributes to a Triassic ophiolitic sequence, referred to as the Aburrá Ophiolite (Figure 2). Permian and/or Triassic igneous and metamorphic rocks have also been recognised in the Guajira Peninsula, Sierra Nevada de Santa Marta (Figure 3), and at the base of boreholes drilled though the Plato–San Jorge Basin located north of the Central Cordillera (Figure 1; Cardona et al., 2010b; Montes et al., 2010; Piraquive, 2017; Weber et al., 2010). Granites from the basement of the Plato–San Jorge Basin are mildly deformed, while the intrusions from the Sierra Nevada de Santa Marta are mylonitised.

Triassic rocks within the Cordillera Real and Amotape Terrane of Ecuador include granitoids of the Tres Lagunas and Moromoro units, migmatites of the Sabanilla unit, geographically scattered amphibolitic dykes and sills (Piedras and Monte Olivo units), and sedimentary rocks of the Piuntza unit (Figure 2). The granites were first described by Colony & Sinclair (1932). Mapping by the British Geological Survey during 1986–1993 linked these occurrences into a semi–continuous belt, and they were grouped into the Loja Terrane (Litherland et al., 1994) along with undifferentiated Paleozoic metamorphic rocks of the Chiguinda and Agoyán units. The Loja Terrane of Litherland et al. (1994) is bound to the

Figure 1. Digital elevation model for northwestern South America showing the cordilleras, terranes, main faults, and the exposure of Permian – Cretaceous magmatic rocks in Ecuador and Colombia. Small black box indicates the location of Figure 3. Inset shows the location of the Arequipa Terrane in southern Perú. Faults: (CAF) Cauca–Almaguer Fault; (GF) Garrapatas Fault; (IF) Ibagué Fault; (InF) Ingapirca Fault; (OF) Oca Fault; (OPF) Otú–Pericos Fault; (PaF) Palestina Fault; (PF) Peltetec Fault; (PuF) Pujili Fault; (SJF) San Jerónimo Fault; (SMF) Santa Marta–Bucaramanga Fault. Other abbreviations: (CC) Central Cordillera; (EC) Eastern Cordillera; (CPV) Cauca–Patía valley; (CR) Cordillera Real; (EBM) El Baúl Massif; (GP) Guajira Peninsula; (IAD) Interandean Depression; (LB) Llanos Basin; (MA) Mérida Andes; (MMV) Middle Magdalena Valley Basin; (OB) Oriente Basin; (PP) Paraguaná Peninsula; (PSB) Plato–San Jorge Basin; (RC) Raspas Complex; (SM) Santander Massif; (SNSM) Sierra Nevada de Santa Marta; (SP) serranía de Perijá; (SZ) Sub–Andean Zone; (UMV) Upper Magdalena Valley Basin; (WC) Western Cordillera. Geology from Litherland et al. (1994) and Gómez et al. (2007).

Jurassic

Metaluminous granitoids
(mainly granodiorite)
Continental arc intrusion

Permian and Triassic

Peraluminous granites and migmatites
(e.g., Cajamarca Complex, Tres
Lagunas Granite, Sabanilla Migmatite).
Amphibolites and ultramafic rocks
(e.g., Piedras unit, Monte Olivo unit).

Paleozoic – Triassic

Undifferentiated para– and ortho– schists
and gneisses
(Ecuador: Agoyán, Chiguinda, Piuntza units
Colombia: Cajamarca unit).

○ City

0   100   200   300 km

244.6 ± 2.4 — U–Pb zircon, monazite. LA–ICP–MS, intrusions.

277.3 ± 3.0 — U–Pb zircon SHRIMP, intrusions.

233.7 ± 4.8 – 2.6 Ga — U–Pb zircon, LA–ICP–MS, detrital zircons, metasedimentary rocks.

213.7 ± 0.9 — ^{40}Ar/^{39}Ar plateau date hornblende, muscovite, biotite, intrusions.

247.2 ± 4.3* — Also dated by apatite U–Pb for t–T analysis

Figure 2. Geology of the Central Cordillera of Colombia and the Cordillera Real and Amotape Complex of Ecuador, showing the distribution of Paleozoic, Permian – Triassic rocks. The Jurassic continental arc is also shown for reference. Concordant Permian and Triassic zircon U–Pb and plateau ^{40}Ar/^{39}Ar dates and their uncertainties (±2σ) obtained by various analytical methods (see Table 1) are shown (see references in Table 1). Cities: (I) Ibagué; (L) Loja; (M) Medellín; (P) Pasto; (Q) Quito. Faults: (BF) Baños Fault; (CAF) Cauca–Almaguer Fault; (SJF) San Jerónimo Fault; (IF) Ibagué Fault; (LF) Llanganates Fault; (OPF) Otú–Pericos Fault; (PF) Peltetec Fault. Map compiled from Litherland et al. (1994) and Gómez et al. (2007). Amphibolite occurrences: (CA) Cajamarca Amphibolites; (CS) Chinchina Stock; (MO) Monte Olivo; (SE) Santa Elena Amphibolites.

Table 1. Summary of data collected from Permian – Triassic rocks of Ecuador and Colombia.

Granitoids and migmatitic leucosomes — Ecuador — Cordillera Real

Sample	Unit	Lithology	Latitude d° m' s''	Longitude W d° m' s''	Zircon $^{206}Pb/^{238}U$ age (Ma) ± 2σ	MSWD	Apatite $^{206}Pb/^{238}U$ ages (Ma)	$^{40}Ar/^{39}Ar$ age (Ma) ± 2σ	εHf zircon ± 2σ	εNd w.r ± 2σ	$(^{87}Sr/^{86}Sr)i$ wr ± 2σ	$(^{206}Pb/^{204}Pb)i$ fs ± 2σ	$(^{207}Pb/^{204}Pb)i$ fs ± 2σ	$\delta^{18}O$ (‰) ± 2σ	Th/U zircon ± 2σ	A/CNK wr	(La/Yb)n wr	Publication
09RC25	Tr. Lagunas	metagranite	1° 23' 51'' S	78° 21' 15''	233.7 ± 0.8	1.1			10.5 to –3.2					15.3 ± 0.2	0.26 ± 0.1	1.99	13.24	Cochrane et al. (2014b)
09RC31	Tr. Lagunas	metagranite	0° 22' 33'' S	78° 08' 32''	234.4 ± 0.9	0.8			–11.0 to +3.2					15.1 ± 0.2	0.04 ± 0.1	1.40	16.16	Cochrane et al. (2014b)
09RC42	Sabanilla	metagranite	4° 27' 43'' S	79° 08' 52''	247.2 ± 4.3	3.0	138–82		–5.3 to –0.5			18.58 ± 0.190	15.64 ± 0.080	16.8 ± 0.2	0.69 ± 0.5	1.23	13.86	Cochrane et al. (2014b)
09RC53	Tr. Lagunas	metagranite	3° 09' 24'' S	78° 48' 45''	231.0 ± 1.9	2.1			–2.63 ± 0.43						0.24 ± 0.1	1.19	12.91	Cochrane et al. (2014b)
09RC44	Sabanilla	paragneiss	4° 29' 02'' S	79° 08' 55''												1.37	15.47	Cochrane et al. (2014b)
09RC45	Sabanilla	paragneiss	3° 58' 41'' S	79° 01' 15''														Cochrane et al. (2014b)
09RC56	Tr. Lagunas	metagranite	1° 23' 57'' S	78° 22' 08''	235.0 ± 1.5	3.0			–6.0 to +1.7					12.1 ± 0.2	0.14 ± 0.1	2.24		Cochrane et al. (2014b)
11RC03	Agoyan Fm.	metagranite	0° 23' 24'' N	77° 51' 44''	207.6 ± 9.2	1.9			–16.3 to –9.0					15.1 ± 0.2	0.01 ± 0.0			Cochrane et al. (2014b)
13AP07	Tr. Lagunas	metagranite	1° 23' 55'' S	78° 21' 39''	232.7 ± 2.8		227–68					18.62 ± 0.001	15.67 ± 0.001		0.35	1.68	13.26	Paul et al. (2018)
13AP20	Tr. Lagunas	metagranite	0° 22' 18'' S	78° 06' 50''	231.2 ± 0.6		210–207					18.75 ± 0.005	15.67 ± 0.005		0.21 ± 0.15	1.05	11.47	Paul et al. (2018)
13AP22	Tr. Lagunas	metagranite	0° 23' 30'' S	78° 03' 31''	238.6 ± 1.3		149–143					18.59 ± 0.006	15.65 ± 0.005		0.14 ± 0.08	1.25	20.91	Paul et al. (2018)
13AP23	Tr. Lagunas	metagranite	0° 22' 55'' S	78° 04' 07''	249.9 ± 1.8		195–171					18.87 ± 0.014	15.65 ± 0.012		0.68 ± 0.25	1.51	13.41	Paul et al. (2018)
13AP24	Tr. Lagunas	metagranite	0° 22' 54'' S	78° 07' 51	243.7 ± 0.7		208–158	164.8 ± 0.9m				18.85 ± 0.015	15.74 ± 0.016		0.74 ± 0.56	1.11	17.45	Paul et al. (2018)
13AP25	Tr. Lagunas	metagranite	0° 22' 44'' S	78° 08' 09''	245.0 ± 3.0		93–85					18.63 ± 0.005	15.63 ± 0.004		0.65 ± 0.17	1.09	8.03	Paul et al. (2018)
13AP35	Sabanilla	leucosome	4° 32' 36'' S	79° 07' 55''	236.0 ± 3.2							18.40 ± 0.101	15.53 ± 0.067		1.22 ± 1.38	1.26	12.9	Paul et al. (2018)
13AP36	Sabanilla	leucosome	4° 32' 36'' S	79° 07' 55''	234.4 ± 3.9		114–69	70.7 ± 0.4m				18.84 ± 0.001	15.67 ± 0.001		0.24 ± 0.19	1.09	4.4	Paul et al. (2018)
13AP37	Sabanilla	leucosome	4° 32' 36'' S	79° 07' 55''	234.4 ± 3.9		101–76	70.7 ± 0.4m				18.55 ± 0.001	15.67 ± 0.001		0.24 ± 0.19	1.12	4.06	Paul et al. (2018)
13AP38	Sabanilla	leucosome	4°35'08'' S	79° 07' 51''	282.7 ± 3.9		99–98					18.56 ± 0.001	15.61 ± 0.001		0.9	1.35	16.19	Paul et al. (2018)
13AP42	Sabanilla	leucosome	4° 34' 19'' S	79° 08' 16''	239.2 ± 0.9		76–75					18.63 ± 0.004	15.63 ± 0.004		0.61 ± 0.12	1.22	11.26	Paul et al. (2018)
13AP43	Sabanilla	leucosome	4° 34' 19'' S	79° 08' 16''	218.1 ± 3.1		106–42	75.3 ± 1.3m							0.04	1.64	6.12	Paul et al. (2018)
13AP46	Sabanilla	leucosome	4° 31' 26'' S	79° 07' 50''	236.5 ± 1.4		80–74								0.02 ± 0.01	1.37	12.9	Paul et al. (2018)
13AP47	Sabanilla	leucosome	4° 27' 43'' S	79° 08' 52''	218.9 ± 4.2		96–81					18.58 ± 0.004	15.64 ± 0.004		0.03 ± 0.03	1.71	11.84	Paul et al. (2018)
13AP51	Sabanilla	leucosome	4° 02' 34'' S	78° 59' 40''	218.3 ± 1.3		129–74					18.53 ± 0.001	15.64 ± 0.001		0.006 ± 0.003	1.33	3.64	Paul et al. (2018)
13AP52	Sabanilla	leucosome	4° 00' 41'' S	79° 01' 17''	230.7 ± 0.7		91–71	72.0 ± 0.6m				18.53 ± 0.001	15.64 ± 0.001		0.23 ± 0.04	1.08	32.12	Paul et al. (2018)
Tr. Lagunas	Tr. Lagunas	granite			227.3 ± 2.2													Litherland et al. (1994)

Amotape Complex

Sample	Unit	Lithology	Latitude d° m' s''	Longitude W d° m' s''	Zircon $^{206}Pb/^{238}U$ age (Ma) ± 2σ	MSWD	Apatite $^{206}Pb/^{238}U$ ages (Ma)	$^{40}Ar/^{39}Ar$ age (Ma) ± 2σ	εHf zircon ± 2σ	εNd w.r ± 2σ	$(^{87}Sr/^{86}Sr)i$ wr ± 2σ	$(^{206}Pb/^{204}Pb)i$ fs ± 2σ	$(^{207}Pb/^{204}Pb)i$ fs ± 2σ	$\delta^{18}O$ (‰) ± 2σ	Th/U zircon ± 2σ	A/CNK wr	(La/Yb)n wr	Publication
09RC40	Moromoro	migmatite	3° 42' 16'' S	79° 51' 07''	237.7 ± 5.2	4.6		214.6 ± 0.9m	–7.5 to +0.8						0.42 ± 0.5	2.38	11.36	Cochrane. (2013)
VI-08–12	La Bocana	migmatite			226.0 ± 1.3*													Riel et al. (2013)
PU-08–10	La Bocana	migmatite	3° 42' 58'' S	80° 03' 18''	223.2 ± 2.2*											1.85		Riel et al. (2013)
AV-08–31	La Bocana	migmatite			229.3 ± 2.4										0.13			Riel et al. (2013)
AV-08–28d	La Bocana	migmatite	3° 40' 41'' S	79° 54' 14''	225.7 ± 6.5										0.10	1.50		Riel et al. (2013)
13AP30	Moromoro	granite	3° 39' 53'' S	79° 45' 28''	227.1 ± 1.9			218.2 ± 0.9m										Paul et al. (2018)
Moromoro	Moromoro	granite			227.5 ± 0.8*													Aspden et al. (1995)

Permian   Triassic

Table 1. Summary of data collected from Permian – Triassic rocks of Ecuador and Colombia (*continued*).

Sample	Unit	Lithology	Latitude d° m' s''	Longitude W d° m' s''	Zircon ^{206}Pb/^{238}U age (Ma) ± 2σ	MSWD	Apatite^V ^{206}Pb/^{238}U ages (Ma)	^{40}Ar/^{39}Ar age (Ma) ± 2σ	εHf zircon ± 2σ	εNd wr ± 2σ	(^{87}Sr/^{86}Sr)i wr ± 2σ	(^{206}Pb/^{204}Pb)i fs ± 2σ	(^{207}Pb/^{204}Pb)i fs ± 2σ	δ^{18}O (‰) ± 2σ	Th/U zircon ± 2σ	A/CNK wr	(La/Yb)n wr	Publication
					Colombia													
					Central Cordillera													
10RC04	Rovira	metagranite	4° 19' 24" N	75° 12' 07"	277.5 ± 1.6	1.2			1.96 ± 0.31					13.6 ± 0.2	1.27 ± 0.6	1.18	16.23	Cochrane et al. (2014b)
10RC40	Cajamarca	metagranite	5° 53' 13" N	75° 25' 28"	236.1 ± 3.3	3.7		221.8 ± 1.0^m	−6.57 ± 0.66					17.4 ± 0.2	0.08 ± 0.1	1.73	8.19	Cochrane et al. (2014b)
10RC41	Cajamarca	metagranite	6° 01' 08" N	75° 07' 28"	234.1 ± 1.2	1.2			−9.5 to −0.2					13.1 ± 0.2	0.23 ± 0.1	1.27	11.49	Cochrane et al. (2014b)
10RC42	Cajamarca	metagranite	5° 59' 17" N	74° 55' 37"	244.6 ± 2.4	2.3			−8.2 to +1.4					13.1 ± 0.2	0.35 ± 0.1	1.33	12.00	Cochrane et al. (2014b)
10RC43	Cajamarca	metagranite	5° 58' 34" N	74° 54' 02"	245.0 ± 2.0	0.6	232–231	213.7 ± 0.9^m	−11.7 to −3.1						0.42 ± 0.4	1.36	15.70	Cochrane et al. (2014b)
10RC53	Cajamarca	metagranite	7° 00' 56" N	75° 22' 28"	236.4 ± 1.8	3.0			−5.9 to +3.1					15.9 ± 0.2	0.30 ± 0.2	1.56	14.27	Cochrane et al. (2014b)
10RC66	Cajamarca	qtz–schist	5° 08' 20" N	75° 09' 47"												1.84	12.63	Cochrane et al. (2014b)
10RC69	Rovira	metagranite	5° 09' 27" N	75° 07' 57"	255.7 ± 1.5	1.2			−3.16 ± 0.7					15.6 ± 0.2	1.10 ± 0.2	1.70	12.81	Cochrane et al. (2014b)
10RC71	Cajamarca	pegmatite	5° 07' 34" N	74° 54' 38"	236.0 ± 0.6	0.9			−6.0 to +0.4						0.31 ± 0.1			Cochrane et al. (2014b)
DV65	Cajamarca	metagranite	5° 59' 16" N	74° 55' 34"	240.9 ± 1.5	0.6			−5.9 to +0.7						0.26 ± 0.2			Cochrane et al. (2014b)
DV82	Rovira	metagranite	4° 17' 16" N	75° 13' 59"	275.8 ± 1.5	3.0			−3.7 to +0.3						0.66 ± 0.1			Cochrane et al. (2014b)
DV02	Cajamarca	paragneiss	4° 46' 42" N	74° 57' 54"	238–582													Villagómez et al. (2011)
DV18	Cajamarca	gneiss	4° 28' 19" N	75° 33' 18"	236.2 ± 6.3	0.6												Villagómez et al. (2011)
DV19	Cajamarca	quartzite	4° 28' 19" N	75° 33' 18"	231–1163													Villagómez et al. (2011)
14API4	Rovira	metagranite	6° 01' 08" N	75° 07' 28"	253.0 ± 2.9		200–198					18.66 ± 0.003	15.67 ± 0.003		0.52 ± 0.62			Paul et al. (2018)
Abejorral	Abejorral	gneiss			250 ± 10^f										0.82			Vinasco et al. (2006)
Palmitas	Palmitas	gneiss			240 ± 4^f										0.25			Vinasco et al. (2006)
Amaga	Amaga	granite			227.6 ± 4.5	1.4									0.30			Vinasco et al. (2006)
La Honda	La Honda	granite						218.7 ± 0.3^b										Vinasco et al. (2006)
El Buey	El Buey	granite						219.3 ± 0.3^m										Vinasco et al. (2006)
Manizales	Manizales	granite						229.7 ± 0.5^b										Vinasco et al. (2006)
GSI1	Santa Isabel	gneiss	6° 57' 34" N	74° 45' 13"	226.7 ± 1.6	1.2									0.19			Restrepo et al. (2011)
GN1	Nechi	gneiss	8° 10' 13" N	74° 46' 55"	236.4 ± 6.6	2.1									0.23			Restrepo et al. (2011)
PALM-1	Palmas	migmatite	6° 09' 14" N	75° 32' 36"	222 ± 10^f										0.24			Restrepo et al. (2011)
P21	Las Palmas	paragneiss			237 ± 2										0.005			Martens et al. (2014)
P22	Las Palmas	gneiss			244 ± 2													Martens et al. (2014)
GCC8	Tierradentro	orthogneiss			244.3 ± 4.8	2.8												Bustamante et al. (2017)
C112	Tierradentro	orthogneiss			271.3 ± 1.3	1.4			−0.1 to −2.5						0.47–1.04			Bustamante et al. (2017)
					Sierra Nevada de Santa Marta													
A14	S.M. mylonite	granite			288.1 ± 4.5	1.0									0.73			Cardona et al. (2010a)
A48	S.M. mylonite	granite			276.5 ± 5.1	1.8									0.57			Cardona et al. (2010a)
EAM-12-05	S.M. mylonite	granite			264.9 ± 4.0	0.0												Cardona et al. (2010a)
MPR-33A	El Encanto	orthogneiss	11° 04' 23" N	74° 04' 26"	274.8 ± 2.1	0.1									0.80	0.66	23.09	Piraquive (2017)
GLV–11	Gaira Schists	gnt–schist	11° 01' 18" N	74° 10' 15"	283.7 ± 6.1										0.84			Piraquive (2017)
MG–063	Gaira Schists	schist	11° 14' 50" N	73° 44' 33"	261.4 ± 2.6										0.75			Piraquive (2017)

Table 1. Summary of data collected from Permian – Triassic rocks of Ecuador and Colombia (*continued*).

Sample	Unit	Lithology	Latitude d° m' s"	Longitude W d° m' s"	Zircon ^{206}Pb/^{238}U age (Ma) ± 2σ	Apatite[v] ^{206}Pb/^{238}U ages (Ma)	MSWD	^{40}Ar/^{39}Ar age (Ma) ± 2σ	εHf zircon ± 2σ	εNd, wr ± 2σ	(^{87}Sr/^{86}Sr)i wr ± 2σ	(^{206}Pb/^{204}Pb)i fs ± 2σ	(^{207}Pb/^{204}Pb)i fs ± 2σ	δ^{18}O (‰)i ± 2σ	Th/U zircon ± 2σ	A/CNK wr	(La/Yb)n wr	Publication
Sierra Nevada de Santa Marta																		
CVI13108	La Secreta	meta–tuff	10°56'04" N	74°08'14"	224.6±2.6										0.17	1.12	9.62	Piraquive (2017)
LRW–21	La Secreta	gabbro	10°54'46" N	74°08'40"	237.4±1.1		3.5								0.21	1.08	10.80	Piraquive (2017)
Plato–San Jorge Basin																		
Cicuco–2a	unknown	granite	9°16'25" N	74°38'53"	241.6±3.9		3.9											Montes et al. (2010)
Cicuco–3	unknown	granite	9°17'39" N	74°38'52"	241.6±3.9		6.0											Montes et al. (2010)
Lobita 1	unknown	granite	9°18'30" N	74°41'31"	239.6±2.9		0.6											Montes et al. (2010)
Guajira Peninsula																		
AVO–03	Uray Gneiss	gneiss			247.6±4.1		0.5								0.20			Weber et al. (2010)
AVO–06	Uray Gneiss	gneiss			245.6±3.9		0.5								0.59			Weber et al. (2010)
Amphibolites																		
Ecuador																		
10RC28	Chinchina	amphibolite	5°03'05" N	75°34'25"	224.7±1.9		0.8		13.31±0.25	9.83	0.70354	17.52	15.40		0.20±0.1	0.66	1.41	Cochrane et al. (2014b)
11RC04	Monte Olivo	amphibolite	0°23'24" N	77°51'44"												0.61	2.59	Cochrane et al. (2014b)
11RC10	Monte Olivo	amphibolite	1°23'56" S	78°22'52"	231.9±3.2		1.6		-6.3 to +11.2	5.03	0.71470	18.71	15.68		0.19±0.1	0.63	1.71	Cochrane et al. (2014b)
11RC14	Piedras	amphibolite	3°39'9" S	79°50'35"	222.7±6.3		1.9		15.00±0.29	9.79	0.70271	17.75	15.48		0.32±0.2	0.61	0.81	Cochrane et al. (2014b)
JR148	Piedras	amphibolite			221±17.0											0.52		Noble et al. (1997)
Colombia																		
10RC39	Santa Elena	amphibolite	5°54'06" N	75°24'31"						8.98	0.70430	18.12	15.61			0.82	2.34	Cochrane et al. (2014b)
10RC39A	Santa Elena	amphibolite	5°53'52" N	75°24'37"	239.7±2.4		1.9		-4.8 to +10.0	4.13	0.70535	18.30	15.64			0.62	2.02	Cochrane et al. (2014b)
10RC50	Tr. Intrusive	amphibolite	6°09'26" N	75°44'31"						10.18	0.70243	16.61	15.53			0.50	0.49	Cochrane et al. (2014b)
AC32B	El Picacho	plagiogranite			216.6±0.4		0.7			3.4	0.70448					0.97	8.00	Correa–Martínez (2007)
CMK040A	El Picacho	metagabbro								8.4							0.61	0.64	Correa–Martínez (2007)
Padua	Padua	amphibolite						243 ± 4[b]										Vinasco et al. (2006)
CAT1A	Tierradentro	amphibolite			234.1±5.3		7.1		+9.2 to +10.9						0.12–0.25			Bustamante et al. (2017)

Abbreviations: (b) biotite; (h) hornblende; (m) muscovite; (fs) feldspar; (wr) whole–rock; A/CNK (Molecular Al_2O_3/CaO + Na_2O + K_2O); (La/Yb)n (normalized to N–MORB).

^{87}Sr/^{86}Sr 2s.d. (ext. reproducibility) = 0.00007%; ^{143}Nd/^{144}Nd = <0.0005 %; ^{206}Pb/^{204}Pb = 0.12 %.

The zircon ^{238}U/^{206}Pb ages are weighted mean ages of concordant analyses.

*Monazite date.

[#]Date obtained from the youngest zircon when a large spread of zircon ages were obtained due to xenocrystic contamination.

Dates acquired by LA–ICP–MS (Cochrane et al., 2014b; Cardona et al., 2010a; Martens et al., 2014; Montes et al., 2010; Paul et al., 2018; Piraquive, 2017; Villagómez et al., 2011; Weber et al., 2010).

Dates acquired by TIMS (Aspden et al., 1995; Litherland et al., 1994).

Dates acquired by SHRIMP (Restrepo et al., 2011; Vinasco et al., 2006).

[v]Dates are from a range of apatite grain sizes, and are shown as largest grain–smallest grain. Grain radii are typically 100 mm and 50 mm. 2σ uncertainties are <5 % (Paul, 2017).

[b]All ^{40}Ar/^{39}Ar dates are plateau dates.

Permian   Triassic
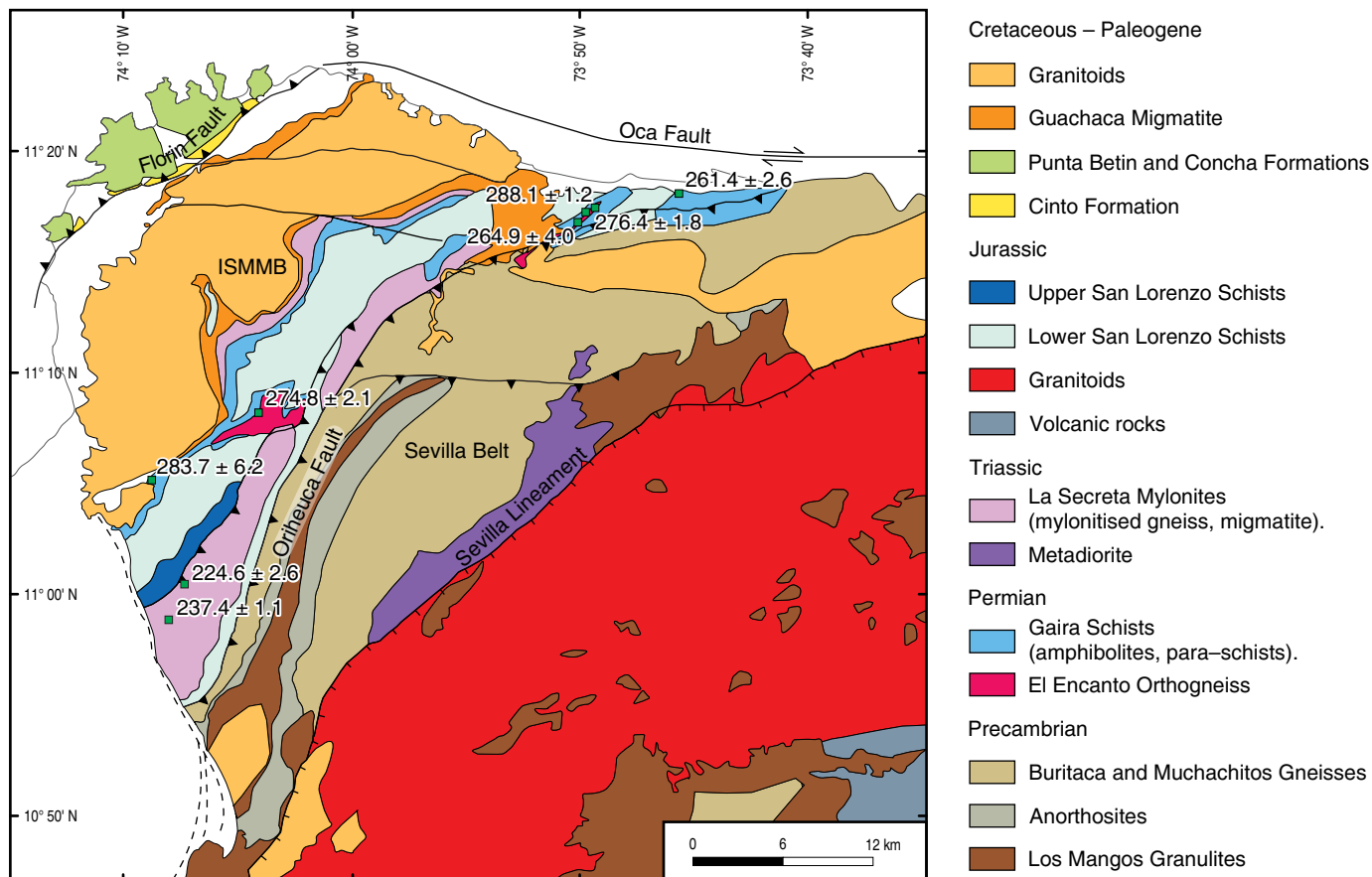
Figure 3. Geological map of the northwestern corner of the Sierra Nevada de Santa Marta after Tschanz et al. (1974), Colmenares et al. (2007a, 2007b), and Piraquive (2017), showing the main structural belts of the Sierra Nevada, Sevilla, and Santa Marta provinces. Concordant zircon U–Pb dates of Permian and Triassic rocks (Table 1) are shown (Cardona et al., 2010a; Piraquive, 2017). ISMMB: Inner Santa Marta Metamorphic Belt (after Piraquive, 2017).

east by the Llanganates Fault and to the west by the Baños Fault (Figure 2). Triassic igneous and metamorphic lithologies are dominated by cordierite and garnet bearing monzogranites and granodiorites (Tres Lagunas unit), and medium– to high–grade, sillimanite and kyanite bearing orthogneisses and migmatites (Sabanilla unit). Litherland et al. (1994), Noble et al. (1997), Riel et al. (2013), Cochrane et al. (2014b), Spikings et al. (2015), and Paul et al. (2018) present a large quantity of geochronological and geochemical data from the igneous and metamorphic rocks in Ecuador (Table 1). The Piuntza unit consists of metamorphosed and skarnified siliciclastic rocks, tuffs, and limestones that host Triassic bivalves (Litherland et al., 1994). The unit is exposed beyond the structural limits of the Loja Terrane of Litherland et al. (1994) along the eastern flank of the southern Cordillera Real (Figure 2), where it is surrounded by the Jurassic Zamora Batholith although the nature of the contact is either unknown or unreported.

4. Geochronology of Permian and Triassic Magmatic Rocks

Early attempts to date the Permian – Triassic crystalline rocks utilised the K/Ar and Rb/Sr methods (e.g., Feininger et al., 1972; Hall et al., 1972; Litherland et al., 1994; McCourt et al., 1984; Ordóñez–Carmona & Pimentel, 2002; Restrepo et al., 1991), resulting in a large scatter of ages spanning between the Permian – Tertiary due to variable degrees of daughter isotope loss. This review of geochronological work is restricted to more accurate measurements of the crystallisation ages of granitoids and mafic intrusions, which have been provided by numerous concordant zircon and few monazite U–Pb dates (Table 1), obtained using TIMS, SHRIMP, and LA–ICP–MS. Unless otherwise stated, the LA–ICP–MS and SHRIMP dates that are reported here were obtained from the rims of zircons, and are considered to date either the most recent phase of magmatic crystallisation or the

most recent metamorphic event that crystallised zircon. Most of these dates have been peer reviewed, with the exception of several data points from PhD theses (e.g., Piraquive, 2017).

4.1. Permian

Permian magmatic rocks in the cordilleras of the northern Andes are sparse compared to the exposure of Triassic rocks. Six granitoids in the central and northern Central Cordillera yield dates spanning between 278 and 253 Ma (Figures 2, 4; Table 1; Bustamante et al., 2017; Cochrane et al., 2014b; Paul et al., 2018; Vinasco et al., 2006). These Permian intrusions are tentatively assigned the name *Rovira Complex*, referring to the locality (close to the town of Ibagué) where Cochrane et al. (2014b) sampled and dated two Permian granites (Table 1). El Encanto Orthogneiss forms the crystalline basement of the Inner Santa Marta Metamorphic Belt of the Sierra Nevada de Santa Marta, and yields a zircon U–Pb age of 274.8 ± 2.1 Ma (Figure 3), which is considered to be the time of initial magmatic crystallisation (Piraquive, 2017). These are overlain by paraschists of the 2000 m thick Gaira Amphibolite sequence, which yields a large range of concordant zircon U–Pb dates (2235–261 Ma), reflecting their sedimentary protoliths. Two schists yield youngest concordant age clusters with U–Pb ages of 283.7 ± 6.2 Ma and 261.5 ± 2.6 Ma (Piraquive, 2017) from laser spots within zircons, constraining their maximum stratigraphic ages. Cardona et al. (2010a) obtained zircon U–Pb concordia ages ranging between 288–265 Ma from mylonitised gneisses within the northern Inner Santa Marta Metamorphic Belt (Figure 3). A migmatite exposed in the southern Cordillera Real is the only Permian magmatic rock identified in Ecuador, and yields a zircon U–Pb age of 282.7 ± 3.9 Ma (Figure 2; Table 1; Paul et al., 2018). The Permian leucosome (rock 13AP38) was previously mapped as part of the Sabanilla Migmatite unit (Litherland et al., 1994). The Sabanilla Migmatite is defined on geochemical and geochronological grounds as Triassic (Spikings et al., 2015), and thus we tentatively assign the Permian leucosome to the newly named *Malacatos Complex*, referring to the nearest town to the sampled location.

4.2. Triassic

Triassic felsic magmatic rocks are abundant in Colombia and Ecuador, and this review includes new data obtained from Paul et al. (2018), and the recent PhD study of Piraquive (2017). Twenty five gneissic granites and pegmatites exposed in the Central Cordillera, the basement of the Plato–San Jorge Basin, the Sierra Nevada de Santa Marta, and the Guajira Peninsula yield zircon U–Pb concordia ages ranging between 247.6 ± 4.1 Ma and 222 ± 10 Ma (Figures 2, 4; Table 1; Bustamante et al., 2017; Cardona et al., 2010a; Cochrane et al., 2014b; Martens et al., 2014; Montes et al., 2010; Piraquive, 2017; Villagómez et al., 2011; Vinasco et al., 2006; Restrepo et al., 2011; Weber et al.,

2010). La Secreta Mylonites form part of the Inner Santa Marta Metamorphic Belt within the Sierra Nevada de Santa Marta, and overthrust the Permian El Encanto Orthogneiss and Gaira Schists (Figure 3; Piraquive, 2017). A peraluminous gabbro from the mylonitic sequence yields a zircon U–Pb date of 237.4 ± 1.1 Ma (Piraquive, 2017), while a mylonite hosts detrital zircons that yield concordant U–Pb dates from cores and rims spanning between 1300–224 Ma, and yields a concordant youngest age cluster of 224.6 ± 2.6 Ma, overlapping with dates from Triassic intrusions (Piraquive, 2017). These dates from Colombian rocks overlap with concordant zircon and monazite U–Pb ages from twenty nine granites and leucosomes of the Tres Lagunas Granite and Sabanilla Migmatite (Cordillera Real), and the Moromoro Granite (Amotape Complex), which range between 249.9 ± 1.8 Ma and 207.6 ± 9.2 Ma (Figure 4; Table 1; Aspden et al., 1995; Chew et al., 2008; Cochrane et al., 2014b; Litherland et al., 1994; Paul et al., 2018; Riel et al., 2013; Spikings et al., 2015).

Multi–phase, plateau $^{40}Ar/^{39}Ar$ dates (Table 1) from Triassic granites and migmatites in Colombia and Ecuador (Cochrane et al., 2014b; Paul et al., 2018; Spikings et al., 2001; Vinasco et al., 2006) are younger than the U–Pb dates obtained from the same rocks, reflecting various degrees of Ar loss. Triassic dates span between 243 ± 4 Ma and 213.7 ± 0.9 Ma and are restricted to the northern Central Cordillera (Table 1). However, Triassic magmatic rocks from the Cordillera Real yield younger plateau muscovite $^{40}Ar/^{39}Ar$ dates that span between 164.8 ± 0.9 Ma and 70.7 ± 0.4 Ma (Table 1; Paul et al., 2018). These reflect the time of cooling of each rock through ~450–400 ºC (Harrison et al., 2009) subsequent to crystallisation and metamorphic retrogression, and the difference in dates between northern (Colombia) and southern (Ecuador) latitudes reveals trench–parallel differences in their thermal histories (see section 7).

A majority of U–Pb dates of zircons extracted from granites and migmatites in Colombia and Ecuador range between 240–230 Ma (Figure 4a), and a comparison with latitude (Figure 4d) does not reveal any trench–parallel trends in Triassic crystallisation. Permian ages are mainly found in Colombia, and are restricted to exposures in the Inner Santa Marta Metamorphic Belt of the Sierra Nevada de Santa Marta, and faulted blocks in the region of the Ibagué Fault (Figures 2, 3). This may reflect exposure, the approximate primary distribution of Permian magmatic intrusions, or the extent of reworking during Triassic anatexis.

Concordant zircon U–Pb dates of amphibolites and a plagiogranite from the Cordilleras Central (Colombia) and Real (Ecuador) range between 243 ± 4 Ma and 216.6 ± 0.4 Ma (Figure 2; Bustamante et al., 2017; Cochrane et al., 2014b; Correa–Martínez, 2007; Noble et al., 1997; Spikings et al., 2015; Vinasco et al., 2006). Within Ecuador, these are exposed as dykes and sills (e.g., the Piedras and Monte Olivo units; see Figure 2), whereas they are more massive in the northern Central Cordillera. The youngest of these ages was obtained from a
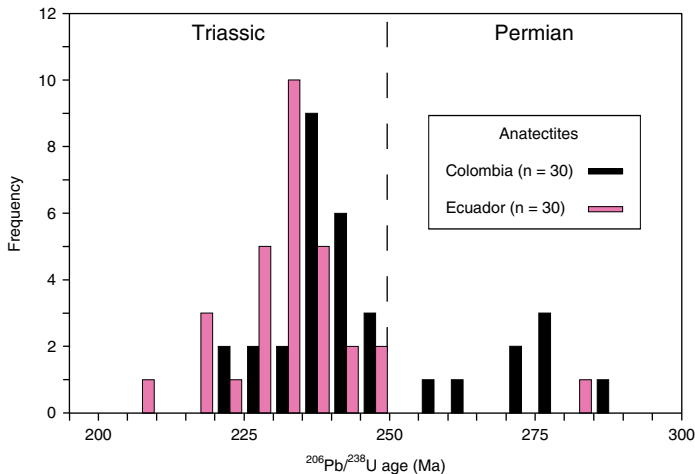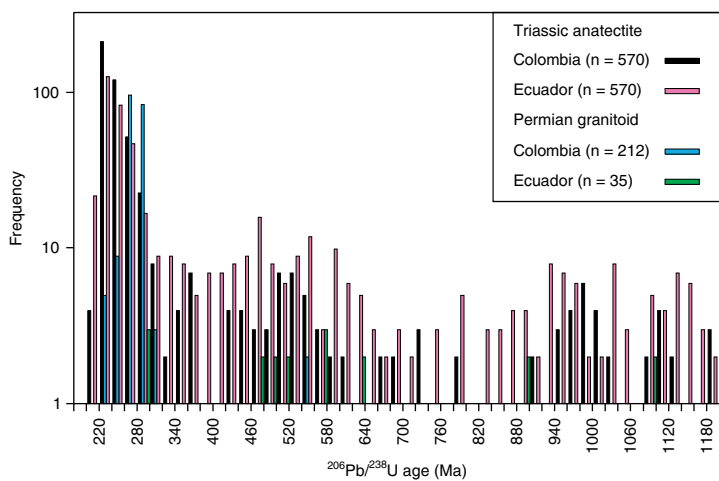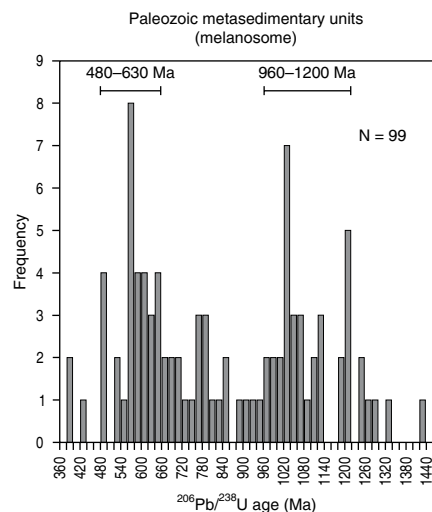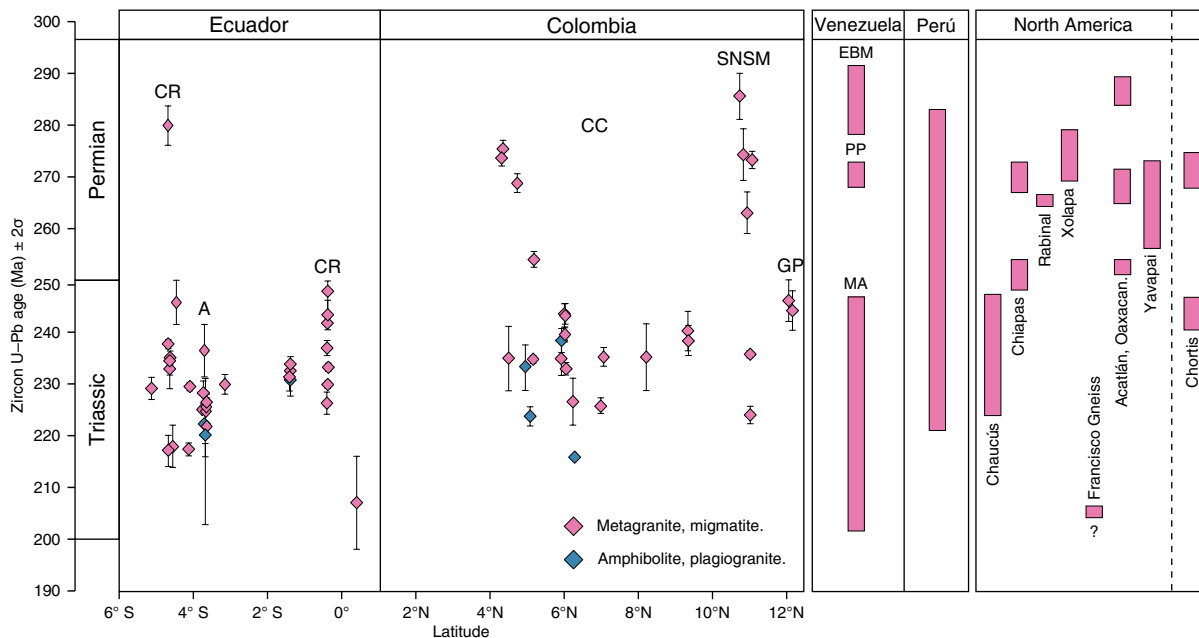
Triassic

Permian

plagiogranite that formed by magmatic fractionation within the Aburrá Ophiolite in northern Colombia, and thus is a minimum age for the ophiolite (Correa–Martínez, 2007).

4.3. Zircons Inherited by Permian and Triassic Magmas

Many concordant zircon U/Pb dates determined by in–situ methods were obtained from the cores of zircon grains that were identified using cathodoluminescence. A frequency analysis of the distribution of these older concordant laser–spot dates from the granitoids and migmatitic leucosomes in Colombia and Ecuador yields broad $^{206}Pb/^{238}U$ age peaks at 580–420 Ma and 1200–950 Ma (Figure 4b), which are the ages of protolith rocks and inherited grains. These age peaks are typical of the distribution of dates obtained from detrital zircons from most Paleozoic rocks distributed along western South America (e.g., Chew et al., 2007). The younger age group broadly corresponds with the age of the Famatinian arc, the Brasiliano Orogeny, and the timing of rifting during the fragmentation of Rodinia and the opening of the Iapetus Ocean. The Famatinian arc (ca. 510–415 Ma; see zircon U–Pb ages presented in Bahlburg et al., 2009; Cardona et al., 2007; Chew et al., 2007; Mišković et al., 2009; Pankhurst et al., 2000; Spikings et al., 2016; Villagómez et al., 2011; van der Lelij et al., 2016) formed during the subduction of Iapetus lithosphere beneath western South America subsequent to the fragmentation of Rodinia, and has been recorded in Venezuela, Colombia, Perú, and Argentina (see previous citations). Inherited zircons with U–Pb dates spanning 650–450 Ma also occur in Cretaceous and Tertiary sedimentary rocks of the Oriente (Amazon retro–foreland; see Figure 1) Basin in Ecuador (Martin–Gombojav & Winkler, 2008). Similarly, Horton et al. (2010) present a large database of U–Pb dates obtained from detrital zircons in the Eastern Cordillera and the western margin of the Llanos Basin in Colombia, which reveal a peak at 520–420 Ma. No Ordovician intrusions of the Famatinian arc have been recorded in Ecuador. However, within Colombia they are recorded within the northern Central Cordillera (470–440 Ma;

La Miel Orthogneiss; Martens et al., 2014; Villagómez et al., 2011), Quetame and Floresta Massifs (Horton et al., 2010), and a majority of the exposed crystalline basement of the Santander Massif (Figure 1; van der Lelij et al., 2016) yields Ordovician dates ranging between 500 and 415 Ma.

Triassic field relationships are clearly exposed in Ecuador (e.g., Litherland et al., 1994), and indicate that the protoliths of the Triassic migmatites and S–type granites within Ecuador were sedimentary rocks of the Paleozoic, fossil bearing Chiguinda and Isimanchi units that are exposed in the Cordillera Real (Figure 2). These sparsely studied sequences yield a detrital zircon U–Pb age spectrum that has the same age peaks as the Triassic anatectites (Figure 4c; Chew et al., 2008), although the tectonic setting within which these potentially Devonian (minimum zircon U–Pb date of 360 ± 2 Ma; Chew et al., 2007) sequences were deposited is undetermined.

The Brasiliano metamorphic belts (Cordani et al., 2003) formed during the late Neoproterozoic amalgamation of Gondwana, and may have supplied some detritus to western South America. However, these belts are located in eastern South America, and a lack of evidence for detritus being sourced from the intervening Amazonia Craton suggests the Brasiliano Orogenic belts were not a major source region (Chew et al., 2008). Finally, most magmatism associated with Neoproterozoic extension is mafic (e.g., the Puncoviscana fold belt in northwestern Argentina; Omarini et al., 1999), which led Chew et al. (2008) to suggest that it is unlikely that these rocks were a major contributor of zircons to Paleozoic sequences along western South America. However, Neoproterozoic rift related dacites occur along the margin of the central Andes (Ramos, 2009), and may have supplied sedimentary detritus towards the west.

4.4. Comparison with the Ages of Permian and Triassic Rocks in Venezuela, Perú, Northern Chile, and Argentina

Rhyolites and granites of El Baúl Massif in Venezuela yield zircon U–Pb dates that span between 291.1 ± 3.1 Ma and 283.3

Figure 4. (a) Histogram of zircon $^{206}Pb/^{238}U$ concordia (crystallisation) ages for Permian and Triassic magmatism and metamorphic zircon growth for variably foliated granites and migmatites (leucosomes) in Ecuador and Colombia (see Table 1 for references). **(b)** $^{206}Pb/^{238}U$ (concordant) age histogram for Permian and Triassic granites and migmatites (leucosomes) from Colombia and Ecuador. Ages are single spot zircon ages determined using LA–ICP–MS and SIMS. **(c)** $^{206}Pb/^{238}U$ age histogram for detrital zircons from the Paleozoic Chiguinda and Isimanchi metasedimentary units of the Cordillera Real of Ecuador (Chew et al., 2008). **(d)** A comparison of Permian and Triassic concordant zircon and monazite U–Pb dates with latitude along the Central Cordillera, Guajira Peninsula, and the Sierra Nevada de Santa Marta of Colombia, and the Cordillera Real and Amotape Complex of Ecuador. The ranges of concordant zircon U–Pb dates obtained from granitoid intrusions and volcano–sedimentary rocks from Venezuela (van der Lelij et al., 2016), the Eastern Cordillera of Perú (Mišković et al., 2009; Spikings et al., 2016), and various regions of the southern North American and western Caribbean Plate (Ducea et al., 2004; Elías–Herrera & Ortega–Gutiérrez, 2002; Helbig et al., 2012; Keppie et al., 2004, 2006; Kirsch et al., 2012; Ortega–Obregón et al., 2014; Ratschbacher et al., 2009; Solari et al., 2001, 2011; Weber et al., 2005, 2007; Yañez et al., 1991) are shown for comparison. Data and citations are presented in Table 1. Abbreviations: (A) Amotape Complex; (CC) Central Cordillera; (CR) Cordillera Real; (EBM) El Baúl Massif; (GP) Guajira Peninsula; (MA) Mérida Andes; (PP) Paraguaná Peninsula; (SNSM) Sierra Nevada de Santa Marta.

± 2.5 Ma (Viscarret et al., 2009), and a zircon U–Pb age of 272.2 ± 2.6 Ma was obtained from a granitic intrusion in the Paraguaná Peninsula (van der Lelij et al., 2016). van der Lelij et al. (2016) report concordant zircon U–Pb dates (LA–ICP–MS) from four granitoid intrusions and a dacitic lava from the Mérida Andes of Venezuela (Figure 1). These dates range between 202.0 ± 1.8 Ma (La Quinta Formation) and 243.5 ± 3.4 Ma, and overlap with dates obtained from Colombia and Ecuador (Figure 4d). No Permian concordant zircon U–Pb dates have been reported from the Mérida Andes.

Voluminous, partly migmatised middle Permian – Triassic magmatic intrusions are exposed throughout the southern and central Eastern Cordillera of Perú (Mišković et al., 2009; Spikings et al., 2016). Zircon U–Pb dates range between 293–223 Ma (Figures 4d, 5; Mišković et al., 2009; Reitsma, 2012; Spikings et al., 2016), with a peak at 245–225 Ma. The crystallisation ages show a southward younging trend, and the oldest plutons south of 13° S are younger than ca. 245 Ma (Spikings et al., 2016). The Mitu Group of the central and southern Eastern Cordillera of Perú hosts abundant Triassic sedimentary and volcanic sequences. Volcanic tuffs and lavas of the Mitu Group yield concordant zircon U–Pb (LA–ICP–MS) dates ranging between 238.7 ± 1.8 Ma and 219.7 ± 1.8 Ma (Chew et al., 2008; Mišković et al., 2009; Spikings et al., 2016). Detrital zircons extracted from oxidised terrigenous sedimentary rocks of the Mitu Group yield minimum dates ranging between 255.4 ± 3.2 Ma and 223.5 ± 7.5 Ma, which constrain their maximum stratigraphic ages (Spikings et al., 2016). Several authors propose that the Mitu Group was deposited within a rift (Laubacher, 1978; Mégard, 1978; Reitsma, 2012; Spikings et al., 2016), which was active during 245–220 Ma (Spikings et al., 2016). This time period precisely overlaps with the majority of Triassic intrusions in Colombia and Ecuador (Figure 5a). Romero et al. (2013) recently published a concordant zircon U–Pb age of 243 ± 0.1 Ma from a basalt exposed in Macabí Island offshore northern Perú (~8° S), although these zircons are probably xenocrystic.

Further south, a series of Middle – Late Triassic rift systems and sinistral pull–apart basins with a NNW–SSE trend in northern and central Chile and Argentina propagated along the hanging wall of previous sutures that separate Paleozoic terranes (e.g., Ramos, 1994; Ramos & Kay, 1991). U–Pb dates of tuffs from the Cuyo Basin span between 246–230 Ma (Potrerillos Formation; Barredo et al., 2012; Spalletti et al., 2008), and a tuff from the rift–related Ischigualasto Formation (Ischigualasto–Villa Unión Basin) yields a sanidine $^{40}Ar/^{39}Ar$ date of 231.4 ± 0.3 Ma (Martínez et al., 2011; recalibration of the 227.8 ± 0.3 Ma age of Rogers et al., 1993). Similarly, ignimbrites within the Los Menucos depocenter yield zircon U–Pb ages of 257–248 Ma (Luppo et al., 2018). Maksaev et al. (2014) compile and present new zircon U–Pb dates from volcanic rocks in northern Chile, which reveals a peak in activity between 240–210 Ma,

temporally overlapping with the peak in magmatic activity in Colombia, Ecuador, and Perú.

4.5. Comparison with the Ages of Permian and Triassic Magmatic Rocks in the Southernmost North American and Western Caribbean Plates

Permian – Triassic intrusive rocks occur along most of the length of México and Central America (e.g., Ortega–Obregón et al., 2014; Weber et al., 2007), and Centeno–García & Keppie (1999), Torres et al. (1999), and Dickinson & Lawton (2001) suggested they are a continuation of exposures in northwestern South America. A plethora of K–Ar dates range between 287–232 Ma (see the review of Torres et al., 1999, and references therein) although interpreting these are crystallisation ages is problematic due to the propensity for Ar loss. Yañez et al. (1991), Solari et al. (2001), Elías–Herrera & Ortega–Gutiérrez (2002), and Ducea et al. (2004) present concordant zircon U–Pb dates from acidic intrusions in southern México (Oaxacan, Xolapa, and Acatlán Complexes; Figures 4d, 5b) ranging between 287–272 Ma. Keppie et al. (2004), Kirsch et al. (2012), and Ortega–Obregón et al. (2014) report Permian concordant zircon U–Pb dates (ID–TIMS) of 298–255 Ma from acidic plutons and dykes within the Acatlán and Oaxacan Complexes, all of which are interpreted as crystallisation ages. Ratschbacher et al. (2009) obtained a concordant U–Pb date of 268.0 ± 0.6 Ma from rounded zircon cores extracted from a migmatitic gneiss of the Rabinal Complex (Maya Block, southern Guatemala). Orthogneisses within the Chiapas Massif of the Maya Block, yield zircon U–Pb discordia intercepts at ca. 251 Ma (Weber et al., 2005), while in–situ dates reveal a Permian U–Pb date of 272 ± 3 Ma from magmatic zones, with metamorphic zircon overgrowths at 254 ± 2 Ma (Weber et al., 2007), which precisely overlaps with anatexis of sedimentary rocks in the same region at 254 ± 2 Ma (Weber et al., 2007). Arvizu et al. (2009) present zircon U–Pb ages (LA–MC–ICP–MS) from monzogranites, granites, and granodiorites ranging between 275–258 Ma from northern México, which intrude crust of the Yavapai Province. Summarising, Permian magmatism intruded large regions of the far southern Northern American Plate, and is also preserved in the Chortis Block (Caribbean Plate). Most zircons formed within magmatic intrusions, although zircon growth and recrystallisation during the latest Permian was associated with metamorphic processes.

Triassic magmatism is scarce in southern North America, and reliable, concordant Triassic zircon U–Pb dates of igneous rocks are mainly exposed in the Chaucús Metamorphic Complex (Guatemala; Maya Block), where they range between 249–226 Ma (Figures 4d, 5b; Solari et al., 2011) and are interpreted as the crystallisation ages of intrusions with a peak at ca. 226 Ma. Ratschbacher et al. (2009) report a single Triassic rim (215.9 ± 0.2 Ma) surrounding a Permian zircon core in the Rabinal Complex (Maya Block). Helbig et al. (2012) obtained a
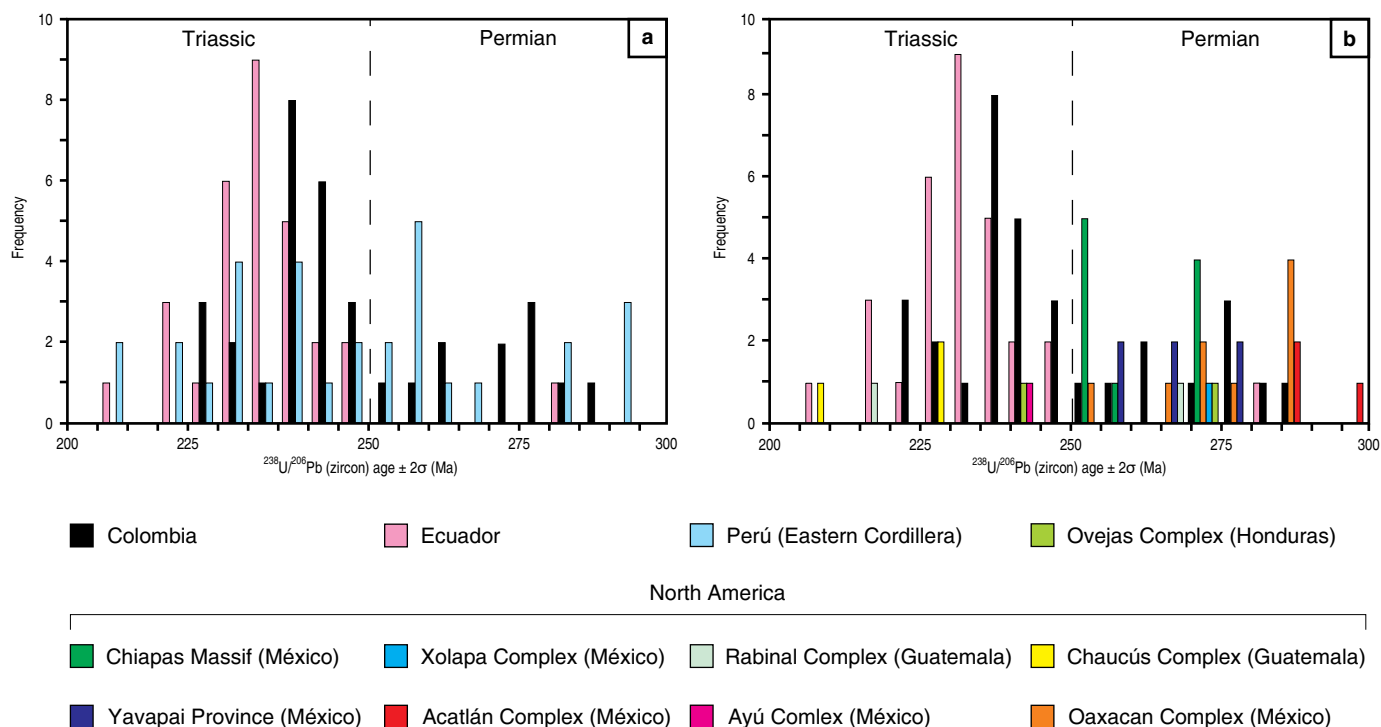
Figure 5. Weighted mean zircon ²⁰⁶Pb/²³⁸U (concordant) age histogram for Permian and Triassic magmatism and metamorphic zircon growth for variably foliated granites and migmatites (leucosomes) in **(a)** the Eastern Cordillera of Perú (Mišković et al., 2009; Spikings et al., 2016), and **(b)** various regions of the southern North American and western Caribbean Plate (references in caption for Figure 4). Concordant ²⁰⁶Pb/²³⁸U zircon dates are also shown for Colombia and Ecuador.

concordant zircon U–Pb age of 244 ± 4 Ma from a granitic dyke within the Ayú Complex, and inherited zircons that yield dates between 242–209 Ma. A migmatite from the Ayú Complex yields inherited zircons with U–Pb dates of 239–225 Ma (Helbig et al., 2012). These overlap with Triassic ages for migmatites and plutons in northwestern South America (Figures 4, 5b). Keppie et al. (2006) present discordant zircon U–Pb dates from migmatitic gneisses of the Francisco Gneiss (Guerrero composite terrane) that span between 216 and 197 Ma. These are not reliable estimates of the timing of crystallisation, although Keppie et al. (2006) suggest they record crystallisation at ca. 206 Ma. If accurate, these would be younger than the timing of anatexis in northwestern South America.

The Chortis Block currently forms part of the western Caribbean Plate, and several Permian and Triassic zircon U–Pb dates have been obtained from intrusions that must be accounted for when reconstructing western Pangaea. Ratschbacher et al. (2009) report U–Pb dates of 272.8 ± 2.8 Ma and 244.8 ± 2.3 Ma from zircon cores in Eocene granitic gneisses of Las Ovejas Complex (northwestern Honduras; Figures 4d, 5b). The Permian cores yield magmatic Th/U ratios (~0.7), while the Triassic group yields Th/U ratios of ~0.04, which is typical of metamorphic, sub–solidus growth.

5. Geochemistry

5.1. Granites and Migmatites: Central Cordillera of Colombia and the Cordillera Real of Ecuador

Major oxide, trace element, and rare earth element (REE) abundances and oxygen isotope compositions (Table 1) have been obtained from Permian and Triassic granites and migmatitic leucosomes from Colombia (Cardona et al., 2010a; Correa–Martínez, 2007; Piraquive, 2017; Spikings et al., 2015; Vinasco et al., 2006) and Ecuador (Cochrane et al., 2014b; Litherland et al., 1994; Paul et al., 2018; Spikings et al., 2015). Both Permian and Triassic granodiorites, monzogranites, and syenogranites (Figure 6a) span the boundaries of calcic to alkali–calcic differentiation trends on the modified alkali–lime index of Peacock (1931) (Figure 6b), with a compositional range of 77–59 (Permian) and 78–65 wt % SiO$_2$ (Triassic). The Triassic acidic rocks plot within the high–K calc–alkaline and calc–alkaline fields when comparing SiO$_2$ with K$_2$O (Figure 7a).

The Triassic anatectites have strongly peraluminous aluminium saturation indices (ASI 1.05–2.38; calculated using Maniar

15
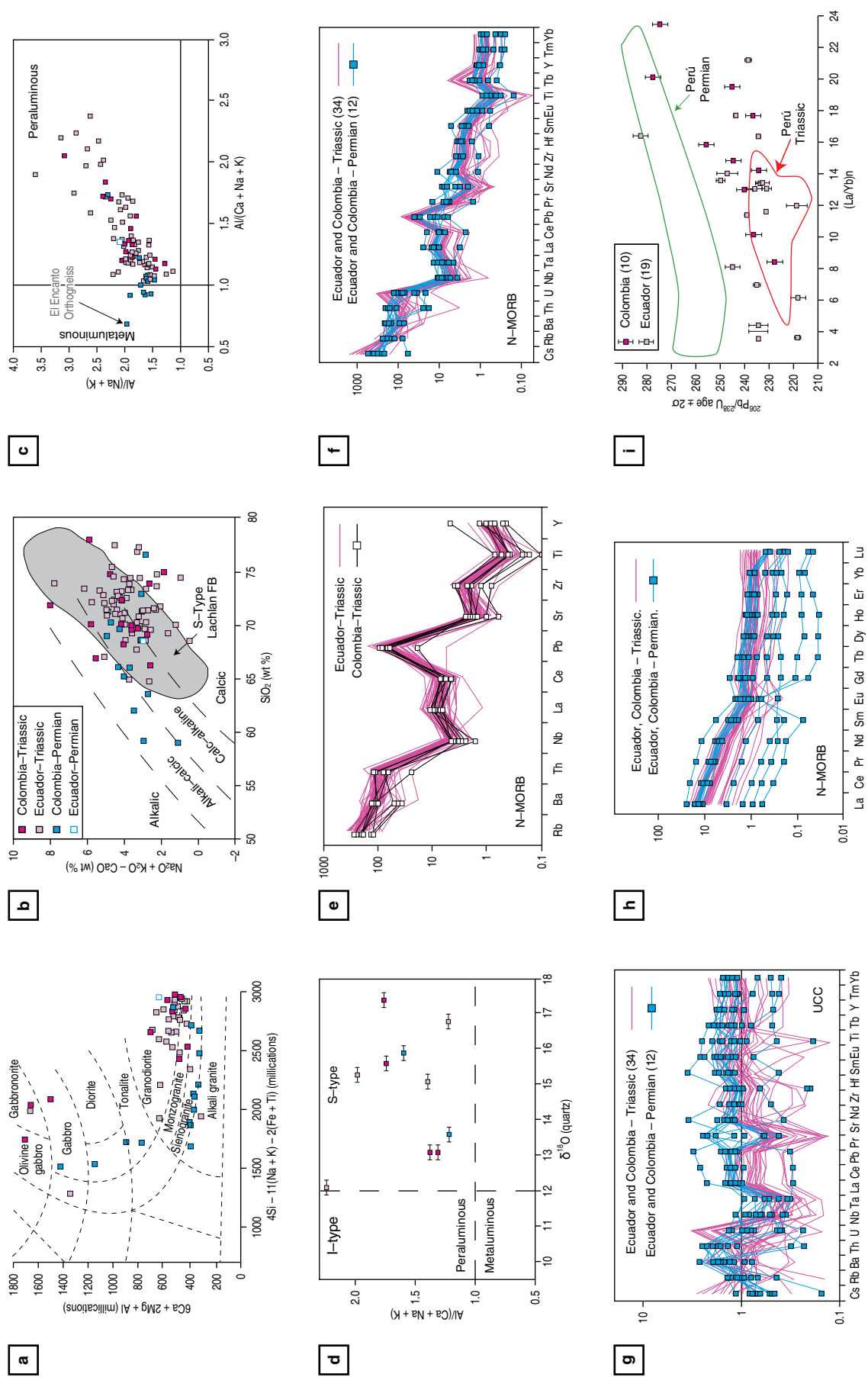
Figure 6. Geochemical data from Permian and Triassic granites and migmatitic leucosomes from the Central Cordillera (Cajamarca and Rovira Complexes) and Inner Santa Marta Metamorphic Belt (El Encanto Orthogneiss and La Secreta Orthogneiss and La Cordillera Real (Sabanilla and Tres Lagunas units) and Amotape Complex (Moromoro unit) of Ecuador. Lithological discriminatory fields shown in **(a)** are from Batchelor & Bowden (1985), while the fields in **(b)**, **(c)**, and **(d)** are from Peacock (1931), Maniar & Piccoli (1989), and Harris et al. (1997), respectively. Fields for Peruvian rocks in **(i)** are from Mišković et al. (2009) and Spikings et al. (2016). Multi-element plots are normalised to N–MORB (Sun & McDonough, 1989) and upper continental crust (UCC) (Taylor & McLennan, 1995). Data from Colombia: Vinasco et al. (2006), Correa–Martínez (2007), Cardona et al. (2010a), Cochrane et al. (2014b), Piraquive (2017). Data from Ecuador: Litherland et al. (1994), Cochrane et al. (2014b), Paul et al. (2018).
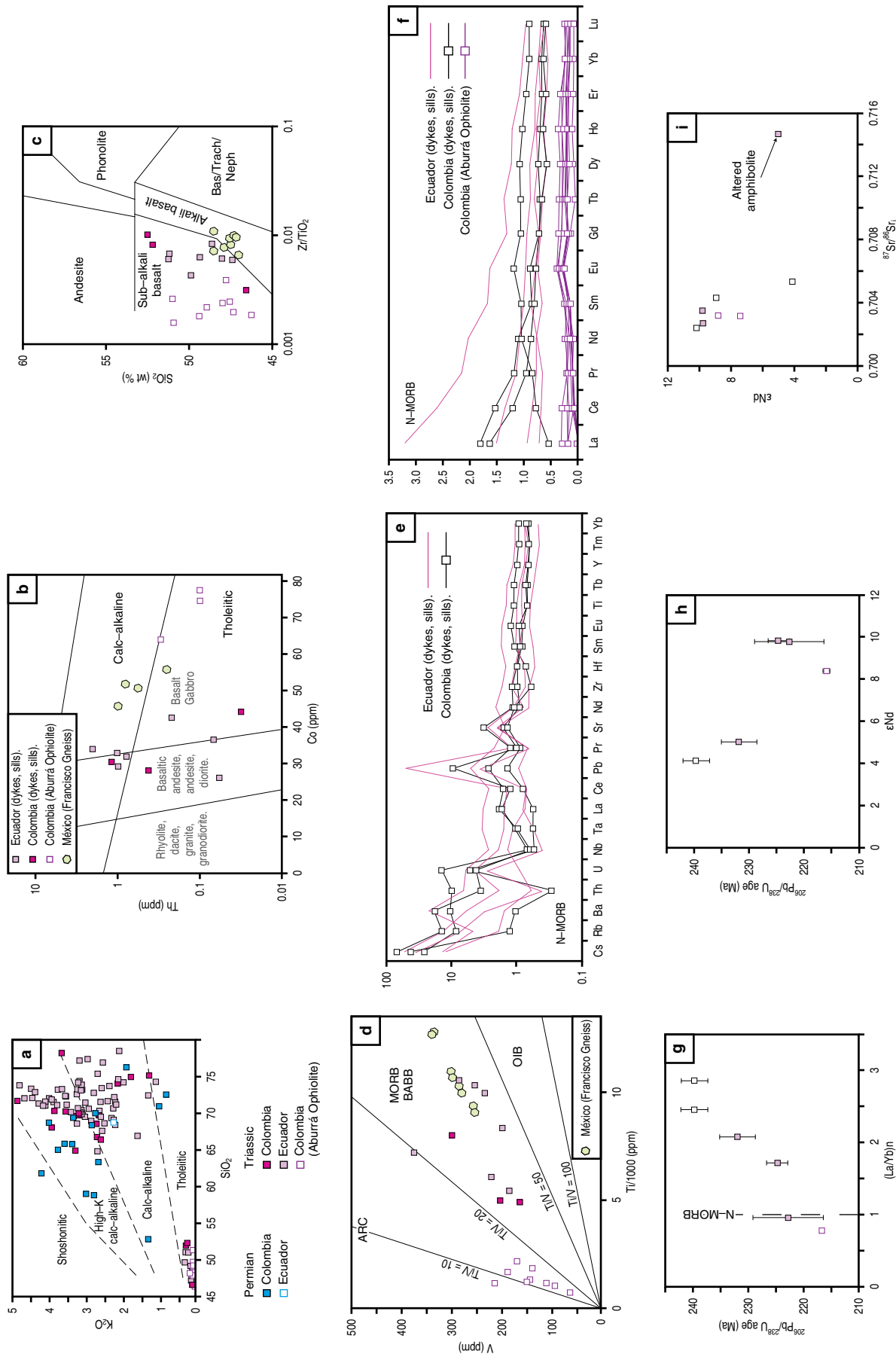
Figure 7. Geochemical data from Triassic amphibolitic dykes and metagabbros of the Central Cordillera (Chinchina and Santa Elena Amphibolites, and the Aburrá Ophiolite), and Cordillera Real (Monte Olivo unit) and Amotape Complex (Piedras unit). Multi-element plots are normalised to N–MORB (Sun & McDonough, 1989). Data is also shown for the Triassic? Francisco Gneiss (México; Keppie et al., 2006). Data from Colombia: Correa-Martínez (2007), Cochrane et al. (2014b). Data from Ecuador: Litherland et al. (1994), Cochrane et al. (2014b). Discriminatory fields in **(a)** are from Peccerillo & Taylor (1976), **(b)** are from Hastie et al. (2007), **(c)** are from Winchester & Floyd (1977), and **(d)** are from Shervais (1982).

17

& Piccoli, 1989; Figure 6c), while the Permian granitoids tend to cluster at slightly lower peraluminous and mildly metaluminous values (ASI 0.92–1.73, with a majority <1.1). The Triassic anatectites yield elevated $\delta^{18}O$ quartz (Figure 6d), which along with their high ASI places these granites and leucosomes within the "S–type granite" field of Chappell & White (1974) and Harris et al. (1997). Normal mid–ocean ridge basalts (N–MORB) normalized trace element abundances of Triassic granitoids from Ecuador and Colombia are identical (Figure 6e), suggesting there are no significant along–strike changes in the fractionation and assimilation history of these high–SiO_2 melts. Trace elements in both the Permian and Triassic granitoids are enriched in light–ion lithophile elements (LILE), and negative Nb, Ta, and Ti anomalies are present (Figure 6f), suggesting that a subduction–derived component was incorporated into these rocks and it is likely that they formed within a continental arc. The Triassic granitoids yield slight negative N–MORB normalized Ba, Eu, Sr, and Ti anomalies, which suggests that plagioclase and Fe–Ti oxides have fractionated, and a positive Pb anomaly that may be derived from a protolith within the continental crust. In contrast, most of the Permian granites do not yield Ba, Eu, and Sr anomalies, although they do have negative Ti anomalies, and positive Pb anomalies are less pronounced, suggesting they evolved via a different fractionation scheme.

Trace element concentrations of Triassic rocks normalized to the composition of average upper continental crust (Taylor & McLennan, 1995) plot close to unity, corroborating the S–type character of these rocks (Figure 6g), whereas a majority of Permian rocks plot slightly above unity. REE abundances in the Triassic granites and leucosomes normalized to N–MORB reveal light–REE enrichment (Figure 6h) with (La/Yb)n ranging between 2.3–19.8 (Figure 6i), with a mildly positive correlation with ^{206}Pb–^{238}U crystallisation age. (La/Yb)n ratios from Permian granites yield values of 23.09–16.1, and the REE concentrations have a larger range to lower values relative to N–MORB, compared to the Triassic rocks (Figure 6h).

5.2. Amphibolites: Central Cordillera of Colombia and the Cordillera Real of Ecuador

A comparison of the abundance of K_2O and SiO_2 (Figure 7a) in all of the Triassic magmatic rocks reveals the bimodal nature of Triassic magmatism within northwestern South America as part of Pangaea between 243 ± 4 Ma and 216.6 ± 0.4 Ma (Table 1). In contrast, Permian intrusions reveal a more continuous spread in SiO_2 abundance (Figure 6a, 6b), and a bimodal character is not evident. Here we review the geochemical characteristics of the mafic intrusions in Colombia and Ecuador, all of which are Triassic.

Amphibolitic dykes and massive metagabbros from the Central Cordillera of Colombia (Chinchina, Santa Elena, Padua, and Aburrá; Figure 2), and the Cordillera Real and Amotape Complex of Ecuador (Monte Olivo and Piedras units) yield low K_2O (<0.5 wt %) relative to SiO_2 (46–55 wt %), placing them within the tholeiitic field of Peccerillo & Taylor (1976) (Figure 7a). However, a comparison of the immobile elements Th and Co (Figure 7b) suggests that amphibolitic dykes straddle the tholeiite and calc–alkaline fields, while the massive metagabbros of the Aburrá Ophiolite plot in the tholeiite field. These discrepancies suggest the amphibolitic dykes may be partially altered. The amphibolites and metagabbros have Zr/TiO_2 that are lower than 0.01 (Figure 7c), placing them within the sub–alkaline basalt field, implying that the tholeiitic nature is primary. The amphibolitic dykes are enriched in Ti relative to V (Figure 7d), and plot in the MORB or back–arc basin basalt (BABB) field of Shervais (1982). The massive metagabbros of the Aburrá Ophiolite (El Picacho Metagabbros) that yield very low K_2O abundances of 0.02–0.12 wt % (Figure 7a), plot closer to the arc field. LILE abundances within the amphibolitic dykes from Colombia and Ecuador (Figure 7e) are enriched (up to ~100 times) relative to N–MORB and lack significant Nb and Ta anomalies. The high field strength elements (HFSE) plot close to parity with N–MORB, which is consistent with the tectonic discrimination plots. Similarly, N–MORB normalised REE plots (Figure 7f) for the amphibolitic dykes plot close to MORB compositions, although the LREE are slightly enriched with (La/Yb)n ratios varying between 3.16–0.59, while the massive metagabbros of the Aburrá Ophiolite yield approximately flat REE patterns that are slightly depleted relative to N–MORB. N–MORB normalised La/Yb ratios from all of these rock sequences show a progressive reduction with crystallisation age from 243 ± 4 Ma to 216.6 ± 0.4 Ma (Figure 7g). Finally, whole–rock εNd_i values for the amphibolitic dykes and the metagabbros range between 10.18 and 3.40, and become more juvenile with younger crystallisation ages (Figure 7h). The most juvenile rocks are characteristic of MORB and back–arc basin basalts (BABB) isotopic compositions.

A single amphibolite from the Monte Olivo unit in the Cordillera Real of Ecuador yields a whole–rock $^{87}Sr/^{86}Sr_i$ of 0.7147 (Figure 7i), which is extremely high relative to its $^{143}Nd/^{144}Nd_i$ of 0.5126 and low La/Yb ratio of 1.71 (Cochrane et al., 2014b). This is consistent with low temperature alteration, which has preferentially mobilized the LILE but had a minimal effect on the REE.

5.3. Comparison with Permian and Triassic Rocks in Perú

Permian granitoids within the Eastern Cordillera of Perú that crystallised during 293–254 Ma are alkali–calcic to calc–alkaline high–SiO_2 monzo–, syeno–, and alkali granites (Figure 8a, 8b), which are mildly metaluminous to peraluminous (ASI 1.0–1.1; Figure 8c) and yield K_2O/Na_2O ratios that mainly range between 0.8 and 1.2 (Mišković et al., 2009). N–MORB
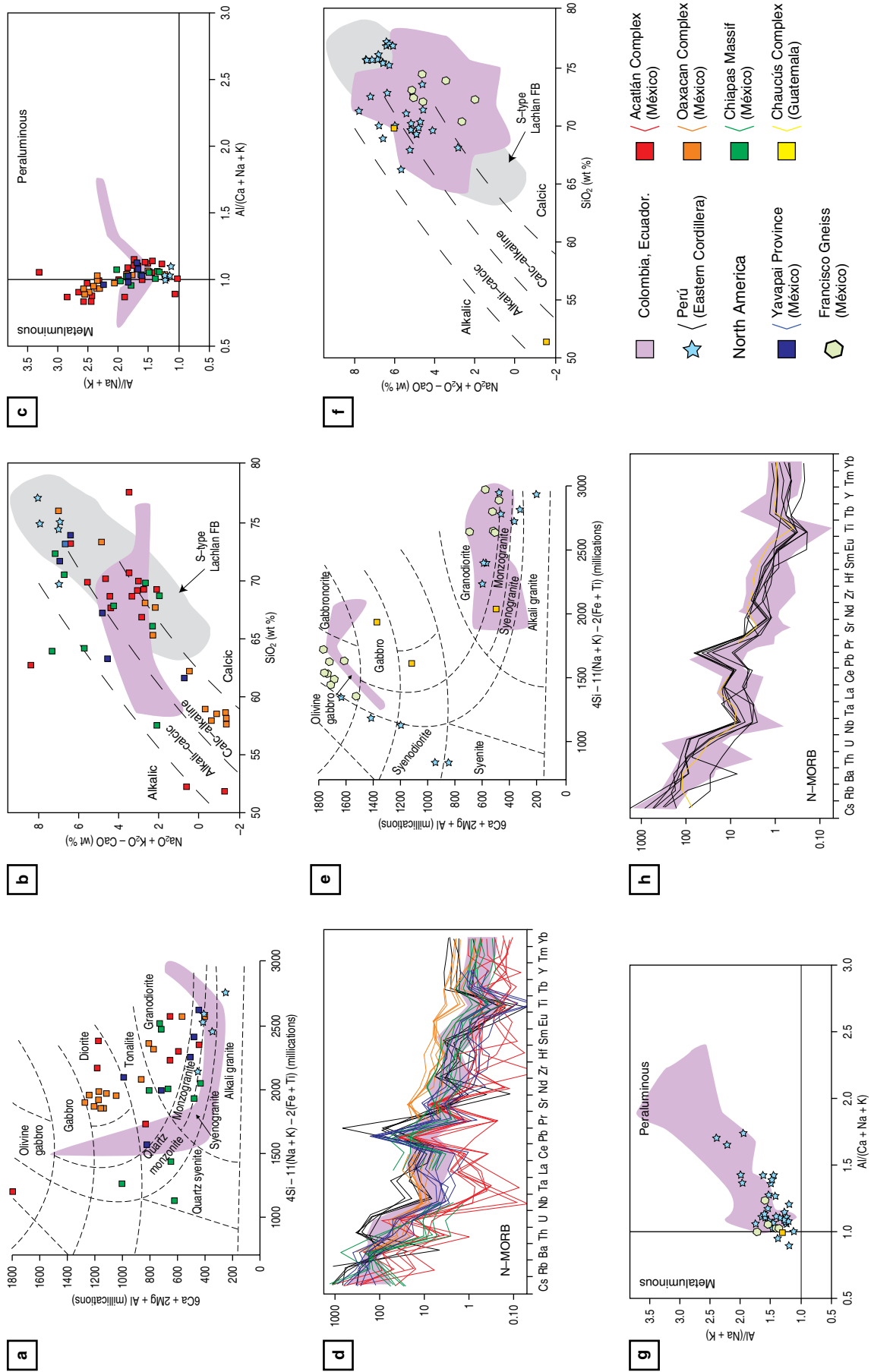
Figure 8. Geochemical data from **(a–d)** Permian and **(e–h)** Triassic granites and migmatitic leucosomes from the Eastern Cordillera of Perú, and various regions in the southern North American and western Caribbean plates. Pink shading shows the data fields obtained from Colombia and Ecuador. Data from Perú published in Mišković et al. (2009) and Spikings et al. (2016). Other data are from Solari et al. (2001; Oaxacan Complex), Keppie et al. (2006; Francisco Gneiss), Weber et al. (2005; Chiapas Massif), Arvizu et al. (2009; Yavapai Province), Solari et al. (2011; Chaucús Complex), Kirsch et al. (2012; Acatlán Complex). Lithological discriminatory fields shown in **(a)** and **(e)** are from Batchelor & Bowden (1985).

normalized multi–element plots reveal negative Nb, Ta, and Ti anomalies (Figure 8d), and resemble the composition of Permian intrusions from Colombia and Ecuador. The Permian intrusions in Perú have high SiO_2 (>69 wt %) and do not reveal a bimodal composition (Figure 8a), which is also the case in Colombia and Ecuador. Mišković et al. (2009) combined major element characteristics with iron oxide number, SiO_2 (e.g., Frost et al., 2001), and trace element abundances, to classify the Permian plutons of the Eastern Cordillera of Perú as late– to post–orogenic.

Triassic intrusions are mainly located in the southern Eastern Cordillera of Perú (Cordillera de Carabaya), and similar to the case of Colombia and Ecuador, they are geochemically distinct from the Permian intrusions (e.g., Mišković et al., 2009; Spikings et al., 2016). Triassic alkali–calcic to calc–alkaline granodiorites, monzo–, syeno–, and alkali granites in Perú (Figure 8e, 8f) are strongly peraluminous (ASI 0.98–1.42; Figure 8g), and yield anomalously high whole–rock K_2O/Na_2O ratios (0.55–2.22, with a majority >1.20; Mišković et al., 2009). N–MORB normalized multi–element plots (Figure 8h) reveal negative Nb, Ta, and Ti anomalies, and a positive Pb anomaly, suggesting the anatectites derived from source rocks with a subduction signature. Geochemically, the Triassic migmatites and granites of the Cordillera Real of Ecuador and the Central Cordillera of Colombia (K_2O/Na_2O 0.77–2.93; ASI 0.92–2.38) resemble the Triassic granites of the Eastern Cordillera of Perú. The Triassic anatectites in Perú were coeval with alkali olivine gabbro to syenitic lavas (Figure 8e) that intercalate oxidised terrigenous sedimentary rocks. Collectively these are referred to as the Mitu Group, which was deposited in a continental rift during 245–220 Ma (Spikings et al., 2016).

5.4. Comparison with Permian and Triassic Rocks in the Southernmost North American Plate

Permian intrusions in the Acatlán Complex, Oaxacan Complex, Chiapas Massif, and Yavapai Province of México are dominated by tonalites, diorites, and granodiorites (Figure 8a) with calcic to alkali–calcic differentiation trends (Figure 8b), while some upper Permian quartz monzogranites and quartz syenites are exposed in the Chiapas Massif. All of these rocks are mildy peraluminous to metaluminous (ASI 0.83–1.14; Figure 8c). All Permian rocks yield N–MORB normalized trace element plots (Figure 8d) with enriched LILE, and negative Nb, Ta, and Ti anomalies, although diorites and tonalites of the Oaxacan Complex are more enriched, while granodiorites of the Aca-tlán Complex are the most depleted. These characteristics generally resemble the Permian intrusions of Colombia, Ecuador, and Perú, suggesting they may have all formed within different regions of the same east–dipping subduction zone along the

western margin of Pangaea (e.g., Dickinson & Lawton, 2001; Kirsch et al., 2012; Ortega–Obregón et al., 2014; Solari et al., 2001; Torres et al., 1999).

Triassic intrusions in México and Central America are sparse (see section 4.5) and thus comparisons with regions within South America are not statistically robust. Nevertheless, orthogneisses in the Chaucús Metamorphic Complex of Guatemala are alkali–calcic, gabbros to monzogranites with mildly peraluminous compositions, and yield N–MORB normalized trace element compositions (Figure 8e–h; Solari et al., 2011) that are very similar to coeval Triassic rocks exposed in Colombia, Ecuador, and Perú. Solari et al. (2011) tentatively suggest these formed in an arc formed by east–dipping subduction of the Pacific lithosphere, and are a temporal extension of the Permian arc rocks found elsewhere in México. Keppie et al. (2006) suggest the Francisco Gneiss, which is exposed within the core of a Tertiary core complex in the Guerrero composite arc terrane is Late Triassic. The magmatic assemblage is bimodal (Figure 8e), and the acidic end–member is moderately peraluminous and calc alkaline rhyolites (Figure 8f, 8g). The mafic end member amphibolites are alkali to sub–alkali basalts with within–plate characteristics (Figure 7b–d) that intruded continental crust. These characteristics closely resemble the Triassic igneous assemblage in Colombia and Ecuador although the accuracy of their crystallisation ages is questionable (see section 4.5).

6. Isotope Geochemistry

Cochrane et al. (2014b) and Paul et al. (2018) report Hf (zircon) and Pb (feldspars) isotopic compositions from thirty seven Triassic migmatitic leucosomes, massive granitoids, and amphibolitic dykes exposed throughout the Central Cordillera of Colombia and the Cordillera Real and Amotape Complex of Ecuador (Table 1). The zircons, which have been dated by LA–ICP–MS (U–Pb), yield a large range of weighted mean (average of several zircon grains) εHf_i values of +15 and –20 (Figure 9; Table 1), which is consistent with the Pb isotopes (Figure 10; Table 1), and suggests that isotopically juvenile material was added to the continental crust during the Triassic, which also introduced heat and recycled continental crust via anatexis, generating the acidic end–member (Cochrane et al., 2014b; Collins et al., 2011; Spikings et al., 2015).

6.1. Zircon Hf: Granites and Migmatitic Leucosomes

Single Triassic leucosomes of migmatites and peraluminous granites generally yield high, intra–sample variations (e.g., εHf_i +3 to –11; Figure 9a) within coeval magmatic rims that surround variably aged xenocrystic cores (Cochrane et al., 2014b), and within samples that lack older cores. These varia-
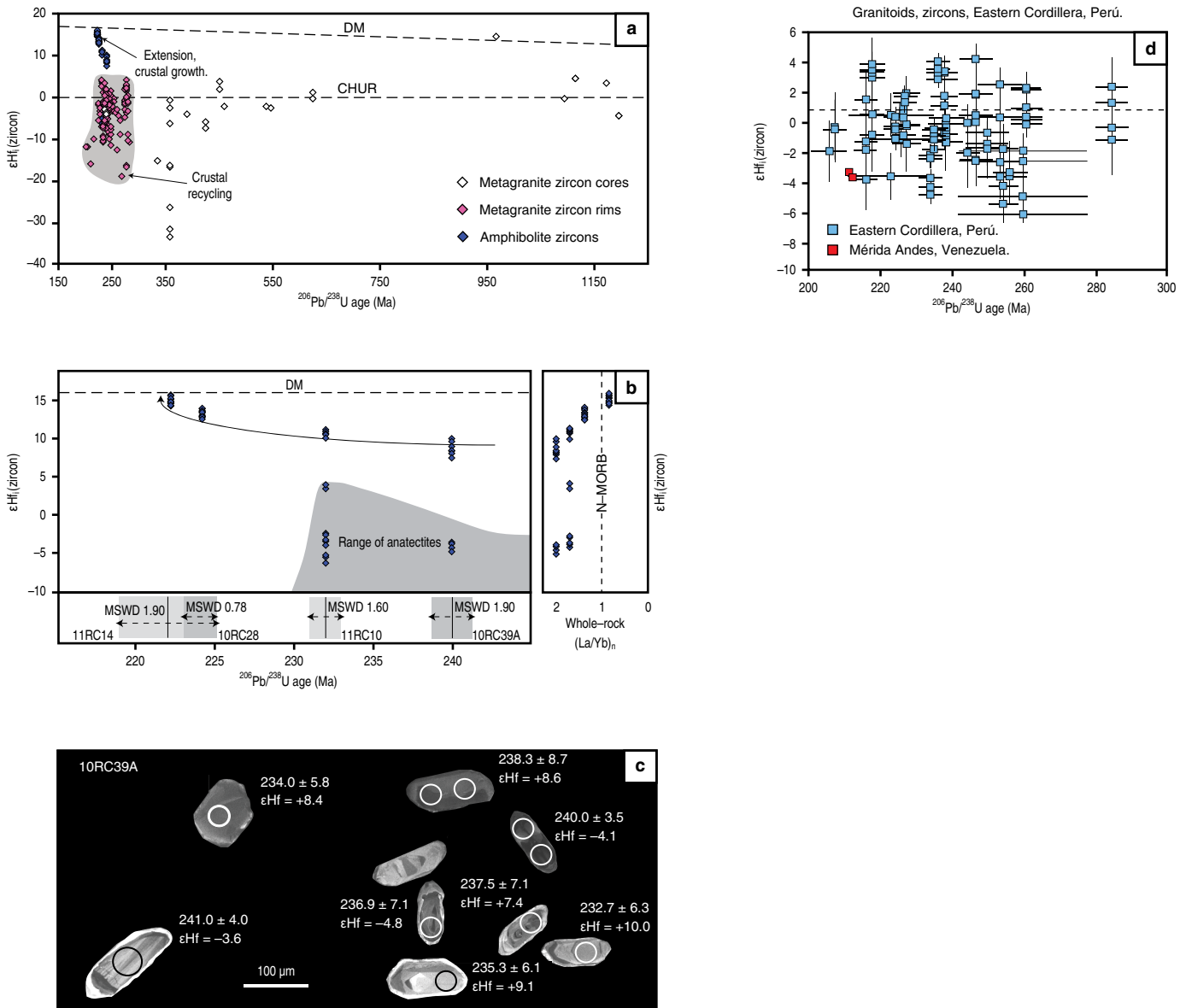
Figure 9. (a) Hf (zircon) isotope data (Cochrane et al., 2014b) acquired from rims and xenocrystic cores (single spots) of Permian and Triassic peraluminous granitoids, migmatitic leucosomes, and amphibolitic dykes and sills of the Central Cordillera, Cordillera Real, and the Amotape Complex. εHf_i was determined using zircon crystallisation dates found using LA–ICP–MS, and the CHUR composition ($^{176}Lu/^{177}Hf$ = 0.0336, $^{176}Hf/^{177}Hf$ = 0.282785; Bouvier et al., 2008). **(b)** Variation in εHf_i (zircon) of the amphibolites with zircon crystallisation date and whole–rock (La/Yb)n (N–MORB), showing a trend towards depleted mantle isotopic and geochemical signatures, with time. **(c)** Representative cathodoluminescence images for amphibolite 10RC39A (Central Cordillera; Table 1) show that juvenile εHf_i values (7.4 to 10) are yielded by patchy or unzoned zircons, whereas less juvenile values (–3.6 to –4.8) are obtained from oscillatory zoned zircons. **(d)** εHf_i (zircon) data from Permian – Triassic granitoids of the Eastern Cordillera of Perú (rims and cores; Mišković et al., 2009; Spikings et al., 2016), and the Mérida Andes (mean values; van der Lelij et al., 2016).

tions are too large for magmatic zircons that crystallised from a single, well–mixed source (e.g., Gerdes et al., 2002), and Cochrane et al. (2014b) conclude that they are mainly derived from multiple crustal sources. A small proportion of granites yield εHf_i (zircon) values that statistically define a single population, suggesting that they were derived from a distinct, homogeneous source. No correlation is found between the εHf_i values obtained from the rims of xenocryst bearing and xenocryst free zircons, and crystallisation age, which is not surprising given the heterogeneous nature of the source rocks within the crust. εHf_i values obtained from xenocrystic zircon cores (Figure 9a) span a large range and are representative of

Triassic

Permian
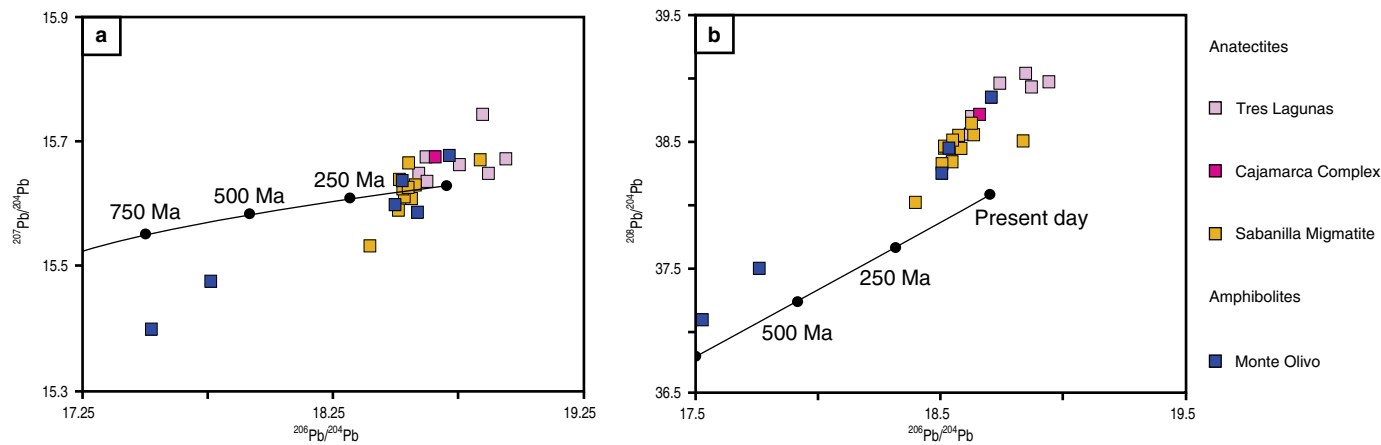
Figure 10. (a) and **(b)** $^{206}Pb/^{204}Pb$, $^{207}Pb/^{204}Pb$ and $^{208}Pb/^{204}Pb$ compositions of feldspar (mixed plagioclase and K–feldspar) extracted from granites and leucosomes of the Cajamarca Complex, Tres Lagunas Granite, and the Sabanilla Migmatite. Data from the Monte Olivo Amphibolites (Figure 2) is also shown. The Stacey & Kramers (1975) two–stage crustal evolution line is drawn as a reference. The data reveal mixing between a mafic end–member defined by amphibolites of the Monte Olivo unit, and the most radiogenic, highly peraluminous melts represented by the Tres Lagunas Granite.

the sedimentary protoliths that melted to form the anatectites. The large heterogeneity in εHf_i corroborates the large range in $^{238}U/^{206}Pb$ dates of the protoliths.

6.2. Zircon Hf: Amphibolites

Cochrane et al. (2014b) report εHf_i (zircon) values from four amphibolites which show a negative correlation with crystallisation age (Figure 9b). The two older amphibolitic dykes (240–232 Ma) yield a large range in εHf_i, with juvenile values (7.4 to 10) obtained from patchy or unzoned (cathodoluminescence) zircons, and crustal compositions (–3.6 to –4.8) from zircons that exhibit oscillatory zoning, similar to the zircons extracted from the anatectites (Figure 9c). The two youngest amphibolites (225–223 Ma) define single populations of εHf_i (13.3–15.0) from unzoned zircons, which approach the depleted mantle array. Crustal contamination of the mafic melts during emplacement was an important process in the petrogenesis of the older amphibolites prior to ca. 225 Ma. However, there is no evidence for the assimilation of significant continental crust after ca. 225 Ma. This interpretation is supported by a negative correlation between (i) εHf_i (zircon) and (La/Yb)n, (Figure 9b), and (ii) crystallisation age and eNd (whole–rock; Figure 7h; Table 1), suggesting that the mafic dykes trend towards MORB compositions with a depleted mantle source, during 240–223 Ma.

6.3. Feldspar Pb: Granites and Migmatitic Leucosomes

Cochrane et al. (2014c) and Paul et al. (2018) present Pb isotopic compositions (measured by ID–TIMS) of a combination of calcic and potassium feldspars (Figure 10; Table 1) extract-

ed from Triassic leucosomes and anatectites of the Cordilleras Central and Real. These data show that the Triassic monzogranites of the Cajamarca Complex (Colombia) and Tres Lagunas Granite (Ecuador) are the most radiogenic suite amongst the Triassic igneous units in the northern Andes (e.g., $^{206}Pb/^{204}Pb$ 18.94–18.59), while the Triassic amphibolitized mafic intrusions yield the least radiogenic compositions ($^{206}Pb/^{204}Pb$ 18.53–18.51) and reveal progressive mixing and contamination with continental crust. Leucosomes of the Sabanilla Migmatite (Ecuador) are slightly less radiogenic than the Tres Lagunas Granite with respect to Pb, and plot between the fields defined by the juvenile mafic intrusions and the Tres Lagunas Granite (Figure 10). This trend corroborates the εHf_i (zircon) values of the amphibolites (Cochrane et al., 2014b) that define a mixing array between the Tres Lagunas Granite end member and depleted mantle during 239.7 ± 2.4 Ma and 216.6 ± 0.4 Ma. These mixing trends are interpreted to reflect progressive contamination of continental crust with juvenile magmas that were emplaced during extensional decompression. Leucosomes of the Sabanilla Migmatite represent incipient melting and moderate crustal contamination of juvenile magmas. Plutons of the Tres Lagunas Granite and Cajamarca Complex are interpreted to be the product of accumulation of leucosomal melts.

6.4. Comparison with Zircon Hf Isotope Compositions in Perú

Hf isotopic compositions obtained from Permian and Triassic peraluminous granitoids of the Eastern Cordillera of Perú yield no clear trends with time, and εHf_t values range between +6 and –8 (Figure 9d; Mišković & Schaltegger, 2009; Spikings et al., 2016). This range overlaps with that obtained from Triassic

granitoids of Ecuador and Colombia, and individual, intra–grain spot analyses show a large spread, reflecting the heterogeneity of the source rocks. Mean zircon εHf_i values from the Early and Late Triassic of 0.02 ± 1.56 and –1.96 ± 1.56 suggest that this period was characterised by the addition of isotopically juvenile, mantle derived magmas, which were underplating previously attenuated continental crust (Mišković & Schaltegger, 2009; Spikings et al., 2016).

7. Thermochronology

Numerous K/Ar dates have been obtained from Paleozoic and Triassic magmatic rocks in the Central Cordillera of Colombia (Aspden et al., 1987; Feininger et al., 1972; Hall et al., 1972; McCourt et al., 1984) and the Cordillera Real of Ecuador (Litherland et al., 1994). Within Ecuador, muscovite, biotite, and whole–rock K/Ar dates of the Tres Lagunas Granite and Sabanilla unit (migmatites) range between 100–50 Ma (Litherland et al., 1994), revealing a clear disturbance to the isotopic system. Unfortunately, we cannot extract useful time–Temperature (t–T) information from these data because the degree of daughter isotope loss cannot be quantified. Nevertheless, McCourt et al. (1984) and Litherland et al. (1994) interpret these data to reflect continental collision at ca. 120 and 65–55 Ma.

Spikings et al. (2000, 2001, 2010) and Villagómez & Spikings (2013) present $^{40}Ar/^{39}Ar$ (white mica, biotite, alkali feldspar) and fission track (zircon, apatite) data from Triassic magmatic rocks in Colombia and Ecuador, which were used to construct time(t)–Temperature(T) paths. However, the collision of the Caribbean Large Igneous Province with South America at ca. 75 Ma drove more than 350 ºC of cooling via exhumation (Spikings et al., 2010), and Triassic thermal histories are not preserved in the isotopic systems.

Recently, Cochrane et al. (2014c) and Paul et al. (2018) published apatite U–Pb data from the Triassic Cajamarca Complex, Sabanilla Migmatite, and Tres Lagunas Granite (Figure 11; Table 1). The authors demonstrate that Pb was lost from the apatite grains by thermally activated diffusion, and thus the dates can be combined with grain sizes and the diffusion properties of Pb in apatite to generate a series of plausible t–T paths at temperatures >380 ºC (Figure 11) using a computed Monte Carlo algorithm. Apatite $^{238}U–^{206}Pb$ dates from the Cajamarca Complex in the northern Central Cordillera are 10–20 my younger than their zircon U–Pb dates (Figure 11a), reflecting rapid cooling through 550–380 °C in the latest Triassic (Figure 11b), and no subsequent re–heating to temperatures >380 °C. In contrast, a majority of $^{238}U–^{206}Pb$ dates from Triassic anatectites in the southern Cordillera Real are younger than 100 Ma (Figure 11a). Numerical modelling suggests these rocks also cooled rapidly through 550–380 °C in the latest Triassic, although the rocks were re–heated to >380 °C in the Cretaceous (Figure 11c). $^{40}Ar/^{39}Ar$ muscovite plateau dates and low temperature thermochronometers (Spikings et al., 2010) support the accuracy of the t–T paths (Table 1).

Rapid cooling from anatectic temperatures to less than ~380 °C during the Triassic is probably mainly a consequence of thermal relaxation subsequent to the removal of the heat source at a local geographic scale. Some component of cooling may also be a consequence of exhumation during Triassic extension (see section 8.2).
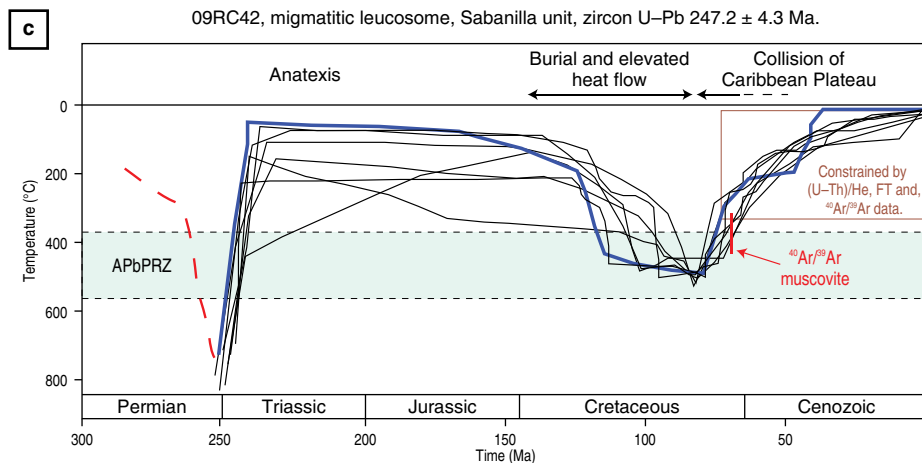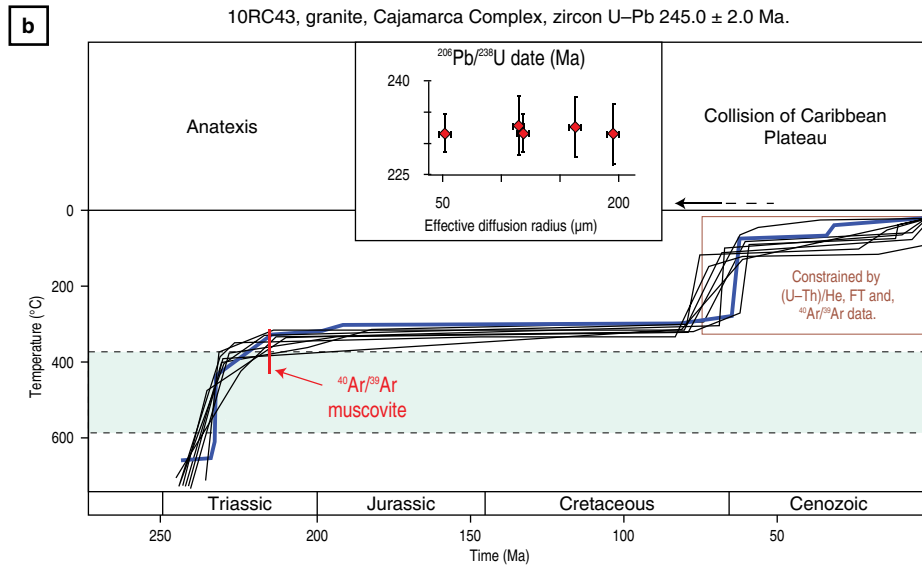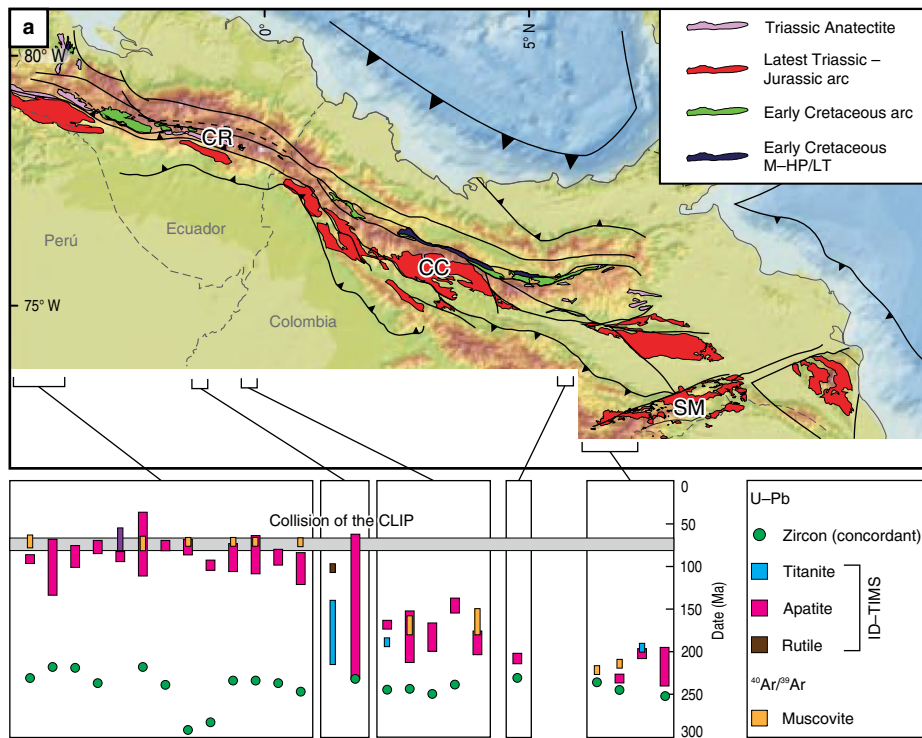
8. Interpretation

8.1. Permian: Arc Magmatism and Metamorphism along Western Pangaea

8.1.1. Arc Magmatism

The exposure of Permian granitoids within the northern Andes (Figure 2) is restricted to the Sierra Nevada de Santa Marta (ca. 288–264 Ma), the central Central Cordillera (ca. 278–253 Ma), and a single rock located in the far southern Cordillera Real (ca. 283 Ma), close to the Peruvian border. Mylonitic granites and orthogneisses from the Sierra Nevada de Santa Marta yield dates spanning between ca. 288–264 Ma, while detrital zircons in metasedimentary rocks have maximum depositional ages of ca. 284–261 Ma. The aluminium saturation index of the Permian alkali–calcic to calcic granites straddles the peraluminous and metaluminous fields, while the $\delta^{18}O$ values (quartz) of 14–17 ‰ suggests that some of these syenogranites formed by partial melting of sedimentary rocks. Zircons yield magmatic Th/U ratios of 0.26–1.27 suggesting that they crystallised from magmas, and have not undergone sub–solidus metamorphic recrystallisation (Figures 12a, 13; Table 1). This is consistent with a high Y content (550–7750 ppm) and negative Eu anomalies in zircons of El Encanto Orthogneiss (Sierra Nevada de Santa Marta; Piraquive, 2017), which is corresponds to with a magmatic origin. The whole–rock trace element abundances are characteristic of subduction related magmatism. Magmatism during this period was not bimodal and thus not accompanied by a mafic end–member, and all rocks yield >58 wt % SiO_2 (Figure 6a, 6b). The Permian granites within the Sierra Nevada de Santa Marta (Cardona et al., 2010a; Piraquive, 2017) and the Central Cordillera of Colombia (Cochrane et al., 2014b; Villagómez et al., 2011) are interpreted to have formed within a continental arc above an east dipping Pacific subduction zone beneath western Pangaea during 288–255 Ma (Figures 13, 14). U–Pb dates of detrital zircons from two metasedimentary schists of the Gaira Schists (Sierra Nevada de Santa Marta) yield maximum depositional ages of ca. 284 and ca. 261 Ma (Piraquive, 2017), and thus these sedimentary rocks were coeval with and probably sourced from the continental arc.

Inherited early Neoproterozoic and Ordovician zircon cores are common in Permian intrusions in Colombia and

a

Triassic Anatectite
Latest Triassic – Jurassic arc
Early Cretaceous arc
Early Cretaceous M–HP/LT

Collision of the CLIP

U–Pb

Zircon (concordant)
Titanite
Apatite
Rutile
ID-TIMS

$^{40}Ar/^{39}Ar$

Muscovite

b 10RC43, granite, Cajamarca Complex, zircon U–Pb 245.0 ± 2.0 Ma.

Anatexis

$^{206}Pb/^{238}U$ date (Ma)

Effective diffusion radius (µm)

Collision of Caribbean Plateau

Constrained by (U–Th)/He, FT and, $^{40}Ar/^{39}Ar$ data.

$^{40}Ar/^{39}Ar$ muscovite

Triassic | Jurassic | Cretaceous | Cenozoic

Time (Ma)

c 09RC42, migmatitic leucosome, Sabanilla unit, zircon U–Pb 247.2 ± 4.3 Ma.

Anatexis

Burial and elevated heat flow

Collision of Caribbean Plateau

Constrained by (U–Th)/He, FT and, $^{40}Ar/^{39}Ar$ data.

$^{40}Ar/^{39}Ar$ muscovite

APbPRZ

Permian | Triassic | Jurassic | Cretaceous | Cenozoic

Time (Ma)

24

Ecuador, and thus the Permian continental arc recycled Sunsas and Famatinian–aged crust (see section 4.3), which is consistent with the mildly peraluminous and calc–alkaline compositions. Cathodoluminescence images show that many detrital zircons from the Gaira Schists (Sierra Nevada de Santa Marta) consist of Ordovician cores (Piraquive, 2017) with Permian rims, which suggests that anatexis of the crust accompanied arc magmatism during the middle part of the Permian. This is consistent with the high $\delta^{18}O$ values (quartz), and thus could be described as a high–temperature metamorphic event at some time between 288 and 264 Ma (Figure 13). Vinasco et al. (2006), suggest that zircon U–Pb (SHRIMP) dates of ca. 275 Ma obtained from the Abejorral granitic gneiss record a metamorphic event, although no evidence is presented for the metamorphic nature of the zircons. Similarly, Piraquive (2017) refers to anatexis at ca. 278 Ma in the Sierra Nevada de Santa Marta as a regional metamorphic event, although evidence for Barrovian metamorphism at that time is lacking, and the Th/U values of zircons is ~1 (Figure 12), suggesting they crystallised in a magmatic environment.

Remnants of Permian magmatism have also been found within the serranía de Perijá (Figure 1; Dasch, 1982), Paraguaná Peninsula (272.2 ± 2.6 Ma; van der Lelij et al., 2016), and El Baúl Massif (294.1 ± 3.1 – 283.3 ± 2.5 Ma) in Venezuela (Figure 4d; Viscarret et al., 2009). The geochemical composition of these rocks is also typical of a calc–alkaline continental arc (e.g., van der Lelij et al., 2016). These dates and geochemical characteristics overlap with Permian intrusions in the Central Cordillera, and the Sierra Nevada de Santa Marta, and thus it is not unrealistic to suggest they all formed within the same subduction zone. However, these Permian intrusions are currently located up to ~500 km to the east of the Sierra Nevada de Santa Marta and the Central Cordillera (Figure 1), whereas there is a magmatic gap between 415–209 Ma in the Santander Massif (van der Lelij et al., 2016), which is only located 200–150 km east of the Central Cordil-

lera (Figure 1). El Baúl Massif may have been closer to the continental margin before north–eastward movement of the Maracaibo Block during the Cenozoic (Figure 14; Pindell & Dewey, 1982). These translations would place the rocks of El Baúl Massif in a similar palinspastic position as the Permian rocks of the Sierra Nevada de Santa Marta. We suggest that the basement of the Santander Massif was located east of the Permian arc axis (Figure 14), and the poorly studied sedimentary rocks of the Tiburón and Bocas Formations, which overly its basement, may host detritus shed from the arc into its back–arc.

Permian granitoids in Colombia, Ecuador, and Venezuela that intruded during 294–255 Ma, were coeval and share the same geochemical characteristics to those found in the southern North American and western Caribbean plates. Permian intrusive magmatism in the Chiapas Massif, the Xolapa, Acatlán, and Oaxacan Complexes, and the Yavapai Province was not bimodal, alkali–calcic to calcic, mildly metaluminous to peraluminous, magmatic (zircon Th/U > 0.1; Figure 12) and includes components derived from subducted oceanic lithosphere (Figure 8). Hf (zircon) isotopic compositions of Permian intrusions in the Acatlán and Oaxacan Complexes suggest that arc magmatism recycled continental crust (Ortega–Obregón et al., 2014). These observations are consistent with previous suggestions that the Permian intrusions in Laurentia and Gondwana formed within a continental arc above the same east–dipping subduction zone along the western margin of Pangaea (Figure 14; e.g., Centeno–García & Keppie, 1999; Dickinson & Lawton, 2001; Kirsch et al., 2012; Ortega–Obregón et al., 2014; Torres et al., 1999; Ratschbacher et al., 2009; Solari et al., 2001).

Using the same logic, the close geochemical similarities between Permian arc intrusions in southern North America, Colombia, Ecuador, and Venezuela with calc–alkaline Permian intrusions in the Eastern Cordillera of Perú (Figure 8; e.g., Mišković et al., 2009) that are older than ca. 260 Ma suggests

Figure 11. (a) Along strike variations of $^{238}U/^{206}Pb$ dates (apatite, titanite, and rutile; ID–TIMS) and plateau $^{40}Ar/^{39}Ar$ dates (biotite and muscovite) from Triassic lithologies (Cajamarca Complex, Tres Lagunas Granite, Sabanilla Migmatite, and various amphibolites). Bars indicate the range of $^{238}U/^{206}Pb$ dates obtained from grains with radii of ~50 (youngest date) and 100 mm (oldest date). The larger grains yield older dates than the smaller grains supporting the premise that Pb has been lost by thermally activated volume diffusion, and thus the data can be used to extract time(t)–Temperature(T) paths. The grey bar represents the timing of the collision and accretion of the Caribbean Large Igneous Province (CLIP), determined using various low–T thermochronometers, sedimentological and palaeomagnetic evidence (Luzieux et al., 2006; Spikings et al., 2001, 2010; Vallejo et al., 2006). $^{238}U/^{206}Pb$ and $^{40}Ar/^{39}Ar$ dates clearly younger towards the south, with the oldest dates in northern Colombia. Time (t)–Temperature (T) solutions to the apatite $^{238}U/^{206}Pb$ data are shown for **(b)** a Triassic granite of the Cajamarca Complex (10RC43), and **(c)** a Triassic leucosome of the Sabanilla Migmatite (09RC42) of the southern Cordillera Real, and the northern Central Cordillera, respectively (locations shown in Figure 2). Data and t–T models are obtained from Cochrane et al. (2014c) and Spikings et al. (2015). $^{40}Ar/^{39}Ar$ muscovite plateau dates are also shown, with the closure temperature range determined from the diffusion parameters presented in Harrison et al. (2009). The t–T paths are determined using a computed Monte Carlo algorithm constrained by the diffusivity and activation energy of diffusion of Pb in apatite (Cherniak et al., 1991), apatite grain size and $^{238}U/^{206}Pb$ date (data shown in (b). Models are only constrained using low–T thermochronological data (Spikings et al., 2010). The thick blue line yields the best fit between measured and predicted data. The red dashed line has not been computed, and only serves to illustrate heating of a Paleozoic sedimentary protolith during anatexis. APbPRZ: Apatite Lead Partial Retention Zone.
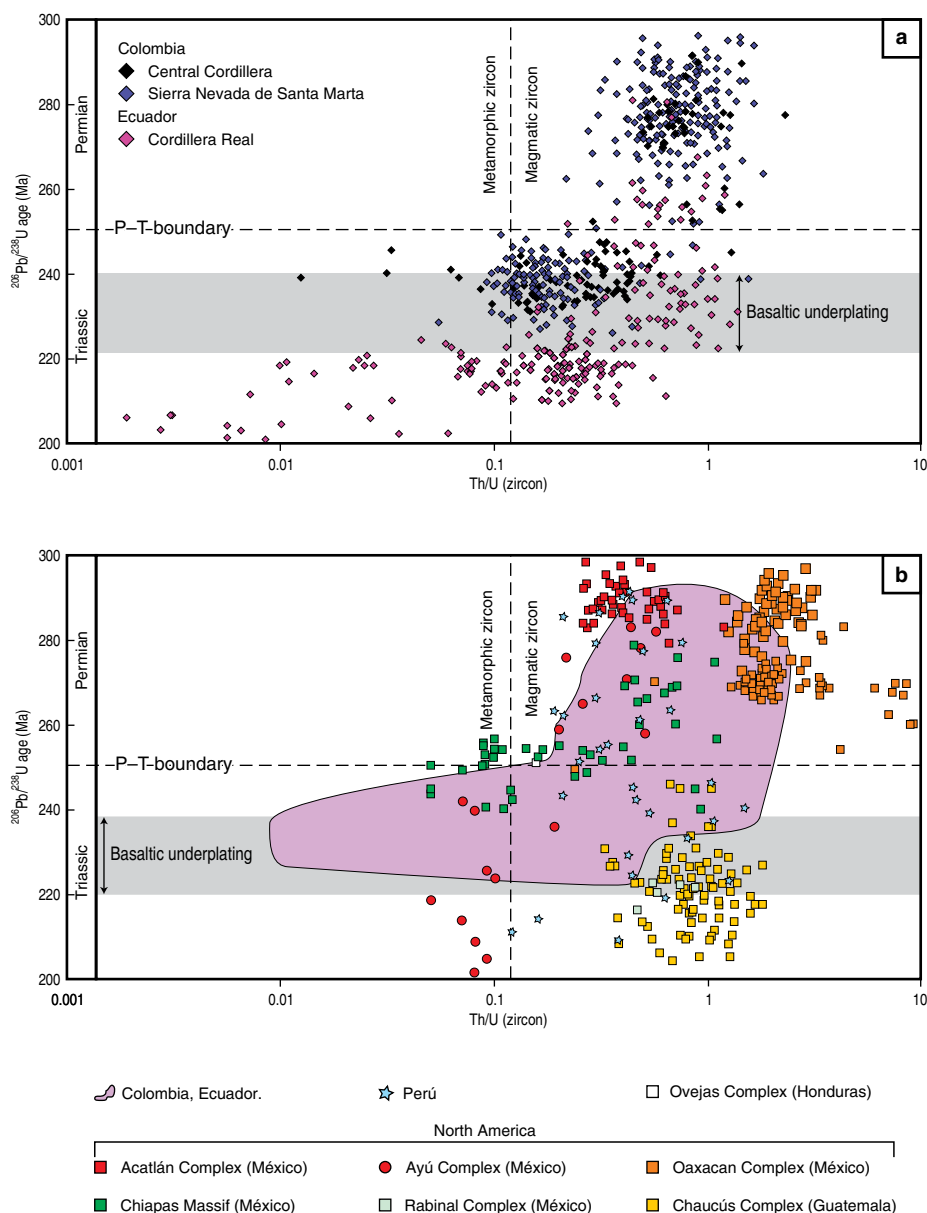
Figure 12. Variations in Th/U ratios with $^{206}Pb/^{238}U$ crystallization age of individual zircons extracted from Permian and Triassic granites and migmatitic leucosomes from **(a)** the Sierra Nevada de Santa Marta, Central Cordillera, and Cordillera Real of Colombia and Ecuador, and **(b)** various regions in the southern North American and western Caribbean plates. The zircon Th/U ratios show a significant reduction in some zircons at ca. 250 Ma in Colombia, Ecuador, the Chiapas Massif (southern Maya Block), the juxtaposing Acatlán and Ayú Complexes (Mixteca Terrane), and the Ovejas Complex (Chortis Block). These are attributed to (i) metamorphic zircon growth during regional metamorphism and crustal thickening (e.g., Weber et al., 2007), and (ii) metamorphic zircon growth, which accompanied anatexis during increased fluid expulsion and geothermal gradients during basaltic underplating (240–223 Ma). Metamorphic and magmatic zircon fields after Hartmann & Santos (2004). Uncertainties of the $^{206}Pb/^{238}U$ ages are ±1 – 2%. Data from Colombia: Cardona et al. (2010a); Cochrane et al. (2014c); Piraquive (2017). Data from Ecuador: Cochrane et al. (2014b), Paul et al. (2018). Other data: Weber et al. (2007; Chiapas Massif), Ratschbacher et al. (2009; Ovejas Complex, Rabinal Complex), Solari et al. (2001, 2011; Chaucús Complex and Oaxacan Complex), Kirsch et al. (2012; Acatlán Complex), Helbig et al. (2012; Ayú Complex), Ortega–Obregón et al. (2014; Oaxacan Complex), Mišković et al. (2009; Perú, Eastern Cordillera).

the arc was geographically extensive and Pacific subduction beneath Pangaea continued towards southern Perú. The shift from a well characterised, calc–alkaline Carboniferous arc in Perú to Permian post–tectonic alkali granites (Mišković et al., 2009) and

ultimately Triassic alkaline bimodal intrusions (see below) and volcanic rocks of the Mitu Group is characteristic of lithospheric thinning (e.g., Spikings et al., 2016; Xu et al., 2007). Mišković et al. (2009) suggest that the Permian granitoids of southern
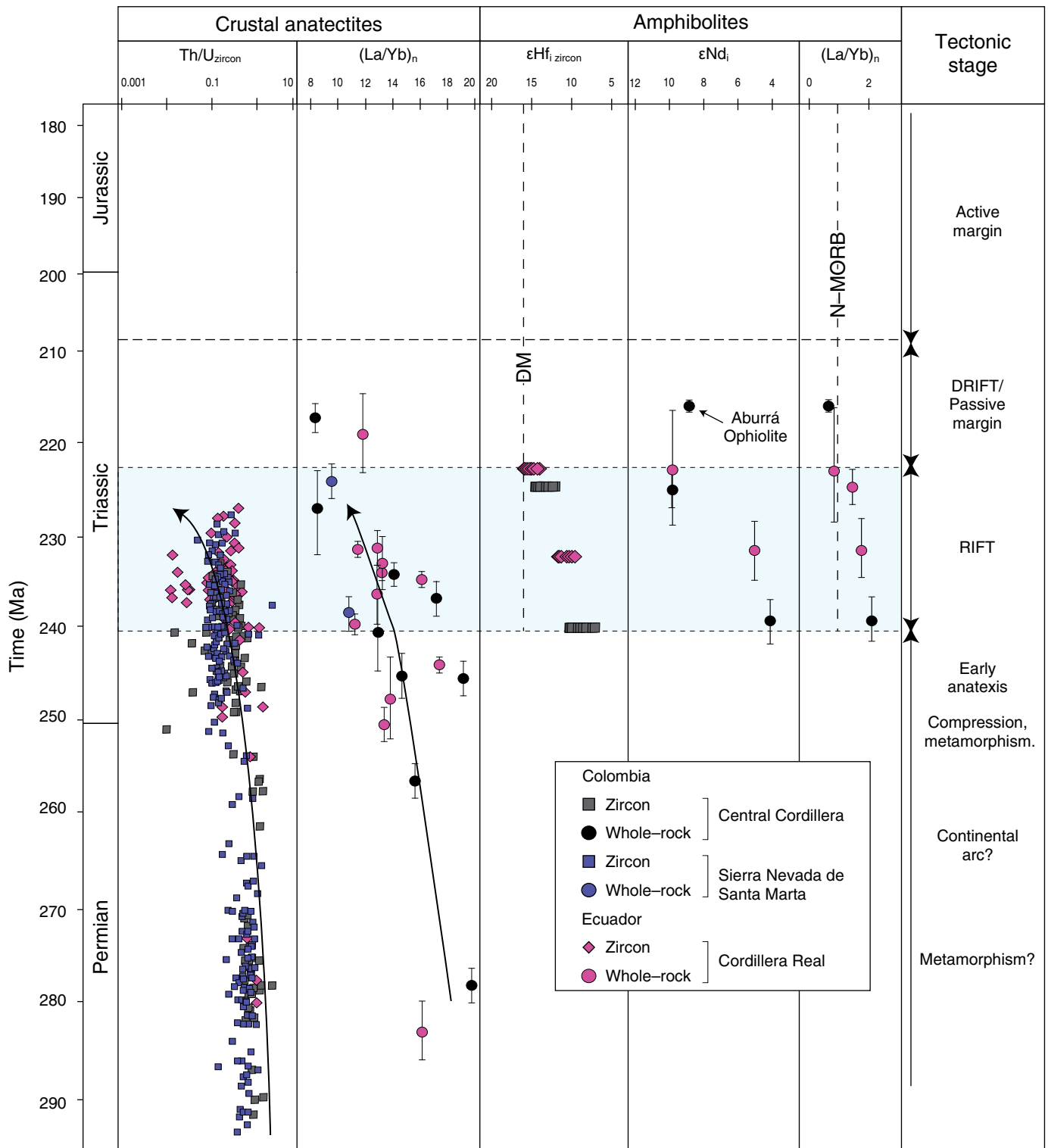
Figure 13. Geochronological and geochemical summary of data from Permian and Triassic granites and leucosomes, tholeiitic basaltic sills and dykes, and the Aburrá Ophiolite. These data define (i) Permian continental arc magmatism, (ii) bimodal magmatism during lithospheric thinning and continental rifting (240–223 Ma), and (iii) a passive margin stage during which oceanic lithosphere was forming (223–209 Ma). Active margin magmatism commences in the Santander Massif at ca. 209 Ma (Spikings et al., 2015; van der Lelij et al., 2016). Regional metamorphism is shown at ca. 275 Ma although this is poorly defined (see 2: 1: 8.1.1). Metamorphism at ca. 250 Ma is obtained from Weber et al. (2007) and Piraquive (2017; see section 8.1.2). Data are from Vinasco et al. (2006), Cochrane et al. (2014b), and Piraquive (2017).
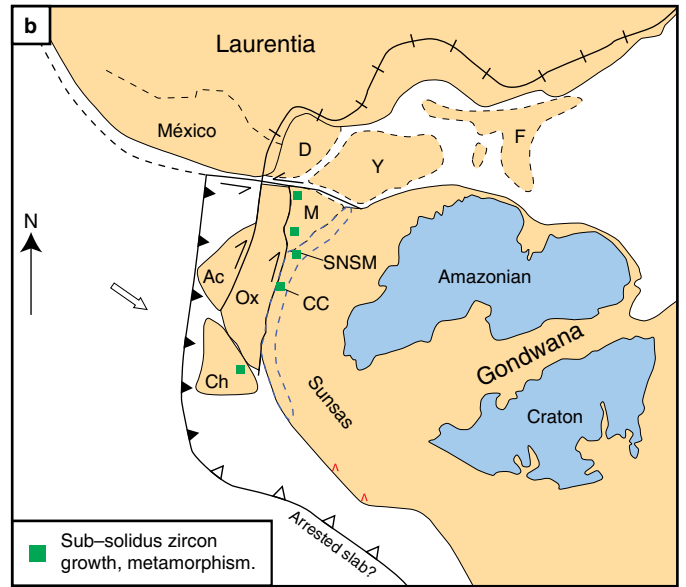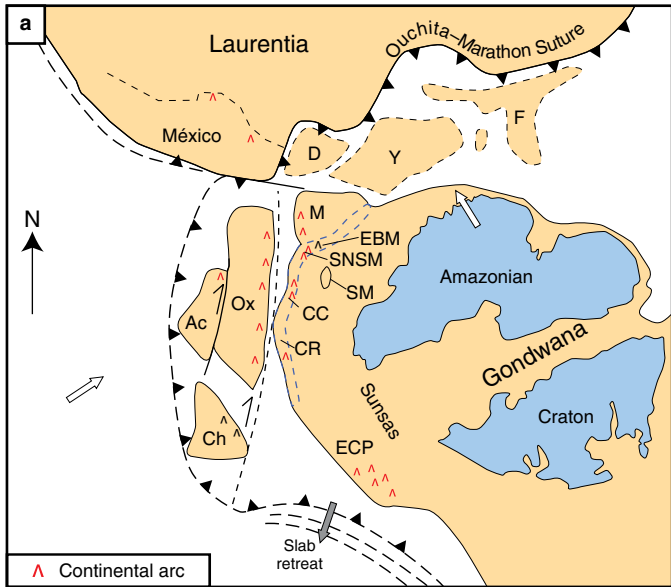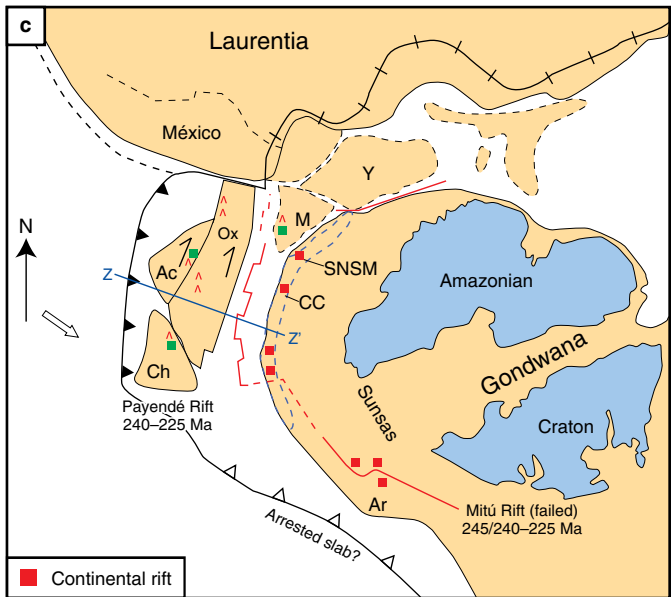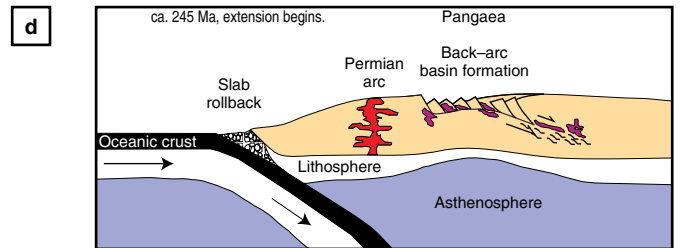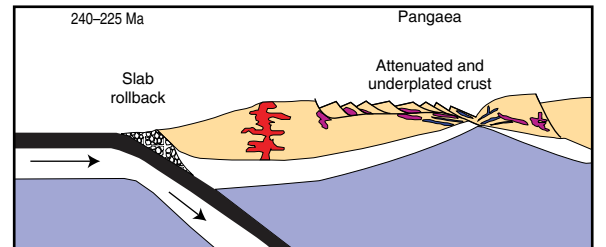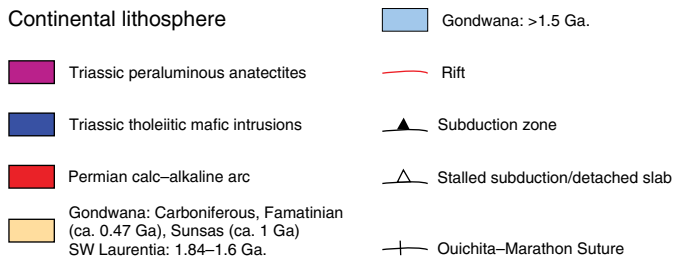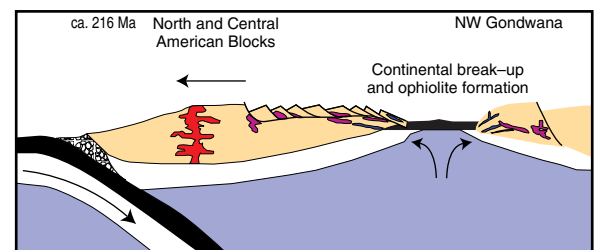
Figure 14. (a–c) Tectonic reconstructions for the Permian and Triassic, modified after Dickinson & Lawton (2001), Elías–Herrera & Ortega–Gutiérrez (2002), and Weber et al. (2007). Africa is not shown. **(d)** Schematic cross sections showing the Triassic rift to drift transition (Payandé Rift), failed rift (Mitu Rift), and early disassembly of Pangaea. Abbreviations: (F) Florida; (D) Delicias; (Y) Yucatán; (M) Maya Block; (EBM) El Baúl Massif; (SNSM) Sierra Nevada de Santa Marta; (SM) Santander Massif; (Ox) Oaxaquia; (CC) Central Cordillera; (Ac) Acatlán Block; (CR) Cordillera Real; (Ch) Chortis Block; (ECP) Eastern Cordillera of Perú.

Perú formed within an extensional regime during extensive slab retreat, which thermally weakened the subducted slab, leading to slab–break–off by ca. 270–260 Ma (Figure 14). Alternatively, orogenic collapse could also be responsible for the switch from a normal magmatic arc to generalised extension, e.g., collapse of the late Paleozoic arc in Chile and Argentina (e.g., Hervé et al., 2014). Rocks of the southern Eastern Cordillera of Perú were deformed by the poorly temporally constrained middle Permian Tardihercynian deformation phase, giving rise to folding and an angular unconformity between Permian – Carboniferous rocks and the overlying Triassic Mitu Group (Laubacher, 1978; Rosas et al., 2007; Spikings et al., 2016).

Any model which includes a Permian arc spanning from North to South America must account for the relatively low volume of Permian arc rocks in Colombia and only a single exposed location in Ecuador, compared to substantial volumes preserved in México and Perú. Most reconstructions (e.g., Dickinson & Lawton, 2001; Elías–Herrera & Ortega–Gutiérrez, 2002) place various Mexican and Central American crustal blocks (Maya, Acatlán–Mixteca, Oaxaquia, Chortis; Figure 14) outboard of the northwestern corner of South America within Pangaea, and therefore it is likely that with the exception of the Inner Santa Marta Metamorphic Belt (Figure 3), a majority of Colombia and Ecuador existed in the Permian back–arc, and most of the Permian arc was displaced northwards during the fragmentation of Pangaea in the Triassic (Spikings et al., 2015). Other blocks, for example the Paraguana Peninsula, El Baúl Massif, and perhaps the Inner Santa Marta Metamorphic Belt were displaced eastwards during the Cenozoic (Pindell & Dewey, 1982).

8.1.2. Latest Permian – Early Triassic Metamorphism

Garnet amphibolites of La Secreta Mylonites of the Inner Santa Marta Metamorphic Belt record prograde metamorphism with peak metamorphic conditions of ~770–830 °C and ~11.5–14 kb (hbl–grt; hbl–plag–qtz), followed by retrogression to 530 °C and 5.5 kb (Piraquive, 2017). Piraquive (2017) identifies sub–solidus metamorphic zircon cores that were coeval with garnet growth at ca. 250 Ma and suggests these date peak metamorphism (Figure 13), while retrogression continued through the Triassic (Spikings et al., 2015). Cardona et al. (2010a) describe kinked plagioclase in mylonitic Permian intrusions (288–264 Ma) of the Sierra Nevada de Santa Marta, which they interpret as a high temperature (>450 °C) deformational event. The same authors interpret amphibole K–Ar dates of ca. 250 Ma (MacDonald & Hurley, 1969) obtained from a gneissic clast located proximal to the mylonites to be the result of a thermal disturbance at ca. 250 Ma, and further suggest that the same thermal event may be responsible for the high–temperature deformation and mylonitisation of the Permian intrusions. The Th/U content

of zircons at ca. 250 Ma approaches 0.1 (Figure 12a), corroborating sub–solidus zircon growth and a metamorphic event at that time (Figure 13).

Weber et al. (2007) report concordant zircon U–Pb dates from migmatites of the Chiapas Massif of 254.0 ± 2.3 Ma – 251.8 ± 3.8 (Figures 4d, 5b). These dates are derived from the rims of zircons which yield Th/U ratios <0.1 (Figure 12b), and they are interpreted to be a result of medium pressure–high temperature (MP–HT) metamorphism during compression, and stacking within an orogenic wedge. Similarly, Ratschbacher et al. (2009) also report zircon rims in Permian intrusions at ca. 250–245 Ma from the Chortis Block of Central America, which yield metamorphic Th/U ratios of ~0.04 (Figure 12b). These dates overlap with, and perhaps add credence to suggestions for latest Permian – earliest metamorphism in Colombia (Figure 13). However, quantitative evidence for the precise timing of a high–temperature metamorphic event in Colombia at ca. 250 Ma is weak, and there is a requirement for further studies to directly date deformation and metamorphism during the Permian and earliest Triassic. Weber et al. (2007) attribute metamorphism in the Chiapas Massif to compression that closed marginal basins, previously formed during extension that accompanied Permian arc magmatism (Figures 13, 14). The cause of compression has been attributed to either terrane accretion, subduction of thickened, topographically prominent and buoyant oceanic lithosphere (e.g., Weber et al., 2007), or increased plate coupling during the waning stages of the amalgamation of Pangaea (Cardona et al., 2010a). The collision event post–dates the early amalgamation of Pangaea by ca. 50 Ma, which is recorded along the diachronous Ouachita–Marathon Suture (Figure 14) that had formed by the early Permian.

Geochemical and isotopic evidence from Permian – Triassic intrusions in Perú provides no clear evidence for compression at ca. 250 Ma (Figure 12; Mišković et al., 2009; U/Th zircons > 0.1). However, rocks of the southern Eastern Cordillera of Perú were deformed by the poorly temporally constrained middle Permian Tardihercynian deformation phase, giving rise to folding and an angular unconformity between Permian – Carboniferous rocks and the overlying Triassic Mitu Group (Laubacher, 1978; Rosas et al., 2007; Spikings et al., 2016). Therefore, it is likely that compression may have also affected the Peruvian margin, although this is not clearly expressed in the composition of magmatic rocks, suggesting that compression may have been less intense to the south of Colombia and Ecuador. A southward waning of compression during the Permian would spatially correlate with the location of continental lithosphere outboard of the Triassic margins of Colombian and Ecuadorian crust within South America, and was perhaps lacking outboard of Perú (Figure 14). This supports a hypothesis that compression at ca. 250 Ma was a consequence of the collision of terranes that now form the basement of México and Central

America. Alternatively, varying stress regimes may be a consequence of varied displacement at the ocean–continent plate interface to the north and south of the Huancabamba Deflection.

8.2. Triassic: Rift to Drift Transition and the Early Disassembly of Pangaea

8.2.1. The Magmatic Record

The Triassic crustal anatectites of the Sierra Nevada de Santa Marta and Central Cordillera of Colombia, and the Amotape Complex and Cordillera Real of Ecuador that formed during 240–225 Ma yield lower whole–rock (La/Yb)n, lower zircon Th/U (Figures 12a, 13), and are significantly more peraluminous than the Permian granitoids in Colombia and Ecuador (Figure 6c), the Eastern Cordillera of Perú (Mišković et al., 2009), and the southwestern North American Plate (Figure 8). These corroborate upper continental crust normalised trace element concentrations close to unity (Figure 6g), and are indicative of increased partial melting of pelitic rocks after ca. 240 Ma, forming metamorphic zircon within the anatectites, and perhaps an overall greater volume of magmatism compared to the Permian, which is reflected by a peak in the quantity of dated samples during 240–225 Ma (Figure 4a). This period was characterised by bimodal magmatism (Figures 7a, 8e), and Cochrane et al. (2014a) suggest that mafic underplating elevated the geothermal gradient, driving fluid expulsion from the pelitic protoliths and lowering their solidus.

The trace element content of the Triassic amphibolitised tholeiitic dykes is characteristic of a back–arc basin or MORB setting (Figure 7d), and the progressive trend in isotopic compositions towards the depleted mantle (Figure 13), combined with progressive depletions in incompatible elements during 240–225 Ma (Figure 7g) suggests they were emplaced within a lithosphere that was thinning. Hafnium isotopic compositions in zircons show that mantle derived tholeiites emplaced during 240–232 Ma assimilated isotopically evolved continental crust (Figure 9), whereas there is little evidence of the assimilation of significant crust after 225 Ma, when εHf$_i$ approaches depleted mantle compositions. Pb isotopes in feldspars (Figure 10) also reveal mixing between a highly radiogenic component that is compatible with upper continental crust, with a juvenile source that approaches the depleted mantle and is represented by the mafic end member rocks.

The geographically widespread occurrence of coeval, Triassic tholeiitic, amphibolitised dykes and crustal anatectites within Colombia and Ecuador (Figure 4a) supports an extensional setting, which probably formed within a region of increased heat flow that is characteristic of an attenuated back–arc basin (e.g., Collins & Richards, 2008). Cochrane et al. (2014b), and Spikings et al. (2015, 2016) suggest that the period between 240–225 Ma was dominated by progressive

thinning of the continental lithosphere during rifting and the disassembly of western Pangaea (Figure 14c). Mafic underplating and anatexis occurred because of doming and decompression of the asthenosphere during extension (Figure 14d), and heat convection during the intrusion of mafic magmas into the crust. Within Colombia, this interpretation is supported by the identification of rapid extension and subsidence located between the present Central and Eastern Cordilleras, resulting in the deposition of red beds of the Luisa and Payandé Formations, and the Chicalá Member of the Saldaña Formation during the Middle – Late Triassic (Mojica & Kammer, 1995; Mojica & Prinz–Grimm, 2000; Senff, 1995). Within Ecuador, Triassic rifting is supported by (i) the tentatively mapped Triassic Zumba Ophiolite in the southernmost Cordillera Real of Ecuador, although its Triassic age is assumed based on its structural position (Figure 2; Litherland et al., 1994), and (ii) late Middle to Upper Triassic continental and marine volcano–sedimentary rocks of the Piuntza unit (southern Cordillera Real) that were deposited in rift grabens (Figure 2; Litherland et al., 1994). Spikings et al. (2016) refer to this rift as the Payandé Rift (w), which was also used by Senff (1995) to describe the tectonic setting of Triassic, red siliciclastic rocks of the Payandé Formation in northern Colombia.

A majority of crustal anatectites are older than 225 Ma, and the basaltic amphibolites that formed during and after 225 Ma yield N–MORB isotopic and geochemical signatures (Figure 13). Cochrane et al. (2014a) suggest that the continental crust was either extremely thin or absent after 225 Ma (Figure 14d). Correa–Martínez (2007) documents a series of metagabbros, amphibolites, and plagiogranites from the northern Central Cordillera, and utilizes petrological observations, isotopic and geochemical analyses, and field mapping to conclude that they are part of an ophiolitic sequence (the Aburrá Ophiolite; Figure 2) that formed within a back–arc basin. U–Pb dating of magmatic zircons from the plagiogranite yields an age of ca. 216 Ma (Table 1) suggesting that seafloor spreading started between ca. 225 and ca. 216 Ma. The youngest plateau ^{40}Ar/^{39}Ar date of 213.7 ± 0.9 Ma (muscovite; Figure 2; Table 1) obtained from an anatectite in Colombia, combined with apatite U–Pb dates of 232–198 Ma (Figure 11) records cooling below ~380 °C as the margin drifted further from the source of elevated heat flow, and possibly exhumation during continued extension. Some regions of the continental margin remained at temperatures that were sufficiently high to form metamorphic zircon rims until ca. 207 Ma (Figures 4d, 12a; Table 1; Cochrane et al., 2014b). The rift and transition to drift occurred over a period of ca. 20–25 my (Figures 13, 14), which is comparable with the duration of other examples of rifting and the transition to a drift phase, including the Lau–Havre–Taupo system (south Pacific; Parson & Wright, 1996), and the west Iberian – Newfoundland conjugate margins (Russell & Whitmarsh, 2003).

Rifting starting at ca. 240 Ma is consistent with the geochronology and geochemistry of bimodal, highly peraluminous granites, alkaline intra–plate basalts, and volcanic tuffs in the central and southern Eastern Cordillera of Perú. Mišković et al. (2009) suggest that decompression melting generated basaltic magmas at the base of the lower crust, resulting in crustal melting during 260–200 Ma, ultimately giving rise to the bimodal Mitu Group within a continental rift. The age of the Mitu Group (245–240 to 220 Ma; Spikings et al., 2016) closely overlaps with the timing of rifting within Colombia and Ecuador. However, unlike the case of Colombia and Ecuador, Spikings et al. (2016) demonstrate that the rift formed in the absence of subduction, either above an arrested slab or a slab that was detached (e.g., Franzese & Spalletti, 2001; Kay, 1993). Alternatively, Noble et al. (1978) and Reitsma (2012) suggested that extension occurred in a back–arc setting, and the Triassic arc was obliterated by Cenozoic tectonic erosion (e.g., Clift & Hartley, 2007). There is no evidence for the formation of Triassic oceanic lithosphere within the Eastern Cordillera of Perú, and the rift foundered during ca. 220–190 Ma, resulting in the deposition of limestones of the Pucará Group during thermal sag (Rosas et al., 2007). Extensive tracts of continental Precambrian – Triassic continental crust, including the Arequipa Terrane (Figure 1), lie outboard of the Mitu Group, and it is likely that the rift failed to advance to a drift phase (Figure 14c). In contrast, no Triassic continental crust is found outboard of the Triassic anatectites within Colombia and Ecuador (Figure 2), and this region advanced to the drift phase. The recent discovery of Triassic xenocrystic zircons in basalt offshore northern Perú (8° S; Romero et al., 2013) suggests this may also be a product of extension of the continental crust. These rocks are exposed along the Outer Shelf High (Romero et al., 2013), and no continental crust has been found to the west, suggesting the Mexican and Central American conjugate margin may have extended into Perú, within Pangaea.

Triassic U–Pb dates obtained from the amphibolites and crustal anatectites from northern Colombia to southernmost Ecuador reveal no trend with latitude (Figure 4d), suggesting that extension and rifting was not diachronous within the northern Andes. Similarly, Spikings et al. (2016) compare U–Pb dates of detrital zircons within the Mitu Group along the strike of the Eastern Cordillera in central and southern Perú, and conclude that the basal strata were coeval everywhere, although Triassic plutons young from central towards southern Perú (Mišković et al., 2009). Rifting along western Pangaea commenced at ca. 240 Ma and affected >2500 km of the Gondwanan margin. Furthermore, Middle to Late Triassic extensional basins are dispersed throughout central and southern Chile, western Argentina (Franzese & Spalletti, 2001), and southern Brazil (Zerfass et al., 2004), suggesting that western Gondwana was placed under tension (e.g., Ramos, 2009) at ca. 240 Ma, culminating in the fragmentation of western Pangaea by ca. 195–180 Ma.

The Pacific margin of northwestern Gondwana remained passive until ca. 209 Ma, after which a prolonged period of latest Triassic – Early Cretaceous magmatism modified the margin of Colombia and Ecuador, and southernmost Perú (Figure 13; Spikings et al., 2015).

8.2.2. Conjugate Margins to Gondwana

Triassic rifting within Colombia and Ecuador is considered to have occurred within a back–arc (Cochrane et al., 2014b; Spikings et al., 2015, 2016). Reconstructions of Pangaea based on Atlantic seafloor magnetic anomalies show that northwestern South America lay close to Laurentia during the Permian and Triassic, and overlapped half of present day México (Dickinson & Lawton, 2001; Pindell & Barrett, 1990). Consequently, it is logical that the rifted margins currently form part of Central America, southern North America, and perhaps parts of the Caribbean Plate. Several lines of evidence suggest that the basement to Mexican and Central American terranes, including the Mixteca Terrane (e.g., the Acatlán and Ayú Complexes), Oaxaquia (including the Oaxacan Complex), the Maya Block (including the Chiapas Massif and Rabinal Complex), and, controversially, the Chortis Block (including the Ovejas Complex) may have been part of Gondwana and were the rifted Triassic conjugate margin to northwestern Gondwana (Figure 14). Other evidence includes (i) Grenville–aged granulite belts with similar Pb isotope signatures (Restrepo–Pace et al., 1997; Ruiz et al., 1999; Weber & Köhler, 1999), (ii) anorthosite complexes (Restrepo–Pace & Cediel, 2010), and (iii) similar Cambrian fauna (Cocks & Torsvik, 2002; Restrepo–Pace & Cediel, 2010).

Triassic igneous rocks are sporadically exposed in (i) the Chaucús Complex (intrusions), (ii) the Chortis Block (Ovejas Complex, zircon inheritance in Eocene intrusions; Figures 5b, 8d), (iii) the Rabinal Complex (intrusions; Maya Block), and (iv) the Ayú Complex (granitic dykes; currently part of the Mixteca Terrane and juxtaposed against the Acatlán Complex). Concordant zircon U–Pb dates from these primary and inherited zircons span between 245–215 Ma, overlapping with the timing of rifting in Colombia and Ecuador. Keppie et al. (2006) present discordant zircon U–Pb dates from migmatitic gneisses of the Francisco Gneiss (northern Guerrero composite terrane, northern México) that span between 216 and 197 Ma, although they interpret these are recording crystallisation at ca. 206 Ma. Their coeval association with mafic amphibolites, combined with intra–plate geochemical characteristics led Keppie et al. (2006) to propose that they formed in a rift located in a continental back–arc. Zircon Th/U values from Triassic zircons in the Chaucús Metamorphic Complex and the Rabinal Complex support an igneous origin (Figure 12b), although zircon Th/U values <0.01 from inherited zircons in the Chortis Block (Ovejas Complex) suggest these may have formed in a sub–solidus,

metamorphic environment (Ratschbacher et al., 2009). Similarly, Th/U (zircon) ratios in the Acatlán Complex and juxtaposed Ayú Complex show a gradual reduction from the Permian to the end of the Triassic (Figure 12). Robust geochemical and isotopic analyses of the Triassic igneous rocks are lacking (e.g., Figure 8), and it is possible that some Triassic rocks formed along an arc axis, whereas others may have formed in the back–arc and resemble the Triassic monzogranites of Colombia and Ecuador. Poorly dated Late Triassic (216–197 Ma) rhyolites and tholeiitic basalts in the Guerrero composite terrane of México are interpreted to have formed in a continental rift (Keppie et al., 2006), and the same authors attribute Upper Triassic rocks of the Oaxaquia Terrane to a back–arc setting. Similarly, Helbig et al. (2012) suggest that Upper Triassic volcanic rocks with E–MORB to MORB characteristics within the Acatlán Complex (Ayú Complex; Figure 5b) formed within a back–arc.

Triassic roll–back of the east–dipping Pacific slab drove widespread extension along most of western Gondwana, resulting in complete rifting of continental crust in the region of northwestern South America. Further south, tensile forces failed to form oceanic lithosphere in Perú (Mitu Rift; Figure 14), western Argentina, and Chile (Cuyo and Ischigualasto–Villa Unión Basins; Spikings et al., 2016), and these regions remain as failed rifts. Perhaps the orthogonal component of roll–back was less severe in these regions, or the continental crust was stronger. The Middle – Late Triassic rifts in Chile and western Argentina, and associated magmatic units are collectively considered to have formed subsequent to slab–detachment, giving rise to intense crustal melting under extensional tectonic conditions during a period of arrested subduction (e.g., Kay et al., 1989; Parada et al., 2007; Spalletti et al., 2008). Consequently, the origin of extension may differ compared to the case of Colombia and Ecuador, where subduction is thought to have continued throughout the Triassic.

9. The Triassic – Jurassic Transition, and the Separation of Pangaea

The magmatic and sedimentary rocks associated with Triassic (240–225 Ma) rifting in Colombia and Ecuador (e.g., Sabanilla Migmatite, Tres Lagunas Granite, and the Cajamarca Complex) are mainly in faulted contact with the younger Late Triassic – Jurassic continental arc, which commenced at ca. 209 Ma in the Santander Massif (Figure 13; Spikings et al., 2015; van der Lelij et al., 2016), and had migrated westwards to the region of the Cordilleras Central and Real by ca. 189 Ma (Spikings et al., 2015). Jurassic extension north of the Huancabamba Deflection (Figure 1) had multiple effects, including (i) trenchward migration of the Jurassic arc (189–145 Ma; Cochrane et al., 2014a; Spikings et al., 2015), (ii) graben formation (e.g., Uribante and Espina grabens; Bartok, 1993), (iii) carbonate (Jaillard et al., 1990; Toussaint & Restrepo, 1994) and red–bed deposition

(e.g., La Quinta Formation; van der Lelij et al., 2016), (iv) the extrusion of the Central Atlantic Magmatic Province during 202–201 Ma (e.g., Davies et al., 2017), and (v) the separation of North America, Yucatán and South America at 195 Ma (e.g., Beutel, 2009; Pindell & Kennan, 2009), forming the proto–Caribbean seaway and the central Atlantic Ocean.

The relationship between the driving forces of Triassic extension in northwestern South America, and Jurassic extension which lead to the fragmentation of western Pangaea is unclear because the rift–related Triassic units are persistently faulted against the Jurassic rocks (Figure 2). Rifting commenced in south–eastern North America at ca. 230 Ma (Schlische, 2002), and possibly also within far southern North America (e.g., northern Florida; Beutel, 2009). Magmatic injection in the form of giant dyke swarms (Central Atlantic Magmatic Province) accompanied rifting within North America at 200 ± 2 Ma (Beutel, 2009 and references therein), and South America at 201.6–201.3 Ma (Davies et al., 2017), which coincides with 202 ± 1.8 Ma tuffs at the base of the rift–related, la Quinta Formation of the Mérida Andes, Venezuela (Figure 1; van der Lelij et al., 2016), and oceanic crust started forming between North and South America at ca. 180 Ma. This sequence of events opens the possibility that plate tectonic forces initiated the early break–up of western Pangaea by attenuating its margins and enhancing mantle upwelling (Figure 14d). Prolonged extension may have propagated along pre–existing weak zones that extended into the continental interior (e.g., the South America–Yucatán–North America–Central African Sutures). These zones captured melts derived from the upwelled mantle (e.g., Buiter & Torsvik, 2014) forming a Large Igneous Province, became hot and eventually lead to the formation of a juvenile ocean.

10. The Suspect Tahamí Terrane

The Tahamí Block (Antioquia Terrane sensu Pindell & Kennan, 2009) of northern Colombia (Restrepo & Toussaint, 1982) is fault bounded by the Otú–Pericos and Palestina Faults to the east, the San Jerónimo Fault to the west, and the Ibagué Fault in the south (Figure 1). It is considered by some authors to be a distinct terrane because (i) it is separated from Rodinia–aged (ca. 1 Ga) crust to the east, (ii) it does not expose Jurassic arc rocks, unlike the region to the east, and (iii) Martens et al. (2014) suggest that the Tahamí Terrane is restricted to Triassic ortho– and paragneiss, and that juxtaposed Ordovician rocks (e.g., La Miel Gneiss; Villagómez et al., 2011) define the separate suspect Anacona Terrane. Thus, the basement rocks in this suspect terrane only yield Triassic (Cajamarca Complex; e.g., Cochrane et al., 2014b; Martens et al., 2014) U–Pb dates, which are intruded by the ca. 90 Ma Antioquia Batholith. We suggest these criteria are insufficient to assign a terrane status to the Triassic rocks of the Tahamí

Block, and it is not proven that they are derived from several hundred km to the south, as is advocated in some models (e.g., Kennan & Pindell, 2009). First, Ordovician basement is widespread in the Mérida Andes, Santander Massif, and the Quetame Massif, and Ordovician zircon cores are abundant in Triassic anatectites of the Cajamarca unit. Ordovician crystalline rocks of the Mérida Andes and Santander Massif yield Pb isotopic compositions that are Gondwanan (van der Lelij, 2013), and thus we propose that the Ordovician basement is autochthonous to South America, and extends to the San Jerónimo Fault. Evidence includes the presence of abundant Ordovician zircon cores in zircons extracted from gneisses of the Triassic Cajamarca Complex (Figure 4). Field relationships in the Cordillera Real of Ecuador reveal in–situ anatexis of undifferentiated Devonian metasedimentary rocks, forming the Triassic Sabanilla Migmatite. We interpret the currently faulted juxtaposition of Ordovician and Triassic gneisses in northern Colombia (e.g., Martens et al., 2014) to be a consequence of exhumation of the Ordovician basement during Jurassic – Early Cretaceous extension. The simplest explanation of rock relationships in a W–E traverse across the Central Cordillera and Cordillera Real (juxtaposition of high–pressure/low–temperature (HP/LT) metamorphic rocks, a Cretaceous arc, Paleozoic and Triassic basement, latest Jurassic arc, and Jurassic – Early Triassic arc), is a consequence of Jurassic – Early Cretaceous attenuation of the margin, followed by a switch to compression starting at ca. 120–115 Ma (Spikings et al., 2015). Jurassic intrusive rocks are not found in the Tahamí Block because the Triassic rocks exposed there did not overlie the arc axis at that time (Spikings et al., 2015). Finally, models which place the Jurassic subduction zone outboard of a hypothetical Tahamí Terrane (e.g., Pindell & Kennan, 2009), create a distance between the trench and the Jurassic arc in South America that is too large (Spikings et al., 2015). Consequently, we do not include these rocks as terranes in our reconstruction (Figure 14). Rather, they are considered to be an attenuated part of autochthonous South America.

11. Conclusions

*   Variably foliated Permian granites, granodiorites tonalites, and gabbros of the Rovira Complex (Central Cordillera), El Encanto Gneiss (Sierra Nevada de Santa Marta), and the Malacatos Complex (Cordillera Real) are calc–alkaline to calcic, metaluminous to mildly peraluminous continental arc intrusions. Concordant U–Pb dates of magmatic zircons constrain Permian arc magmatism to 288–253 Ma. The arc reworked and assimilated Sunsas (ca. 1 Ga) and Famatinian (Ordovician) continental crust, and is partly composed of S–type granites. The geochemical compositions and crystallisation ages of Permian intrusions in Colombia and Ecuador are ex-

tremely similar to (i) intrusions and volcanic rocks in the far southern North American and western Caribbean plates (298–255 Ma), (ii) intrusions in the serranía de Perijá, Paraguaná Peninsula, and El Baúl Massif (Venezuela; 294–272 Ma), and (iii) intrusions and volcanic rocks in the southern Eastern Cordillera of Perú (293–252 Ma). Collectively these are considered to have formed within the same east–dipping subduction system, which consumed oceanic lithosphere of the Pacific Ocean beneath western Pangaea. A majority of the arc is preserved in far northern Colombia (Sierra Nevada de Santa Marta) and conjugate margin blocks that are currently preserved in México and Central America. A majority of Ordovician and older basement in Colombia and Ecuador is interpreted to have resided in the Permian back–arc, while rocks of the Santander Massif were located further east, beyond the magmatic reach of the arc.

*   Vinasco et al. (2006) and Piraquive (2017) suggest that a regional metamorphic event affected the Permian intrusions in the Central Cordillera and Sierra Nevada de Santa Marta, respectively, at ca. 278 Ma. We find that this is extremely tentative because evidence for a widespread metamorphic event at that time is lacking, and a majority of zircon growth at ca. 278 Ma occurred in a magmatic environment. Further studies are required to identify a metamorphic event in South American lithosphere, which may have formed in response to the early collisional events that lead to the formation of Pangaea in the earliest Permian.

*   The margin of western Pangaea was compressed at ca. 250 Ma, driving regional metamorphism with peak conditions of 770–830 °C and 11.5–14 kb in the Sierra Nevada de Santa Marta of northern Colombia. Metamorphism at ca. 250 Ma has also been observed in the western Maya Block and the Chortis Block (México and Honduras, respectively), where it induced anatexis and perhaps sub–solidus zircon recrystallisation. Compression drove deformation in Perú prior to the onset of rifting at 245–240 Ma, although there is no evidence for regional metamorphism. Compressive forces may have been weaker south of the Huancabamba Deflection, revealing large–scale trench–parallel differences in the prevailing stress regime. Stronger compression and Barrovian metamorphism towards the north may be due to either terrane accretion (e.g., the Chortis Block; Figure 14), or the subduction of thickened and relatively buoyant continental lithosphere. The lack of metamorphism in southern Perú coincides with reconstructions that do not place Mexican and Central American terranes outboard of Perú, supporting a model whereby compression towards the north was driven by terrane accretion.

*   Magmatic underplating and anatexis of continental crust throughout 245/240–225 Ma occurred during progressive

thinning of the continental lithosphere over rifting along western Pangaea. Rifting advanced to complete separation of continental crust by ca. 216 Ma, and the formation of oceanic lithosphere between the conjugate margins of northwestern South America and basement terranes of México and Central America. The rifting event is recorded by amphibolitised tholeiitic basaltic dykes and extensive tracts of migmatites and S–type granites within the conjugate margins. These are the Cajamarca Complex and La Secreta Mylonites (Colombia), and the Tres Lagunas Granite, Sabanilla Migmatite, and Moromoro Granite (Ecuador) in northwestern South America. Various Triassic units in the Chaucús Complex, Chortis Block, Maya Block, the Mixteca Terrane (México and Central America), and perhaps in the lower plate of Tertiary metamorphic core complexes in the Guerrero composite terrane formed within the Triassic arc and back–arc. Rifting north of the Huancabamba Deflection was accompanied by subduction, and occurred within a backarc. The rift axis propagated southwards, and extension is recorded along western Perú (the Mitu Aulacogen), western Argentina, Chile, and southern Brazil. Rifting along northwestern South America started as a back–arc basin to a Permian arc, and represents the early break–up of western Pangaea, leading to the separation of North and South America by ca. 180 Ma.

✑ The relationship between Triassic plate margin extension and the final fragmentation of Pangaea is unclear. However, the sequence of events: Plate margin rifting during ca. 245–220 Ma, the extrusion of a Large Igneous Province at ca. 201 Ma, and the opening of the proto–Caribbean seaway and central Atlantic at ca. 195 Ma opens the possibility that plate tectonic forces initiated the early break–up of Pangaea by attenuating its margins and enhancing mantle upwelling. Prolonged extension may have propagated along pre–existing weak zones that extended into the continental interior (e.g., the South America–Yucatán–North America–Central African Sutures). These zones captured melts derived from the upwelled mantle (e.g., Buiter & Torsvik, 2014) forming the Central Atlantic Magmatic Province, became hot and weak and eventually lead to the formation of a juvenile ocean.

✑ We suggest that there is very little evidence for the existence of the allochthonous continental Tahamí Terrane, which is considered by some authors to have been outboard of northwestern South America during the Jurassic – Early Cretaceous. Triassic zircon rims around Ordovician zircon cores, combined with field relationships that reveal melting of Paleozoic basement rocks, forming the Triassic anatectites are evidence that Triassic rocks of the Tahamí Block are melts of Ordovician basement. Ordovician basement can be traced eastwards to the Santander Massif and

Mérida Andes, where it yields Pb isotope signatures that are Gondwanan. We conclude that the rocks of the Tahamí Block are autochthonous.

References

Arvizu, H.E., Iriondo, A., Izaguirre, A., Chávez–Cabello, G., Kamenov, G.D., Solís–Pichardo, G., Foster, D.A. & Lozano–Santa Cruz, R. 2009. Rocas graníticas pérmicas en la Sierra Pinta, NW de Sonora, México: Magmatismo de subducción asociado al inicio del margen continental activo del SW de Norteamérica. Revista Mexicana de Ciencias Geológicas, 26(3): 709–728.

Aspden, J.A. & Litherland, M. 1992. The geology and Mesozoic collisional history of the Cordillera Real, Ecuador. Tectonophysics, 205(1–3): 187–204. https://doi.org/10.1016/0040-1951(92)90426-7

Aspden, J.A. & McCourt, W.J. 1986. Mesozoic oceanic terrane in the central Andes of Colombia. Geology, 14(5): 415–418. https://doi.org/10.1130/0091-7613(1986)14<415:MOTITC>2.0.CO;2

Aspden, J.A., McCourt, W.J. & Brook, M. 1987. Geometrical control of subduction–related magmatism: The Mesozoic and Cenozoic plutonic history of western Colombia. Journal of the Geological Society, 144(6): 893–905. https://doi.org/10.1144/gsjgs.144.6.0893

Aspden, J.A., Bonilla, W. & Duque, P. 1995. The El Oro Metamorphic Complex, Ecuador: Geology and economic mineral deposits. British Geological Survey, Overseas Geology and Mineral Resources 67, 63 p. Nottingham, United Kingdom.

Bahlburg, H., Vervoort, J.D., Du Frane, S.A., Bock, B., Augustsson, C. & Reimann, C. 2009. Timing of crust formation and recycling in accretionary orogens: Insights learned from the western margin of South America. Earth–Science Reviews, 97(1–4): 215–241. https://doi.org/10.1016/j.earscirev.2009.10.006

Barredo, S., Chemale, F., Marsicano, C., Ávila, J.N., Ottone, E.G. & Ramos, V.A. 2012. Tectono–sequence stratigraphy and U–Pb zircon ages of the Rincón Blanco depocenter, northern Cuyo

Rift, Argentina. Gondwana Research, 21(2–3): 624–636. https://doi.org/10.1016/j.gr.2011.05.016

Bartok, P. 1993. Prebreakup geology of the Gulf of Mexico–Caribbean: Its relation to Triassic and Jurassic rift systems of the region. Tectonics, 12(2): 441–459. https://doi.org/10.1029/92TC01002

Batchelor, R.A. & Bowden, P. 1985. Petrogenetic interpretation of granitoid rock series using multicationic parameters. Chemical Geology, 48(1–4): 43–55. https://doi.org/10.1016/0009-2541(85)90034-8

Bayona, G., Rapalini, A. & Costanzo–Álvarez, V. 2006. Paleomagnetism in Mesozoic rocks of the northern Andes and its implications in Mesozoic tectonics of northwestern South America. Earth, Planets and Space, 58(10): 1255–1272. https://doi.org/10.1186/BF03352621

Bayona, G., Jiménez, G., Silva, C., Cardona, A., Montes, C., Roncancio, J. & Cordani, U. 2010. Paleomagnetic data and K–Ar ages from Mesozoic units of the Santa Marta Massif: A preliminary interpretation for block rotation and translations. Journal of South American Earth Sciences, 29(4): 817–831. https://doi.org/10.1016/j.jsames.2009.10.005

Beutel, E.K. 2009. Magmatic rifting of Pangaea linked to onset of South American Plate motion. Tectonophysics, 468(1–4): 149–157. https://doi.org/10.1016/j.tecto.2008.06.019

Bouvier, A., Vervoort, J.D. & Patchett, P.J. 2008. The Lu–Hf and Sm–Nd isotopic composition of CHUR: Constraints from unequilibrated chondrites and implications for the bulk composition of terrestrial planets. Earth and Planetary Science Letters, 273(1–2): 48–57. https://doi.org/10.1016/j.epsl.2008.06.010

Buiter, S.J.H. & Torsvik, T.H. 2014. A review of Wilson cycle plate margins: A role for mantle plumes in continental break–up along sutures? Gondwana Research, 26(2): 627–653. https://doi.org/10.1016/j.gr.2014.02.007

Bustamante, A., Juliani, C., Essene, E.J., Hall, C.M. & Hyppolito, T. 2012. Geochemical constraints on blueschist– and amphibolite–facies rocks of the Central Cordillera of Colombia: The Andean Barragán region. International Geology Review, 54(9): 1013–1030. https://doi.org/10.1080/00206814.2011.594226

Bustamante, C., Archanjo, C.J., Cardona, A., Bustamante, A. & Valencia, V.A. 2017. U–Pb ages and Hf isotopes in zircons from parautochthonous Mesozoic terranes in the western margin of Pangea: Implications for the terrane configurations in the northern Andes. The Journal of Geology, 125(5): 487–500. https://doi.org/10.1086/693014

Cardona, A., Cordani, U. & Sánchez, A. 2007. Metamorphic, geochronological and geochemical constraints from the pre–Permian basement of the eastern Peruvian Andes (10° S): A Paleozoic extensional–accretionary orogen? 20th Colloquium on Latin American Earth Sciences, p. 29–30. Kiel, Germany.

Cardona, A., Valencia, V., Garzón, A., Montes, C., Ojeda, G., Ruiz, J. & Weber, M. 2010a. Permian to Triassic I to S–type magmatic switch in the northeast Sierra Nevada de Santa Marta and adjacent regions, Colombian Caribbean: Tectonic setting and implications within Pangea paleogeography. Journal of South American Earth Sciences, 29(4): 772–783. https://doi.org/10.1016/j.jsames.2009.12.005

Cardona, A., Valencia, V., Bustamante, C., García–Casco, A., Ojeda, G., Ruiz, J., Saldarriaga, M. & Weber, M. 2010b. Tectonomagmatic setting and provenance of the Santa Marta Schists, northern Colombia: Insights on the growth and approach of Cretaceous Caribbean oceanic terranes to the South American continent. Journal of South American Earth Sciences, 29(4): 784–804. https://doi.org/10.1016/j.jsames.2009.08.012

Centeno–García, E. & Keppie, J.D. 1999. Latest Paleozoic – early Mesozoic structures in the central Oaxaca Terrane of southern Mexico: Deformation near a triple junction. Tectonophysics, 301(3–4): 231–242. https://doi.org/10.1016/S0040-1951(98)00213-3

Chappell, B.W. & White, A.J.R. 1974. Two contrasting granite types. Pacific Geology, 8: 173–174.

Charrier, R., Pinto, L. & Rodríguez, M.P. 2007. Tectonostratigraphic evolution of the Andean Orogen in Chile. In: Moreno, T. & Gibbons, W. (editors), The geology of Chile. The Geological Society, p. 21–114. London. https://doi.org/10.1144/GOCH.3

Cherniak, D.J., Lanford, W.A. & Ryerson, F.J. 1991. Lead diffusion in apatite and zircon using ion implantation and Rutherford backscattering techniques. Geochimica et Cosmochimica Acta, 55(6): 1663–1673. https://doi.org/10.1016/0016-7037(91)90137-T

Chew, D.M., Schaltegger, U., Košler, J., Whitehouse, M.J., Gutjahr, M., Spikings, R. & Mišković, A. 2007. U–Pb geochronologic evidence for the evolution of the Gondwanan margin of north–central Andes. Geological Society of America Bulletin, 119(5–6): 697–711. https://doi.org/10.1130/B26080.1

Chew, D.M., Magna, T., Kirkland, C.L., Mišković, A., Cardona, A., Spikings, R. & Schaltegger, U. 2008. Detrital zircon fingerprint of the proto–Andes: Evidence for a Neoproterozoic active margin? Precambrian Research, 167(1–2): 186–200. https://doi.org/10.1016/j.precamres.2008.08.002

Clift, P.D. & Hartley, A.J. 2007. Slow rates of subduction erosion and coastal underplating along the Andean margin of Chile and Peru. Geology, 35(6): 503–506. https://doi.org/10.1130/G23584A.1

Cochrane, R. 2013. U–Pb thermochronology, geochronology and geochemistry of NW South America: Rift to drift transition, active margin dynamics and implications for the volume balance of continents. Doctoral thesis, University of Geneva, 191 p. Geneva, Switzerland. https://doi.org/10.13097/archive-ouverte/unige:30029

Cochrane, R., Spikings, R., Gerdes, A., Winkler, W., Ulianov, A., Mora, A. & Chiaradia, M. 2014a. Distinguishing between in–situ and accretionary growth of continents along active margins. Lithos, 202–203: 382–394. https://doi.org/10.1016/j.lithos.2014.05.031

Triassic

Permian

Cochrane, R., Spikings, R., Gerdes, A., Ulianov, A., Mora, A., Villagómez, D., Putlitz, B. & Chiaradia, M. 2014b. Permo–Triassic anatexis, continental rifting and the disassembly of western Pangaea. Lithos, 190–191: 383–402. https://doi.org/10.1016/j.lithos.2013.12.020

Cochrane, R., Spikings, R., Chew, D., Wotzlaw, J.F., Chiaradia, M., Tyrrell, S., Schaltegger, U. & van der Lelij, R. 2014c. High temperature (>350 °C) thermochronology and mechanisms of Pb loss in apatite. Geochimica et Cosmochimica Acta, 127: 39–56. https://doi.org/10.1016/j.gca.2013.11.028

Cocks, L.R.M. & Torsvik, T.H. 2002. Earth geography from 500 to 400 million years ago: A faunal and palaeomagnetic review. Journal of the Geological Society, 159(6): 631–644. https://doi.org/10.1144/0016-764901-118

Collins, W.J. & Richards, S.W. 2008. Geodynamic significance of S–type granites in circum–Pacific orogens. Geology, 36(7): 559–562. https://doi.org/10.1130/G24658A.1

Collins, W.J., Belousova, E.A., Kemp, A.I.S. & Murphy, J.B. 2011. Two contrasting Phanerozoic orogenic systems revealed by hafnium isotope data. Nature Geoscience, 4: 333–337. https://doi.org/10.1038/NGEO1127

Colmenares, F.H., Mesa, A.M., Roncancio, J.H., Arciniegas, E.G., Silva, C.A., Romero, A.J., Pedraza, P.E., Alvarado, S.I., Romero, O.A., Vargas, A.F., Santamaría, J.C. & Cardona, A. 2007a. Geologic map of the Sierra Nevada de Santa Marta. Scale 1:200 000. Ingeominas–Invemar–Ecopetrol–ICP–Geosearch Ltda. Bogotá.

Colmenares, F.H., Mesa, A.M., Roncancio, J.H., Arciniegas, E.G., Pedraza, P.E., Cardona, A., Romero, A.J., Silva, C.A., Alvarado, S.I., Romero, O.A. & Vargas, A.F. 2007b. Geología de las planchas 11, 12, 13, 14, 18, 19, 20, 21, 25, 26, 27, 33, 34 y 40. Proyecto: Evolución geohistórica de la Sierra Nevada de Santa Marta. Invemar–Ingeominas–ICP–Ecopetrol–Geosearch Ltda., 401 p. Bogotá.

Colony, R.J. & Sinclair, J.H. 1932. Metamorphic and igneous rocks of eastern Ecuador. Annals of the New York Academy of Sciences, 34(1): 1–53. https://doi.org/10.1111/j.1749-6632.1932.tb56973.x

Cordani, U.G., Brito–Neves, B.B. & D'Agrella, M.S. 2003. From Rodinia to Gondwana: A review of the available evidence from South America. Gondwana Research, 6(2): 275–283. https://doi.org/10.1016/S1342-937X(05)70976-X

Correa–Martínez, A.M. 2007. Petrôgenese e evolução do Ofiolito de Aburrá, Cordilhera Central dos Andes colombianos. Doctoral thesis, Universidade de Brasília, 204 p. Brasilia.

Dasch, L.E. 1982. U–Pb geochronology of the Sierra de Perijá, Venezuela. Master thesis, Case Western Reserve University, 183 p. Cleveland, USA.

Davies, J.H.F.L., Marzoli, A., Bertrand, H., Youbi, N., Ernesto, M. & Schaltegger, U. 2017. End–Triassic mass extinction started by intrusive CAMP activity. Nature Communications, 8(15996): 1–8. https://doi.org/10.1038/ncomms15596

Dickinson, W.R. & Lawton, T.F. 2001. Carboniferous to Cretaceous assembly and fragmentation of Mexico. Geological Society of America Bulletin, 113(9): 1142–1160. https://doi.org/10.1130/0016-7606(2001)113<1142:CTCAAF>2.0.CO;2

Ducea, M.N., Gehrels, G.E., Shoemaker, S., Ruiz, J. & Valencia, V.A. 2004. Geologic evolution of the Xolapa Complex, southern Mexico: Evidence from U–Pb zircon geochronology. Geological Society of America Bulletin, 116(7–8): 1016–1025. https://doi.org/10.1130/B25467.1

Elías–Herrera, M. & Ortega–Gutiérrez, F. 2002. Caltepec Fault zone: An early Permian dextral transpressional boundary between the Proterozoic Oaxacan and Paleozoic Acatlán Complexes, southern Mexico, and regional tectonic implications. Tectonics, 21(3): 4-1–4-18. https://doi.org/10.1029/2000TC001278

Feininger, T., Barrero, D. & Castro, N. 1972. Geología de parte de los departamentos de Antioquia y Caldas (sub–zona II–B). Boletín Geológico, 20(2): 1–173.

Franzese, J.R. & Spalletti, L.A. 2001. Late Triassic – Early Jurassic continental extension in southwestern Gondwana: Tectonic segmentation and pre–break–up rifting. Journal of South American Earth Sciences, 14(3): 257–270. https://doi.org/10.1016/S0895-9811(01)00029-3

Frost, B.R., Barnes, C.G., Collins, W.J., Arculus, R.J., Ellis, D.J. & Frost, C.D. 2001. A geochemical classification for granitic rocks. Journal of Petrology, 42(11): 2033–2048. https://doi.org/10.1093/petrology/42.11.2033

Gerdes, A.G., Montero, P.M., Bea, F.B., Fershater, G.F., Borodina, N.B., Osipova, T.O. & Shardakova, G.S. 2002. Peraluminous granites frequently with mantle–like isotope compositions: The continental–type Murzinka and Dzhabyk Batholiths of the eastern Urals. International Journal of Earth Sciences, 91(1): 3–19. https://doi.org/10.1007/s005310100195

Gómez, J., Nivia, Á., Montes, N.E., Jiménez, D.M., Tejada, M.L., Sepúlveda, M.J., Osorio, J.A., Gaona, T., Diederix, H., Uribe, H. & Mora, M., compilers. 2007. Geological Map of Colombia 2007. Scale 1:1 000 000. Ingeominas, 2 sheets. Bogotá.

González, H. 1980. Geología de las planchas 167 Sonsón y 187 Salamina. Scale 1:100 000. Ingeominas, Internal report 1760, 262 p. Medellín.

Hall, R.B., Álvarez, J. & Rico, H. 1972. Geología de parte de los departamentos de Antioquia y Caldas (sub–zona II–A). Boletín Geológico, 20(1): 1–85.

Harris, C., Faure, K., Diamond, R.E. & Scheepers, R. 1997. Oxygen and hydrogen isotope geochemistry of S– and I–type granitoids: The Cape Granite Suite, South Africa. Chemical Geology, 143(1–2): 95–114. https://doi.org/10.1016/S0009-2541(97)00103-4

Harrison, T.M., Célérier, J., Aikman, A.B., Hermann, J. & Heizler, M.T. 2009. Diffusion of [40]Ar in muscovite. Geochimica et Cosmochimica Acta, 73(4): 1039–1051. https://doi.org/10.1016/j.gca.2008.09.038

Hartmann, L.A. & Santos, J.O.S. 2004. Predominance of high Th/U, magmatic zircon in Brazilian Shield sandstones. Geology, 32(1): 73–76. https://doi.org/10.1130/G20007.1

Hastie, A.R., Kerr, A.C., Pearce, J.A. & Mitchell, S.F. 2007. Classification of altered volcanic island arc rocks using immobile trace elements: Development of the Th–Co discrimination diagram. Journal of Petrology, 48(12): 2341–2357. https://doi.org/10.1093/petrology/egm062

Hatcher, R.D. 2002. Alleghanian (Appalachian) Orogeny, a product of zipper tectonics: Rotational transpressive continent–continent collision and closing of ancient oceans along irregular margins. In: Martínez, J.R., Hatcher, R.D., Arenas, R. & Díaz–García, F. (editors), Variscan–Appalachian dynamics: The building of the late Paleozoic basement. Geological Society of America, Special Paper 364, p. 199–208. https://doi.org/10.1130/0-8137-2364-7.199

Helbig, M., Keppie, J.D., Murphy, J.B. & Solari, L.A. 2012. U–Pb geochronological constraints on the Triassic – Jurassic Ayú Complex, southern Mexico: Derivation from the western margin of Pangea–A. Gondwana Research, 22(3–4): 910–927. https://doi.org/10.1016/j.gr.2012.03.004

Hervé, F., Fanning, C.M., Calderón, M. & Mpodozis, C. 2014. Early Permian to Late Triassic batholiths of the Chilean Frontal Cordillera (28°–31° S): SHRIMP U–Pb zircon ages and Lu–Hf and O isotope systematics. Lithos, 184–187: 436–446. https://doi.org/10.1016/j.lithos.2013.10.018

Horton, B.K., Saylor, J.E., Nie, J., Mora, A., Parra, M., Reyes–Harker, A. & Stockli, D.F. 2010. Linking sedimentation in the northern Andes to basement configuration, Mesozoic extension, and Cenozoic shortening: Evidence from detrital zircon U–Pb ages, Eastern Cordillera, Colombia. Geological Society of America Bulletin, 122(9–10): 1423–1442. https://doi.org/10.1130/B30118.1

Jaillard, E., Soler, P., Carlier, G. & Mourier, T. 1990. Geodynamic evolution of the northern and central Andes during early to middle Mesozoic times: A Tethyan model. Journal of the Geological Society, 147(6): 1009–1022. https://doi.org/10.1144/gsjgs.147.6.1009

Jaillard, E., Sempere, T., Soler, P., Carlier, G. & Marocco, R. 1995. The role of Tethys in the evolution of the northern Andes between late Permian and late Eocene times. In: Nairn, A.E.M., Ricou, L.E., Vrielynck, B., Dercourt, J., (editors), The ocean basins and margins: The Tethys Ocean. Springer Science+Business Media, p. 463–492. New York. https://doi.org/10.1007/978-1-4899-1558-0_15

John, T., Scherer, E.E., Schenk, V., Herms, P., Halama, R. & Garbe–Schönberg, D. 2010. Subducted seamounts in an eclogite–facies ophiolite sequence: The Andean Raspas Complex, SW Ecuador. Contributions to Mineralogy and Petrology, 159(2): 265–284. https://doi.org/10.1007/s00410-009-0427-0

Kay, S.M. 1993. Late Paleozoic tectonics in southern South America: A global perspective. Douzième Congrés International de la Stratigraphie et Géologie du Carbonifére et Permien. Comptes Rendus, I, p. 109–122.

Kay, S.M., Ramos, V.A., Mpodozis, C. & Sruoga, P. 1989. Late Paleozoic to Jurassic silicic magmatism at the Gondwana margin: Analogy to the middle Proterozoic in North America? Geology, 17(4): 324–328. https://doi.org/10.1130/0091-7613(1989)017<0324:LPTJSM>2.3.CO;2

Kennan, L. & Pindell, J.L. 2009. Dextral shear, terrane accretion and basin formation in the northern Andes: Best explained by interaction with a Pacific–derived Caribbean Plate? In: James, K.H., Lorente, M.A. & Pindell, J.L. (editors), The origin and evolution of the Caribbean Plate. Geological Society of London, Special Publication 328, p. 487–531. https://doi.org/10.1144/SP328.20

Keppie, J.D., Sandberg, C.A., Miller, B.V., Sánchez–Zavala, J.L., Nance, R.D. & Poole, F.G. 2004. Implications of latest Pennsylvanian to middle Permian paleontological and U–Pb SHRIMP data from the Tecomate Formation to re–dating tectonothermal events in the Acatlán Complex, southern Mexico. International Geology Review, 46(8): 745–753. https://doi.org/10.2747/0020-6814.46.8.745

Keppie, J.D., Dostal, J., Miller, B.V., Ortega–Rivera, A., Roldán–Quintana, J. & Lee, J.W.K. 2006. Geochronology and geochemistry of the Francisco Gneiss: Triassic continental rift tholeiites on the Mexican margin of Pangea metamorphosed and exhumed in a Tertiary core complex. International Geology Reviews, 48(1): 1–16. https://doi.org/10.2747/0020-6814.48.1.1

Kerr, A.C., Marriner, G.F., Tarney, J., Nivia, Á., Saunders, A.D., Thirlwall, M.F. & Sinton, C.W. 1997. Cretaceous basaltic terranes in western Colombia: Elemental, chronological and Sr–Nd isotopic constraints on petrogenesis. Journal of Petrology, 38(6): 677–702. https://doi.org/10.1093/petrology/38.6.677

Kerr, A.C., Aspden, J.A., Tarney, J. & Pilatasig, L.F. 2002. The nature and provenance of accreted oceanic terranes in western Ecuador: Geochemical and tectonic constraints. Journal of the Geological Society, 159(5): 577–594. https://doi.org/10.1144/0016-764901-151

Kirsch, M., Keppie, J.D., Murphy, J.B. & Solari, L.A. 2012. Permian – Carboniferous arc magmatism and basin evolution along the western margin of Pangea: Geochemical and geochronological evidence from the eastern Acatlán Complex, southern Mexico. Geological Society of America Bulletin, 124(9–10): 1607–1628. https://doi.org/10.1130/B30649.1

Laubacher, G. 1978. Géologie des Andes Péruviennes. Géologie de la Cordillère Orientale et de l'Altiplano au nord et nord–ouest du lac Titicaca, Pérou. ORSTOM, 217 p. Paris.

Laya, J.C. & Tucker, M.E. 2012. Facies analysis and depositional environments of Permian carbonates of the Venezuelan Andes: Palaeogeographic implications for northern Gondwana. Palaeogeography, Palaeoclimatology, Palaeoecology, 331–332: 1–26. https://doi.org/10.1016/j.palaeo.2012.02.011

Triassic

Permian

Litherland, M., Aspden, J.A. & Jemielita, R.A. 1994. The metamorphic belts of Ecuador. Overseas Memoir of the British Geological Survey 11, 147 p. Nottingham, England.

Luppo, T., López de Luchi, M.G., Rapalini, A.E., Martínez–Dopico, C.I. & Fanning, C.M. 2018. Geochronologic evidence of a large magmatic province in northern Patagonia encompassing the Permian – Triassic boundary. Journal of South American Earth Sciences, 82: 346–355. https://doi.org/10.1016/j.jsames.2018.01.003

Luzieux, L.D.A., Heller, F., Spikings, R., Vallejo, C.F. & Winkler, W. 2006. Origin and Cretaceous tectonic history of the coastal Ecuadorian forearc between 1° N and 3° S: Paleomagnetic, radiometric and fossil evidence. Earth and Planetary Science Letters, 249(3–4): 400–414. https://doi.org/10.1016/j.epsl.2006.07.008

MacDonald, W.D. & Hurley, P.M. 1969. Precambrian gneisses from northern Colombia, South America. Geological Society of America Bulletin, 80(9): 1867–1872. https://doi.org/10.1130/0016-7606(1969)80[1867:PGFNCS]2.0.CO;2

Maksaev, V., Munizaga, F. & Tassinari, C. 2014. Timing of magmatism of the paleo–Pacific border of Gondwana: U–Pb geochronology of late Paleozoic to early Mesozoic igneous rocks of the north Chilean Andes between 20° and 31° S. Andean Geology, 41(3): 447–506. https://doi.org/10.5027/andgeoV41n3-a01

Maniar, P.D. & Piccoli, P.M. 1989. Tectonic discrimination of granitoids. Geological Society of America Bulletin, 101(5): 635–643. https://doi.org/10.1130/0016-7606(1989)101<0635:TDOG>2.3.CO;2

Martens, U., Restrepo, J.J., Ordóñez–Carmona, O. & Correa–Martínez, A.M. 2014. The Tahamí and Anacona Terranes of the Colombian Andes: Missing links between South American and Mexican Gondwana margins. The Journal of Geology, 122(5): 507–530. https://doi.org/10.1086/677177

Martínez, R.N., Sereno, P.C., Alcober, O.A., Colombi, C.E., Renne, P.R., Montañez, I.P. & Currie, B.S. 2011. A basal dinosaur from the dawn of the dinosaur era in southwestern Pangaea. Science, 331(6014): 206–210. https://doi.org/10.1126/science.1198467

Martin–Gombojav, N. & Winkler, W. 2008. Recycling of Proterozoic crust in the Andean Amazon foreland of Ecuador: Implications for orogenic development of the northern Andes. Terra Nova, 20(1): 22–31. https://doi.org/10.1111/j.1365-3121.2007.00782.x

Maya, M. & González, H. 1995. Unidades litodémicas en la cordillera Central de Colombia. Boletín Geológico, 35(2–3): 43–57.

McCourt, W.J., Aspden, J.A. & Brook, M. 1984. New geological and geochronological data from the Colombian Andes: Continental growth by multiple accretion. Journal of the Geological Society, 141(5): 831–845. https://doi.org/10.1144/gsjgs.141.5.0831

Mégard, F. 1978. Etude géologique des Andes du Pérou central. ORSTOM, 310 p. Paris.

Mišković, A. & Schaltegger, U. 2009. Crustal growth along a non–collisional cratonic margin: A Lu–Hf isotopic survey of the eastern cordilleran granitoids of Peru. Earth and Planetary Science Letters, 279(3–4): 303–315. https://doi.org/10.1016/j.epsl.2009.01.002

Mišković, A., Spikings, R.A., Chew, D.M., Košler, J., Ulianov, A. & Schaltegger, U. 2009. Tectonomagmatic evolution of western Amazonia: Geochemical characterization and zircon U–Pb geochronologic constraints from the Peruvian eastern cordilleran granitoids. Geological Society of America Bulletin, 121(9–10): 1298–1324. https://doi.org/10.1130/B26488.1

Mitouard, P., Kissel, C. & Laj, C. 1990. Post–Oligocene rotations in southern Ecuador and northern Peru and the formation of the Huancabamba Deflection in the Andean Cordillera. Earth and Planetary Science Letters, 98(3–4): 329–339. https://doi.org/10.1016/0012-821X(90)90035-V

Mojica, J. & Kammer, A. 1995. Eventos jurásicos en Colombia. Geología Colombiana, 19: 165–172.

Mojica, J. & Prinz–Grimm, P. 2000. La fauna de amonitas del Triásico Tardío en el Miembro Chicalá (parte baja de la Formación Saldaña) en Payandé, Tolima, Colombia. Geología Colombiana, 25: 13–23.

Montes, C., Guzman, G., Bayona, G., Cardona, A., Valencia, V. & Jaramillo, C. 2010. Clockwise rotation of the Santa Marta Massif and simultaneous Paleogene to Neogene deformation of the Plato–San Jorge and Cesar–Ranchería Basins. Journal of South American Earth Sciences, 29(4): 832–848. https://doi.org/10.1016/j.jsames.2009.07.010

Nivia, Á., Marriner, G.F., Kerr, A.C. & Tarney, J. 2006. The Quebradagrande Complex: A Lower Cretaceous ensialic marginal basin in the Central Cordillera of the Colombian Andes. Journal of South American Earth Sciences, 21(4): 423–436. https://doi.org/10.1016/j.jsames.2006.07.002

Noble, D.C., Silberman, M.L., Megard, F. & Bowman, H.R. 1978. Comendite (peralkaline rhyolite) and basalt in the Mitu Group, Peru: Evidence of Permian – Triassic lithospheric extension in the central Andes. U.S. Geological Survey Journal of Research, 6(4): 453–457.

Noble, S.R., Aspden, J.A. & Jemielita, R. 1997. Northern Andean crustal evolution: New U–Pb geochronological constraints from Ecuador. Geological Society of America Bulletin, 109(7): 789–798. https://doi.org/10.1130/0016-7606(1997)109<0789:NACENU>2.3.CO;2

Omarini, R.H., Sureda, R.J., Götze, H.J., Seilacher, A. & Pflüger, F. 1999. Puncoviscana folded belt in northwestern Argentina: Testimony of late Proterozoic Rodinia fragmentation and pre–Gondwana collisional episodes. International Journal of Earth Sciences, 88(1): 76–97. https://doi.org/10.1007/s005310050247

Ordóñez–Carmona, O. & Pimentel, M.M. 2002. Rb–Sr and Sm–Nd isotopic study of the Puquí Complex, Colombian Andes. Journal of South American Earth Sciences, 15(2): 173–182. https://doi.org/10.1016/S0895-9811(02)00017-2

Ordóñez–Carmona, O., Restrepo, J.J. & Pimentel, M.M. 2006. Geochronological and isotopical review of pre–Devonian crustal

basement of the Colombian Andes. Journal of South American Earth Sciences, 21(4): 372–382. https://doi.org/10.1016/j.jsames.2006.07.005

Ortega–Obregón, C., Solari, L., Gómez–Tuena, A., Elías–Herrera, M., Ortega–Gutiérrez, F. & Macías–Romo, C. 2014. Permian – Carboniferous arc magmatism in southern Mexico: U–Pb dating, trace element and Hf isotopic evidence on zircons of earliest subduction beneath the western margin of Gondwana. International Journal of Earth Sciences, 103(5): 1287–1300. https://doi.org/10.1007/s00531-013-0933-1

Pankhurst, R.J., Rapela, C.W. & Fanning, C.M. 2000. Age and origin of coeval TTG, I– and S–type granites in the Famatinian belt of NW Argentina. Transactions of the Royal Society of Edinburgh: Earth and Environmental Sciences, 91(1–2): 151–168. https://doi.org/10.1017/S0263593300007343

Parada, M.A., López–Escobar, L., Oliveros, V., Fuentes, F., Morata, D., Calderón, M., Aguirre, L., Féraud, G., Espinoza, F., Moreno, H., Figueroa, O., Muñoz–Bravo, J., Troncoso–Vásquez, R. & Stern, C.R. 2007. Andean magmatism. In: Moreno, T. & Gibbons, W. (editors), The geology of Chile. The Geological Society, p. 115–146. London. https://doi.org/10.1144/GOCH.4

Parson, L.M. & Wright, I.C. 1996. The Lau–Havre–Taupo back–arc basin: A southward–propagating, multi–stage evolution from rifting to spreading. Tectonophysics, 263(1–4): 1–22. https://doi.org/10.1016/S0040-1951(96)00029-7

Paul, A. 2017. Advancing U–Pb high–temperature thermochronology by combining single grain and intra–grain dating. Doctoral thesis, University of Geneva. Geneva, 201 p., Switzerland. https://doi.org/10.13097/archive-ouverte/unige:102601

Paul, A., Spikings, R., Ulianov, A. & Ovtcharova, M. 2018. High temperature (>350 °C) thermal histories of the long lived (>500 Ma) active margin of Ecuador and Colombia: Apatite, titanite and rutile U–Pb thermochronology. Geochimica et Cosmochimica Acta, 228: 275–300. https://doi.org/10.1016/j.gca.2018.02.033

Peacock, M.A. 1931. Classification of igneous rock series. The Journal of Geology, 39(1): 54–67.

Peccerillo, A. & Taylor, S.R. 1976. Geochemistry of Eocene calc–alkaline volcanic rocks from the Kastamonu area, northern Turkey. Contributions to Mineralogy and Petrology, 58(1): 63–81. https://doi.org/10.1007/BF00384745

Pindell, J.L. 1985. Alleghenian reconstruction and subsequent evolution of the Gulf of Mexico, Bahamas, and proto–Caribbean. Tectonics, 4(1): 1–39. https://doi.org/10.1029/TC004i001p00001

Pindell, J. & Barrett, S.F. 1990. Geological evolution of the Caribbean region; a plate–tectonic perspective. In: Dengo, G. & Case, J.E. (editors), The Caribbean region. Geological Society of America, p. 405–432. https://doi.org/10.1130/DNAG-GNA-H.405

Pindell, J. & Dewey, J.F. 1982. Permo–Triassic reconstruction of western Pangaea and the evolution of the Gulf of Mexico/Caribbean region. Tectonics, 1(2): 179–211. https://doi.org/10.1029/TC001i002p00179

Pindell, J.L. & Kennan, L. 2009. Tectonic evolution of the Gulf of Mexico, Caribbean and northern South America in the mantle reference frame: An update. In: James, K.H., Lorente, M.A. & Pindell, J.L. (editors), The origin and evolution of the Caribbean Plate. Geological Society of London, Special Publication 328, p. 1–55. https://doi.org/10.1144/SP328.1

Pindell, J.L., Higgs, R. & Dewey, J.F. 1998. Cenozoic palinspastic reconstruction, paleogeographic evolution and hydrocarbon setting of the northern margin of South America. In: Pindell, J.L. & Drake, C. (editors), Paleogeographic evolution and non–glacial eustasy, northern South America. Society for Sedimentary Geology, Special Publication 58, p. 45–85. https://doi.org/10.2110/pec.98.58.0045

Piraquive, A. 2017. Structural framework, deformation and exhumation of the Santa Marta Schists: Accretion and deformational history of a Caribbean Terrane at the north of the Sierra Nevada de Santa Marta. Doctoral thesis, Université Grenoble Alpes and Universidad Nacional de Colombia, 393 p. Grenoble–Bogotá.

Pratt, W.T., Duque, P. & Ponce, M. 2005. An autochthonous geological model for the eastern Andes of Ecuador. Tectonophysics, 399(1–4): 251–278. https://doi.org/10.1016/j.tecto.2004.12.025

Ramos, V.A. 1988. The tectonics of the central Andes; 30° to 33° S latitude. In: Clark Jr., S.P., Burchfiel, B.C. & Suppe, J. (editors), Processes in continental lithospheric deformation. Geological Society of America, Special Paper 218, p. 31–54. https://doi.org/10.1130/SPE218-p31

Ramos, V.A. 1994. Terranes of southern Gondwanaland and their control in the Andean structure (30°–33° S latitude). In: Reutter, K.J., Scheuber, E. & Wigger, P.J. (editors), Tectonics of the southern central Andes. Springer–Verlag, p. 249–261. Heidelberg. https://doi.org/10.1007/978-3-642-77353-2_18

Ramos, V.A. 2009. Anatomy and global context of the Andes: Main geologic features and the Andean orogenic cycle. In: Kay, S.M., Ramos, V.A. & Dickinson, W.R. (editors), Backbone of the Americas: Shallow subduction, plateau uplift, and ridge and terrane collision. Geological Society of America, Memoirs 204, p. 31–65. https://doi.org/10.1130/2009.1204(02)

Ramos, V.A. & Kay, S.M. 1991. Triassic rifting and associated basalts in the Cuyo Basin, central Argentina. In: Harmon, R. & Rapela, C. (editors), Andean magmatism and its tectonic setting. Geological Society of America, Special Paper 265, p. 79–92. https://doi.org/10.1130/SPE265-p79

Ratschbacher, L., Franz, L., Min, M., Bachmann, R., Martens, U., Stanek, K., Stübner, K., Nelson, B.K., Herrmann, U., Weber, B., López–Martínez, M., Jonckheere, R., Sperner, B., Tichomirowa, M., Mcwilliams, M.O., Gordon, M., Meschede, M. & Bock, P. 2009. The North American–Caribbean Plate boundary in Mexico–Guatemala–Honduras. In: James, K.H.,

Triassic

Permian

Lorente, M.A. & Pindell, J.L. (editors), The origin and evolution of the Caribbean Plate. Geological Society of London, Special Publication 328, p. 219–293. https://doi.org/10.1144/SP328.11

Reitsma, M.J. 2012. Reconstructing the late Paleozoic: Early Mesozoic plutonic and sedimentary record of south–east Peru: Orphaned back–arcs along the western margin of Gondwana. Doctoral thesis, University of Geneva, 226 p. Geneva. https://doi.org/10.13097/archive-ouverte/unige:23095

Restrepo, J.J. & Toussaint, J.F. 1982. Metamorfismos superpuestos en la cordillera Central de Colombia. V Congreso Latinoamericano de Geología, p. 505–512. Buenos Aires, Argentina.

Restrepo, J.J. & Toussaint, J.F. 1988. Terranes and continental accretion in the Colombian Andes. Episodes, 11(3): 189–193. https://doi.org/10.18814/epiiugs/1988/v11i3/006

Restrepo, J.J., Toussaint, J.F., González, H., Cordani, U., Kawashita, K., Linares, E. & Parica, C. 1991. Precisiones geocronológicas sobre el occidente colombiano. Simposio sobre magmatismo andino y su marco tectónico. Memoirs, I, p. 1–22. Manizales.

Restrepo, J.J., Ordóñez–Carmona, O., Armstrong, R. & Pimentel, M.M. 2011. Triassic metamorphism in the northern part of the Tahamí Terrane of the Central Cordillera of Colombia. Journal of South American Earth Sciences, 32(4): 497–507. https://doi.org/10.1016/j.jsames.2011.04.009

Restrepo–Pace, P.A. & Cediel, F. 2010. Northern South America basement tectonics and implications for paleocontinental reconstructions of the Americas. Journal of South American Earth Sciences, 29(4): 764–771. https://doi.org/10.1016/j.jsames.2010.06.002

Restrepo–Pace, P.A., Ruiz, J., Gehrels, G. & Cosca, M. 1997. Geochronology and Nd isotopic data of Grenville–age rocks in the Colombian Andes: New constraints for late Proterozoic – early Paleozoic paleocontinental reconstructions of the Americas. Earth and Planetary Science Letters, 150(3–4): 427–441. https://doi.org/10.1016/S0012-821X(97)00091-5

Riel, N., Guillot, S., Jaillard, E., Martelat, J.E., Paquette, J.L., Schwartz, S., Goncalves, P., Duclaux, G., Thebaud, N., Lanari, P., Janots, E. & Yuquilema, J. 2013. Metamorphic and geochronological study of the Triassic El Oro Metamorphic Complex, Ecuador: Implications for high–temperature metamorphism in a forearc zone. Lithos, 156–159: 41–68. https://doi.org/10.1016/j.lithos.2012.10.005

Rogers, R.R., Swisher, C.C., Sereno, P.C., Monetta, A.M., Forster, C.A. & Martínez, R.N. 1993. The Ischigualasto tetrapod assemblage (Late Triassic, Argentina) and ^{40}Ar/^{39}Ar dating of dinosaur origins. Science, 260(5109): 794–797. https://doi.org/10.1126/science.260.5109.794

Romero, D., Valencia, K., Alarcón, P., Peña, D. & Ramos, V.A. 2013. The offshore basement of Perú: Evidence for different igneous and metamorphic domains in the forearc. Journal of South American Earth Sciences, 42: 47–60. https://doi.org/10.1016/j.jsames.2012.11.003

Rosas, S., Fontboté, L. & Tankard, A. 2007. Tectonic evolution and paleogeography of the Mesozoic Pucará Basin, central Peru. Journal of South American Earth Sciences, 24(1): 1–24. https://doi.org/10.1016/j.jsames.2007.03.002

Ruiz, J., Tosdal, R.M., Restrepo, P.A. & Murillo–Muñetón, G. 1999. Pb isotope evidence for Colombia–southern México connections in the Proterozoic. In: Ramos, V.A. & Keppie, J.D. (editors), Laurentia–Gondwana connections before Pangea. Geological Society of America, Special Paper 336, p. 183–197. https://doi.org/10.1130/0-8137-2336-1.183

Russell, S.M. & Whitmarsh, R.B. 2003. Magmatism at the west Iberia non–volcanic rifted continental margin: Evidence from analyses of magnetic anomalies. Geophysical Journal International, 154(3): 706–730. https://doi.org/10.1046/j.1365-246X.2003.01999.x

Schlische, R.W. 2002. Progress in understanding the structural geology, basin evolution, and tectonic history of the eastern North American rift system. In: LeTourneau, P.M. & Olsen, P.E. (editors), The Great Rift valleys of Pangaea in eastern North America, 1. Columbia University Press, p. 21–64. New York. https://doi.org/10.7312/leto11162-003

Senff, M. 1995. Sedimentologie, fauna und fazies des präkretazischen Mesozoikum im Oberen Magdalenatal von zentralkolumbien unter besonderer berüecksichtigung der obertriassischen Payande Formation. Doctoral thesis, Univeristät Giessen, 114 p. Germany.

Shervais, J.W. 1982. Ti–V plots and the petrogenesis of modern and ophiolitic lavas. Earth and Planetary Science Letters, 59(1): 101–118. https://doi.org/10.1016/0012-821X(82)90120-0

Sinton, C.W., Duncan, R.A., Storey, M., Lewis, J. & Estrada, J.J. 1998. An oceanic flood basalt province within the Caribbean Plate. Earth and Planetary Science Letters, 155(3–4): 221–235. https://doi.org/10.1016/S0012-821X(97)00214-8

Solari, L.A., Dostal, J., Ortega–Gutiérrez, F. & Keppie, J.D. 2001. The 275 Ma arc–related La Carbonera stock in the northern Oaxacan Complex of southern Mexico: U–Pb geochronology and geochemistry. Revista Mexicana de Ciencias Geológicas, 18(2): 149–161.

Solari, L., Gómez–Tuena, A., Ortega–Gutiérrez, F. & Ortega–Obregón, C. 2011. The Chuacús Metamorphic Complex, central Guatemala: Geochronological and geochemical constraints on its Paleozoic – Mesozoic evolution. Geologica Acta, 9(3–4): 329–350. https://doi.org/10.1344/105.000001695

Spalletti, L.A., Fanning, C.M. & Rapela, C.W. 2008. Dating the Triassic continental rift in the southern Andes: The Potrerillos Formation, Cuyo Basin, Argentina. Geologica Acta, 6(3): 267–283. https://doi.org/10.1344/105.000000256

Spikings, R., Seward, D., Winkler, W. & Ruiz, G.M. 2000. Low–temperature thermochronology of the northern Cordillera Real, Ecuador: Tectonic insights from zircon and apatite fission track analysis. Tectonics, 19(4): 649–668. https://doi.org/10.1029/2000TC900010

Spikings, R., Winkler, W., Seward, D. & Handler, R. 2001. Along–strike variations in the thermal and tectonic response of the continental Ecuadorian Andes to the collision with heterogeneous oceanic crust. Earth and Planetary Science Letters, 186(1): 57–73. https://doi.org/10.1016/S0012-821X(01)00225-4

Spikings, R., Crowhurst, P.V., Winkler, W. & Villagómez, D. 2010. Syn– and post–accretionary cooling history of the Ecuadorian Andes constrained by their in–situ and detrital thermochronometric record. Journal of South American Earth Sciences, 30(3–4): 121–133. https://doi.org/10.1016/j.jsames.2010.04.002

Spikings, R., Cochrane, R., Villagómez, D., van der Lelij, R., Vallejo, C., Winkler, W. & Beate, B. 2015. The geological history of northwestern South America: From Pangaea to the early collision of the Caribbean Large Igneous Province (290–75 Ma). Gondwana Research, 27(1): 95–139. https://doi.org/10.1016/j.gr.2014.06.004

Spikings, R., Reitsma, M.J., Boekhout, F., Mišković, A., Ulianov, A., Chiaradia, M., Gerdes, A. & Schaltegger, U. 2016. Characterization of Triassic rifting in Peru and implications for the early disassembly of western Pangaea. Gondwana Research, 35: 124–143. https://doi.org/10.1016/j.gr.2016.02.008

Stacey, J.S. & Kramers, J.D. 1975. Approximation of terrestrial lead isotope evolution by a two–stage model. Earth and Planetary Science Letters, 26(2): 207–221. https://doi.org/10.1016/0012-821X(75)90088-6

Sun, S.S. & McDonough, W.F. 1989. Chemical and isotopic systematics of oceanic basalts: Implications for mantle composition and processes. In: Saunders, A.D. & Norry, M.J. (editors), Magmatism in the ocean basins. Geological Society of London, Special Publication 42, p. 313–345. https://doi.org/10.1144/GSL.SP.1989.042.01.19

Taylor, S.R. & McLennan, S.M. 1995. The geochemical evolution of the continental crust. Reviews of Geophysics, 33(2): 241–265. https://doi.org/10.1029/95RG00262

Torres, R., Ruiz, J., Patchett, P.J. & Grajales–Nishimura, J.M. 1999. Permo–Triassic continental arc in eastern Mexico: Tectonic implications for reconstructions of southern North America. In: Bartolini, C., Wilson, J.L. & Lawton, T.F. (editors), Mesozoic sedimentary and tectonic history of north–central Mexico. Geological Society of America, Special Paper 340, p. 191–196. https://doi.org/10.1130/0-8137-2340-X.191

Toussaint, J.F. & Restrepo, J.J. 1994. The Colombian Andes during Cretaceous times. In: Salfity, J.A. (editor), Cretaceous tectonics of the Andes. Earth Evolution Sciences. Vieweg + Teubner Verlag, p. 61–100. Wiesbaden, Germany. https://doi.org/10.1007/978-3-322-85472-8_2

Tschanz, C.M., Marvin, R.F., Cruz, J., Mehnert, H.H. & Cebula, G.T. 1974. Geologic evolution of the Sierra Nevada de Santa Marta, northeastern Colombia. Geological Society of America Bulletin, 85(2): 273–284. https://doi.org/10.1130/0016-7606(1974)85<273:GEOTSN>2.0.CO;2

Vallejo, C., Spikings, R., Luzieux, L., Winkler, W., Chew, D. & Page, L. 2006. The early interaction between the Caribbean Plateau and the NW South American Plate. Terra Nova, 18(4): 264–269. https://doi.org/10.1111/j.1365-3121.2006.00688.x

Vallejo, C., Winkler, W., Spikings, R.A., Luzieux, L., Heller, F. & Bussy, F. 2009. Mode and timing of terrane accretion in the forearc of the Andes in Ecuador. In: Kay, S.M., Ramos, V.A. & Dickinson, W.R. (editors), Backbone of the Americas: Shallow subduction, plateau uplift, and ridge and terrane collision. Geological Society of America, Memoirs 204, p. 197–216. https://doi.org/10.1130/2009.1204(09)

van der Lelij, R. 2013. Reconstructing north–western Gondwana with implications for the evolution of the Iapetus and Rheic Oceans: A geochronological, thermochronological and geochemical study. Doctoral thesis, University of Geneva, 248 p. Geneva. https://doi.org/10.13097/archive-ouverte/unige:31653

van der Lelij, R., Spikings, R., Kerr, A.C., Kounov, A., Cosca, M., Chew, D. & Villagómez, D. 2010. Thermochronology and tectonics of the Leeward Antilles: Evolution of the southern Caribbean Plate boundary zone. Tectonics, 29(6): 1–30. https://doi.org/10.1029/2009TC002654

van der Lelij, R., Spikings, R., Ulianov, A., Chiaradia, M. & Mora, A. 2016. Palaeozoic to Early Jurassic history of the northwestern corner of Gondwana, and implications for the evolution of the Iapetus, Rheic and Pacific Oceans. Gondwana Research, 31: 271–294. https://doi.org/10.1016/j.gr.2015.01.011

Vilas, J.F. & Valencio, D.A. 1978. Palaeomagnetism and K–Ar age of the Upper Ordovician Alcaparrosa Formation, Argentina. Geophysical Journal International, 55(1): 143–154. https://doi.org/10.1111/j.1365-246X.1978.tb04753.x

Villagómez, D. & Spikings, R. 2013. Thermochronology and tectonics of the Central and Western Cordilleras of Colombia: Early Cretaceous – Tertiary evolution of the northern Andes. Lithos, 160–161: 228–249. https://doi.org/10.1016/j.lithos.2012.12.008

Villagómez, D., Spikings, R., Magna, T., Kammer, A., Winkler, W. & Beltrán, A. 2011. Geochronology, geochemistry and tectonic evolution of the Western and Central Cordilleras of Colombia. Lithos, 125(3–4): 875–896. https://doi.org/10.1016/j.lithos.2011.05.003

Vinasco, C.J., Cordani, U.G., González, H., Weber, M. & Peláez, C. 2006. Geochronological, isotopic, and geochemical data from Permo–Triassic granitic gneisses and granitoids of the Colombian central Andes. Journal of South American Earth Sciences, 21(4): 355–371. https://doi.org/10.1016/j.jsames.2006.07.007

Viscarret, P., Wright, J. & Urbani, F. 2009. New U–Pb zircon ages of El Baúl Massif, Cojedes state, Venezuela. Revista Técnica de la Facultad de Ingeniería, Universidad del Zulia, 32(3): 210–221.

Weber, B. & Köhler, H. 1999. Sm–Nd, Rb–Sr and U–Pb geochronology of a Grenville Terrane in southern Mexico: Origin and geologic history of the Guichicovi Complex. Precambrian

Triassic

Permian

Research, 96(3–4): 245–262. https://doi.org/10.1016/S0301-9268(99)00012-1

Weber, B., Cameron, K.L., Osorio, M. & Schaaf, P. 2005. A late Permian tectonothermal event in Grenville crust of the southern Maya Terrane: U–Pb zircon ages from the Chiapas Massif, southeastern Mexico. International Geology Review, 47(5): 509–529. https://doi.org/10.2747/0020-6814.47.5.509

Weber, B., Iriondo, A., Premo, W.R., Hecht, L. & Schaaf, P. 2007. New insights into the history and origin of the southern Maya Block, SE México: U–Pb–SHRIMP zircon geochronology from metamorphic rocks of the Chiapas Massif. International Journal of Earth Sciences, 96(2): 253–269. https://doi.org/10.1007/s00531-006-0093-7

Weber, M., Cardona, A., Valencia, V., García–Casco, A., Tobón, M. & Zapata, S. 2010. U/Pb detrital zircon provenance from Late Cretaceous metamorphic units of the Guajira Peninsula, Colombia: Tectonic implications on the collision between the Caribbean Arc and the South American margin. Journal of South American Earth Sciences, 29(4): 805–816. https://doi.org/10.1016/j.jsames.2009.10.004

Winchester, J.A. & Floyd, P.A. 1977. Geochemical discrimination of different magma series and their differentiation products using immobile elements. Chemical Geology, 20: 325–343. https://doi.org/10.1016/0009-2541(77)90057-2

Xu, H., Ma, C. & Ye, K. 2007. Early Cretaceous granitoids and their implications for the collapse of the Dabie Orogen, eastern China: SHRIMP zircon U–Pb dating and geochemistry. Chemical Geology, 240(3–4): 238–259. https://doi.org/10.1016/j.chemgeo.2007.02.018

Yañez, P., Ruiz, J., Patchett, P.J., Ortega–Gutiérrez, F. & Gehrels, G.E. 1991. Isotopic studies of the Acatlan Complex, southern Mexico: Implications for Paleozoic North American tectonics. Geological Society of America Bulletin, 103(6): 817–828. https://doi.org/10.1130/0016-7606(1991)103<0817:ISOTAC>2.3.CO;2

Zerfass, H., Chemale, F., Schultz, C.L. & Lavina, E. 2004. Tectonics and sedimentation in southern South America during Triassic. Sedimentary Geology, 166(3–4): 265–292. https://doi.org/10.1016/j.sedgeo.2003.12.008

Explanation of Acronyms, Abbreviations, and Symbols:

BABB	Back–arc basin basalt
CHUR	Chondritic uniform reservoir
E–MORB	Enriched mid–ocean ridge basalt
HFSE	High field strength elements
HP/LT	High–pressure/low–temperature
ID–TIMS	Isotope dilution thermal ionization mass spectrometry
ISMMB	Inner Santa Marta Metamorphic Belt
LA–ICP–MS	Laser ablation inductively coupled plasma mass spectrometry
LA–MC–ICP–MS	Laser ablation multi–collector inductively coupled plasma mass spectrometry
LILE	Light–ion lithophile element
LREE	Light rare earth element
MORB	Mid–ocean ridge basalt
MP–HT	Medium pressure–high temperature
N–MORB	Normal mid–ocean ridge basalt
REE	Rare earth element
SHRIMP	Sensitive high–resolution ion microprobe
SIMS	Secondary ion mass spectrometry

Authors' Biographical Notes
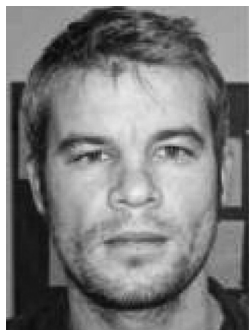
Richard SPIKINGS graduated in geochemistry at the University of St. Andrews in 1993. His research in thermochronology earned a PhD in geology in 1998 from La Trobe University, Melbourne. Since 1998, he has worked as a postdoctoral fellow at the ETH–Zurich, and as tenured research staff at the University of Geneva where he currently manages the $^{40}Ar/^{39}Ar$ laboratory. His research has focussed on thermochronology and geochronology of the Andean cordilleras in Ecuador, Colombia, Venezuela, Perú, and Chile. More recently, Richard has focussed his research efforts on bulk and in–situ U–Pb thermochronology of accessory phases.

Andre Navin PAUL obtained a BSc in geoscience in 2010 and a MS in geoscience in 2012 at the University of Hamburg, Germany. He then completed his PhD at the University of Geneva, Switzerland in 2017, where he studied U–Pb thermochronology. Since then Andre has been investigating Boron isotope systematics in the earth's mantle as a post–doctoral research assistant at the University of Edinburgh, in collaboration with the University of Bristol and University of Leeds, United Kingdom. His research is focused on the use of radiogenic and stable isotope systematics, with high spatial resolution and high precision analyses.

Triassic

Permian

43